ACCSCIENCE PUBLISHING

Explora: Environment and Resource

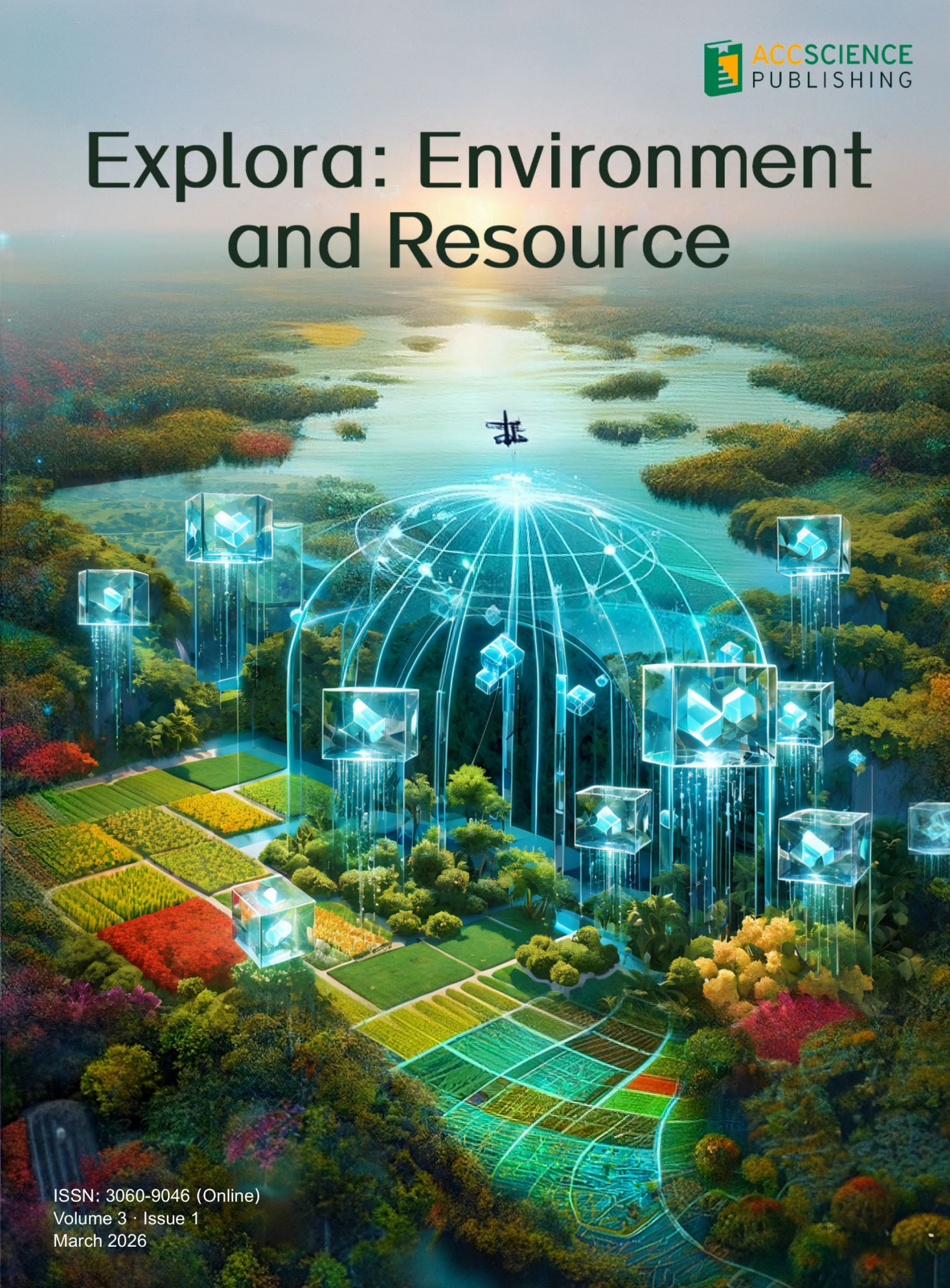

ISSN: 3060-9046 (Online)
Volume 3 · Issue 1
March 2026

Explora: Environment and Resource

Online ISSN: 3060-9046

Explora: Environment and Resource is an international and multidisciplinary journal covering all aspects of the environmental impacts of socio-economic development. It is concerned with the complex interactions among society, development, and the environment, aiming to explore ways and means of achieving sustainability in all human activities related to development. The journal welcomes scientific research papers, review papers, and discussion papers addressing environmental sustainability issues from various fields, including the biological sciences, agriculture, geology, meteorology, energy, food sciences, soil and water sciences, geography, nutrition, physical sciences, politics, economics, and law.

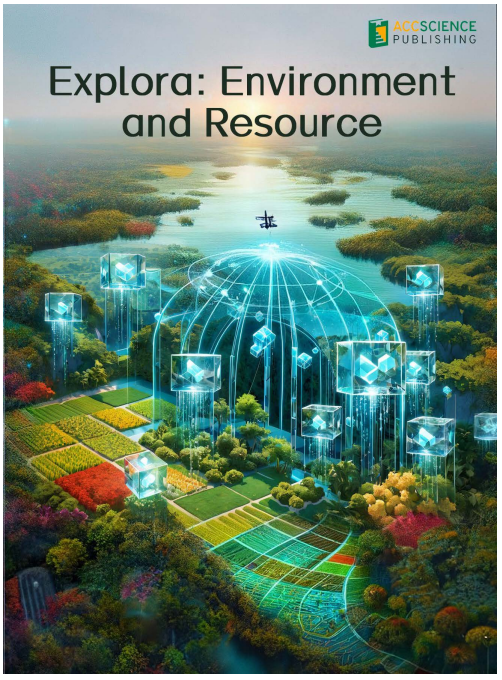

About the Publisher

AccScience Publishing is a publishing company based in Singapore. We publish a range of high-quality, open-access, peer-reviewed journals and books from a broad spectrum of disciplines.

Contact Us

Managing Editor
eer.office@accscience.sg

AccScience Publishing
2 Venture Drive, #07-06 Vision Exchange,Singapore 608526.

Volume 3 • Issue 1 • March 2026
ISSN 3060-9046 (online)

EXPLORA: ENVIRONMENT AND RESOURCE

ACCSCIENCE PUBLISHING

Access Science Without Barriers

EXPLORA: ENVIRONMENT AND RESOURCE

ISSN: 3060-9046 (online)

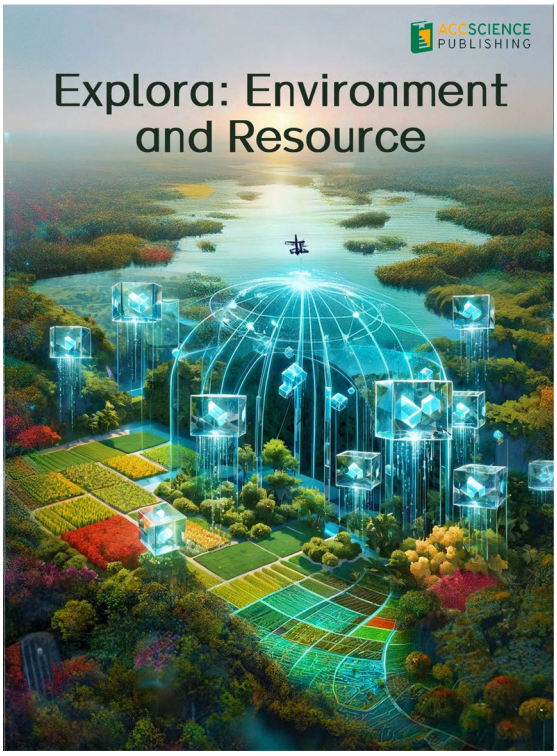

Editorial and Production Credits

Publisher: AccScience Publishing
Managing Editor: Dora Zhang
Production Editor: Sharmila Velapasamy
Article Layout and Typeset: Sinjore Technologies (India)

For all advertising queries, contact eer.office@accscience.sg.

Supplementary file

Supplementary files of articles can be obtained at https://accscience.com/journal/EER/3/1.

Explora: Environment and Resource

Editorial Board

*Editorial Board Members as of March 16, 2026

ACCSCIENCE PUBLISHING

Volume 3 | Issue 1 | March 2026 |

Explora: Environment and Resource

https://accscience.com/journal/EER

CONTENTS

ACCSCIENCE PUBLISHING

Explora: Environment and Resource

REVIEW ARTICLE

Navigating microplastic-related challenges in the Arabian Gulf: Prospects of artificial intelligence and bioremediation

Amani Almaabadi[1†], Mona Alshahrani[2†], Bandar Sendy[1], and Hany M. Almotairy[3†*]

[1]Institute of Wellness and Preventative Medicine, Health Sector, King Abdulaziz City for Science and Technology, Riyadh, Saudi Arabia

[2]Research and Development Center, Saudi Aramco, Dhahran, Saudi Arabia

[3]Executive Department of Monitoring and Risk Assessment, Food Sector, Saudi Food and Drug Authority, Riyadh, Saudi Arabia

Abstract

Microplastics (MPs) have emerged as contaminants of growing concern due to their widespread distribution, high mobility, and ability to act as vectors for pollutants in marine ecosystems. This review examines MP contamination in the Arabian Gulf, one of the world's most environmentally vulnerable semi-enclosed seas. The Gulf's extreme conditions, including high salinity, elevated temperatures, restricted water circulation, and intensive coastal development, promote MP accumulation and biological exposure, increasing potential risks to marine organisms, aquaculture, and human health. Conventional detection and quantification techniques, including Fourier-transform infrared (FTIR) and Raman spectroscopy, as well as pyrolysis–gas chromatography/mass spectrometry, are critically assessed with emphasis on limitations related to size detection thresholds, analytical throughput, and processing efficiency. The review highlights artificial intelligence (AI) as a transformative approach for MP analysis. Machine-learning algorithms applied to FTIR and Raman spectral data improve polymer classification accuracy, whereas computer-vision models such as U-Net and Mask R-convolutional neural network enable automated particle segmentation and sizing. These tools reduce manual bias, enhance reproducibility, and facilitate high-throughput analysis across laboratories. Meanwhile, eco-friendly bioremediation strategies are reviewed. Microorganisms, algae, and aquatic plants have demonstrated the ability to adsorb, colonize, or partially degrade MPs, offering sustainable alternatives to conventional remediation methods. However, the effectiveness of these biological approaches under the harsh environmental conditions of the Arabian Gulf remains limited. Finally, this review proposes a Gulf-specific roadmap that includes standardized monitoring protocols and shared spectral and image databases to support AI-based detection, interlaboratory proficiency testing, and pilot-scale bioremediation studies tailored to regional conditions.

Keywords: Microplastic; Arabian Gulf; Marine pollution; Artificial intelligence prediction; Artificial intelligence in pollution management; Machine learning; Bioremediation; Aquatic ecosystems

†These authors contributed equally to this work.

***Corresponding author:**
Hany M. Almotairy
(hmmotairy@sfda.gov.sa)

Citation: Almaabadi A, Alshahranl M, Sendy B, Almotairy HM. Navigating microplastic-related challenges in the Arabian Gulf: Prospects of artificial intelligence and bioremediation. *Explora Environ Resour*. 2026;3(1):025370068. doi: 10.36922/EER025370068

Received: September 11, 2025

1st revised: October 29, 2025

2nd revised: November 20, 2025

Accepted: December 16, 2025

Published online: January 28, 2026

1. Introduction

1.1. History

The history of plastics can be traced back over a century, with significant developments in our understanding of their environmental impact. In 1972, Carpenter and Smith[1] published a study that marked an early examination of marine plastic pollution. In the early 1980s, small-scale research and case studies began highlighting the detrimental effects of plastic in the ocean. By 1988, governmental policies were implemented to prevent ships from discharging plastic waste into marine habitats, driven by concerns over the impact of plastic on marine life.[2]

Further insights into the role of plastic deformation in the cracking process of metallic materials were discussed by Wang *et al.*[3] in 1998. However, it was not until 2004 that serious discussions and analyses specific to microplastics (MPs) emerged, primarily led by Thompson *et al.*[2,4] Their study introduced the term "microplastics" to describe these minuscule plastic particles, sparking a significant increase in research interest.[5]

The growing awareness of the MP issue led to a research revolution after 2004. In a milestone event, the National Oceanic and Atmospheric Administration organized the First International Research Symposium on the Occurrence, Effects, and Fate of Microplastic Marine Debris, during which MPs were well-defined as plastic particles <5 mm in diameter.[6]

To date, numerous studies have underscored MPs as a global threat to various living organisms, including potential effects on human respiratory health,[7] the well-being of aquatic life, such as fish,[8] and even microbial communities.[9] These findings emphasize the need for continuous research and proactive measures to address MP pollution.

Plastics, in general, are characterized as long chains of high molecular-weight organic polymers.[10] The significant components of plastics' organic composition are derived from fossil fuels, reflecting the recurring hydrocarbon-based chemical structures that constitute plastic polymers.[11]

The inception of plastics marked a significant advancement in materials science, with early household products made from materials such as bakelite, a phenol-formaldehyde thermoset, representing one of the earliest synthetic plastics produced in the 20th century.[12] Subsequently, after World War II, plastic production experienced exponential growth, with annual production reaching approximately 5 million tonnes in the 1950s.[13] This accelerated production trend continued, dramatically increasing, reaching 359 million tonnes by 2018. Global plastic production is projected to continue increasing, reaching 590 million tonnes by 2050 (Figure 1).[14,15]

Plastics possess various unique characteristics, making them highly desirable for consumers and industrial applications. These attributes include strength, cost-effectiveness, extended durability, lightweight properties, resistance to corrosion, and flexibility.[16] These inherent qualities have facilitated the incorporation of various plastic polymers, such as polyethylene (PE), nylon, polystyrene (PS), and polypropylene (PP), in diverse roles such as fillers, plasticizing agents, antimicrobial components, adhesives, and coloring agents. This versatility enhances plastic performance and accessibility for end-users.[17]

1.2. MPs classification: A closer look

MPs encompass a wide array of particle sizes, shapes, and polymer types.[18] These plastic fragments can be categorized by size into several groups: Macroplastics (over 25 mm), mesoplastics (5–25 mm), and MPs (<5 mm).[19] Interestingly, small-scale plastic particles were detected in aquatic habitats as early as the 1970s before they were formally recognized and labeled as MPs.[20] To date, any fragments smaller than 5 mm are referred to as MPs,[21] and it is well understood that plastic particles can continue to degrade into even smaller sizes, eventually producing nanoplastics.[22]

Other than size categorization, MPs are generally categorized into two main classes: primary and secondary MPs.[23] Primary MP particles are intentionally manufactured at the microscale. They can be found in products such as scrubs, handwashing soaps, cleansers, toothpaste, and biomedical products.[24] These particles, especially those with diameters between 1 μm and 5 μm, tend to be spherical and are typically composed of materials such as PP, PS, or PE.[25] Notably, some of these particles can bypass filtration systems during sewage treatment and enter freshwater environments, posing a threat to various living organisms.[26]

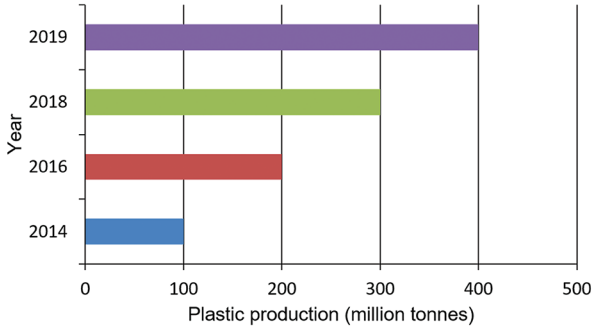

Figure 1. Global plastic production (million tonnes) has steadily increased from 2014 to 2019. Image created by the authors.

Meanwhile, secondary MPs are formed when larger plastic waste is fragmented.[27] Physical forces and ultraviolet (UV) radiation from the sun play a role in breaking down larger plastics into micro- and nanoparticles.[28] Exposure to waves, sunlight, and high temperatures can make plastics brittle, rendering them more susceptible to fragmentation.[29]

The main objective of this study is to shed light on the MP issue in the Arabian Gulf as an example and evaluate its negative impact on marine ecosystems and human health. We discuss promising methods for monitoring, detecting, and mitigating the risk of MPs, highlighting the central role of artificial intelligence (AI) in improving detection accuracy and the potential of bioremediation strategies as an eco-friendly tool to address this environmental threat, with particular applicability to the Arabian Gulf. In addition, we highlight how these innovations can be integrated into broader resource management and governance strategies, such as Circular Economy approaches, to help mitigate the region's growing plastic dependency. With rapid urbanization, high consumption patterns, and heavy reliance on single-use plastics shaping daily life, the challenge is both urgent and complex. By connecting technological tools, such as AI-powered monitoring, with policy measures that promote recycling, sustainable waste practices, and eco-friendly product design, this study suggests a practical and forward-looking pathway for building stronger, more resilient environmental governance across the Arabian Gulf. This compelling analysis underlines the pressing nature of the MP pollution crisis, proposing innovative solutions that can guide policymakers and shape future research endeavors in marine conservation.

The methodology for this review involved a systematic survey of literature on MP contamination in marine environments, emphasizing the Arabian Gulf. Articles from 2000 onwards were retrieved by searching scientific databases such as the Web of Science, Scopus, and PubMed. The focus was on peer-reviewed articles discussing MP types, sources, impacts, and remediation. Information on study location, MP concentration, and remediation effectiveness was extracted and compiled. The data were synthesized narratively to present an updated overview of MP pollution and potential solutions.

1.3. MPs in the Arabian Gulf

The MP issue has garnered increasing global attention. Recent evidence suggests that MPs are found in different habitats around the globe, such as the deep sea of the western Pacific Ocean,[30] the Indian Ocean,[31] and the Atlantic Ocean.[32] However, there has been relatively little focus on MPs in the Gulf Cooperation Council countries, particularly in the Arabian Gulf region of Saudi Arabia. The Arabian Gulf, a geologically young sea basin, boasts rich and diverse marine habitats, including mangrove forests, seagrass beds, and coral reefs.[33] This unique region is surrounded by eight countries: Saudi Arabia, Qatar, Oman, the United Arab Emirates (UAE), Kuwait, Bahrain, Iraq, and Iran.[34]

Several factors contribute to the Arabian Gulf's relevance as a setting for MP research. First, it receives minimal river inflow into the Gulf.[35] Second, rainfall is limited between October and January.[36] Third, the region experiences high salinity (44 practical salinity units) and extreme thermal variations, with surface seawater temperatures ranging from 20°C in spring to 38°C in summer.[37] Given the impact of global warming on seawater temperature, the Gulf's environment has become a focal point for researchers studying climate change.

Despite these favorable conditions, limited studies have assessed the presence of MPs in the Arabian Gulf, particularly from the perspective of Saudi Arabia (Table 1).[38-44] One such study analyzed 18 MP particles—13 isolated from sediments and 5 from seawater [38]. Their findings revealed the ubiquitous presence of MPs in beach sediments and surface seawaters along the coast of Qatar. PP and PE polymers dominated the MPs in intertidal sediments and seawater samples. Furthermore, fibers, measuring 1–5 mm in size, represented the dominant type of particle in all samples, comprising 93.8% of the total isolates.

Naji *et al.*[39] examined the presence of MPs in several types of shellfish found in the coastal waters of the Arabian Gulf. Their study confirmed the presence of MPs through Fourier-transform infrared (FTIR) analysis with common polymers, including PE, polyethylene terephthalate (PET), and nylon. Notably, their study highlighted fibers and microfibers as the most prevalent shapes of MPs in the marine environment and shellfish.

A study investigated the bioaccumulation,

Table 1. Timeline of the significant stages in microplastic research in the Arabian Gulf

Time	Location	Sample source	Reference
2017	Qatar	Sediments/seawater	37
2018	Arabian Gulf	Shellfish	38
2019	Arabian Gulf	Fish, crab, prawn	39
2020	Kuwait	Fish, sediments	40
2021	Arabian Gulf	Sediment and bivalve	41
2022	United Arab Emirates	Sediment and oysters	42
2023	East of the Arabian Gulf	Sediments	43

biomagnification, and potential human exposure to MPs in the muscles and gills of five commonly consumed species (including three fish, one crab, and one prawn) from the Arabian Gulf.[40] Among the species examined, *Penaeus semisulcatus* and *Epinephelus coioides* had the highest (average of 0.360 items/g muscle) and lowest (average of 0.158 items/g muscle) levels of MPs in their muscles, respectively. Interestingly, the number of MPs extracted from the gills exceeded that from the muscle tissue. Calculations of the trophic magnification factor and biomagnification factor indicated that MPs did not biomagnify within the edible portions of the marine food web in the Arabian Gulf. Contrary to prior beliefs, MPs experienced dilution rather than concentration in seafood's edible parts. Assessing the human intake of MPs highlighted potential risks associated with seafood consumption, particularly for individuals with a seafood-heavy diet.

Saeed *et al.*[41] studied MP influences in Kuwait's coastal areas using several sampling techniques to collect data. For example, sediment samples were taken from 44 intertidal locations, short trawls were conducted at 40 sites to gather samples from the water, and the gastrointestinal contents of 87 fish and mussels were examined to assess the ingestion of materials. MPs were identified using Raman spectroscopy, and contrary to expectations, the results revealed a relatively low presence of MP particles. Only 37 MPs were found in beach sediments at 15 locations, and seawater trawls detected MPs in just 2 samples from Kuwait Bay and 2 from the southern areas. In biota, only three pieces of plastic were recovered from the gastrointestinal tracts of Hamour fish. Moreover, they found that the most common MPs were PP, PE, and PS. While MP levels in Kuwait were lower than in neighboring areas, they were comparable to those in Qatar and Oman.

Jahromi *et al.*[42] investigated heavy metals and MPs in coastal sediments and edible bivalves along the Arabian Gulf in the Hormozgan province. Sampling sites were strategically selected to represent industrial, urban, and protected forest areas. The results indicated heavy metal concentrations in sediments were generally below typical geological baseline values, except for nickel (Ni) and cadmium (Cd). Furthermore, areas with significant human activity, such as ports, exhibited elevated concentrations of several heavy metals. The study identified a moderate environmental risk associated with arsenic (As), cobalt, zinc, and copper (Cu). However, it concluded that health risks from heavy metals in bivalve consumption were generally low, except for As, which posed a potential carcinogenic risk. Regarding MPs, the predominant type identified was fibrous, with lengths ranging from 100 to 250 μm, primarily composed of PET and PP.

Al Hammadi *et al.*[43] examined MP pollution in the UAE oyster bed ecosystems. They assessed MP levels in sediment and oysters from five coastal sites, considering abundance, shape, size, color, and composition. MPs averaged 191.7 ± 95.5 MPs/kg of dry weight in sediment samples, whereas in oysters, it was 101.2 ± 93.8 MPs/kg. MPs were found in all sediment samples and 51% oysters, with no clear correlation between sediment and oyster MP levels. Fibers were the primary MP shape (93%), and black was the most common color (53%). This study, the region's first investigation into oyster bed MPs, highlights the widespread presence of MPs in sediment, necessitating further research into sources and management to protect the marine ecosystem.

In a more recent study, Ali *et al.*[44] aimed to be the first to assess MP pollution in Saudi Arabia's east coast sediment, specifically at beaches in four cities: Khafji, Jubail, Dammam, and Salwa. Samples were collected from high and low tide zones. A total of 586 MP particles were found, with an average size of 1.55 ± 0.94 mm. Most particles (77%) were with a size smaller than 2 mm. The MP levels exhibited a range of values, with the low tide region ranging from 5.5 ± 1.55 to 21.2 ± 0.68 particles/kg and the high tide region ranging from 6.3 ± 4.05 to 16.5 ± 4.98 particles/kg. Transparent (34%) and blue (30%) were the predominant colors, whereas fibers (96%) were the most common shape. PET was the common polymer type in fibers, whereas PE and high-density PE were prevalent in fragments and filaments.

Nevertheless, comprehensive datasets on MP abundance, polymer typology, and degradation behavior within the Arabian Gulf are notably limited, highlighting an urgent need for systematic, region-specific investigations that account for its distinct hydrographic and climatic characteristics.

2. Impacts of MP pollution on the marine ecosystem

Saudi Arabia's aquaculture sector has shown remarkable growth, with total production reaching approximately 140,000 tonnes in 2023, reflecting a 56.4% increase compared to previous years.[45] Shrimp (66,000 tonnes) and Nile tilapia (45,000 tonnes) dominate aquaculture output, driven by intensive marine and freshwater farming practices. However, the sector may face significant challenges due to MP contamination in the Arabian Gulf, a major production area. MPs threaten the health and reproduction of key species and compromise water quality, impacting aquaculture sustainability and regional food security. These risks emphasize the urgent need for monitoring and mitigation strategies tailored to the Gulf's unique environmental conditions.

2.1. Impact on aquatic life

Marine organisms consuming MPs can experience severe physical harm, including digestive blockages, reduced feeding efficiency, and internal injuries. These impacts have been documented across various species, from plankton to top predators. For example, an increasing trend of MP ingestion, including PE and PP, has been observed globally in commercially important fish species (*Acanthopagrus latus* and *E. coioides*) from the Arabian Gulf.[46,47] MPs tend to accumulate in the digestive tracts of plankton and small fish, impairing nutrient absorption and disrupting metabolic processes, adversely impacting growth and reproduction.[48]

In the Arabian Gulf, economically valuable species face heightened risks due to high levels of plastic pollution predominantly originating from fishing gear, domestic wastewater, and industrial activities.[47,49] These MPs disrupt physiological functions and introduce contaminants such as heavy metals and persistent organic pollutants, exacerbating their impacts. Recent studies have highlighted that MPs in the region are dominated by fibers and fragments, commonly ingested by fish, mistaking them for prey.[46,49] The ingestion of MPs by these species poses significant threats to fisheries production and food security.

Furthermore, the trophic transfer of MPs within marine ecosystems can result in the bioaccumulation of contaminants, leading to cascading ecological effects.[48,49] This emphasizes the need for rigorous research to quantify MP ingestion rates and assess long-term ecological consequences in the Arabian Gulf. Strategic policy measures targeting plastic waste reduction and improving wastewater treatment systems are essential to mitigate these risks.[47,48]

MPs are ubiquitous in marine environments and linked to biochemical disturbances in aquatic organisms. They interact with cellular processes, disrupting metabolic pathways and overall organismal health. Understanding these biochemical interactions is essential for assessing the broader ecological implications of MPs in marine ecosystems.

Recent studies have demonstrated the extent and complexity of these disruptions. For example, adult zebrafish exposed to high-density PE and PS MPs exhibited altered gene expression, notably impacting immune system functions and epithelial integrity.[50] Histological assessments further revealed increased neutrophils in the gills and intestinal epithelium, suggesting vulnerabilities in defense mechanisms and altered energy utilization due to MPs exposure.

MPs exacerbate biochemical risks in the Arabian Gulf by acting as vectors for hazardous substances, including heavy metals and endocrine disruptors.[48] These contaminants amplify physiological stress, resulting in oxidative damage, diminished immune responses, and cellular dysfunction. Such impacts may jeopardize marine food web stability and ecosystem health in this unique and vulnerable region.[49,51]

Moreover, oxidative stress caused by MPs is a primary biochemical concern. MPs promote the generation of reactive oxygen species, leading to lipid peroxidation, protein denaturation, and DNA damage.[52] These processes impair organism health and disrupt trophic interactions, amplifying ecological consequences across marine systems.[53]

The dual role of MPs as physical and biochemical disruptors underscores the urgency of further research, particularly in regions such as the Arabian Gulf, where unique environmental conditions may exacerbate these impacts. Identifying Gulf-specific biomarkers for oxidative stress and immune dysfunction could aid in effectively monitoring and mitigating these risks.

MPs are ubiquitous across marine ecosystems and pose substantial risks to the reproduction and growth of marine organisms. When ingested, MPs can release harmful agents that disrupt endocrine systems and inhibit reproductive success in marine species.[54,55] These disturbances have cascading effects on population dynamics and marine ecosystem stability. Studies have highlighted the reproductive challenges faced by key species. For example, MPs have been shown to impair oyster reproduction by interfering with gamete development and larval growth.[54] Similarly, zooplankton exposed to MPs experience feeding disturbances that reduce reproductive output, threatening their critical role in the marine food web.[56]

In the Arabian Gulf, unique environmental conditions such as high salinity and elevated temperatures may exacerbate the reproductive impacts of MPs on local species. A study has reported significant MP ingestion among commercially valuable species, including shrimp and groupers, potentially leading to reproductive challenges such as reduced fecundity and growth disturbances.[57] Although specific data quantifying these effects are sparse, the ecological implications of chronic MP exposure underline the urgent need for targeted research in the region.[57,58]

Marine turtles are particularly vulnerable to MP ingestion, which has been documented to cause gastrointestinal blockages, reduced stomach capacity, and mortality. Such outcomes indirectly affect turtle

populations by limiting reproductive potential and disrupting nesting success.[59] These findings highlight the urgent need for targeted research in the Arabian Gulf to evaluate the long-term reproductive consequences of MPs on ecologically and economically significant species.

Exposure to and ingestion of MPs by marine organisms have prompted various behavioral shifts. For example, post-MP consumption, zooplankton have been observed to alter their swimming behaviors, increasing their susceptibility to predators.[60] Similarly, when exposed to MPs, mussels exhibit diminished mobility and compromised defensive reactions.[61] Research on gastropods links MP interactions with various adverse effects, from developmental issues to behavioral shifts.[62]

The proliferation of MPs, especially in delicate areas such as coral reefs and benthic habitats, is also a growing concern. Reports indicate that MPs injure corals, hampering their growth, smothering entire communities, and transmitting toxic substances.[63,64] Furthermore, MPs serve as vectors for detrimental pathogens, potentially altering benthic community structures and threatening their diversity.[65] These extensive damages (Figure 2) highlight the urgency of addressing this rising menace to uphold marine ecosystem health.[66]

2.2. Responses and adaptive mechanisms

Marine organisms exhibit a range of responses to MP exposure. Recognizing these intrinsic tactics can offer valuable insights for devising holistic solutions.

Mollusks, such as oysters, have been observed to incorporate MPs into their shells as a potential defense mechanism.[67] According to a study by Onyena *et al.*,[68] essential marine organisms such as phytoplankton and zooplankton alter their feeding habits to avoid MP-rich areas. Several other studies have investigated the impact of MPs on the feeding of phytoplankton and zooplankton.[69-74] The effects depend on various factors, including size, shape, concentration, organism species, and polymer type. Table 2 concludes the most significant findings. These studies indicated that at elevated concentrations of spherical MPs, algal consumption of certain organisms, such as cladocerans, diminished. In contrast, realistic microfiber concentrations (5.7–9.0 fibers/mL) do not inhibit diatom clearance in calanoid copepods or doliolids, regardless of observable ingestion and egestion through fecal pellets. Most promisingly, recent research hints at the capability of certain marine species to biodegrade MPs courtesy of unique enzymes or metabolic processes.[75]

These findings could pave the way for biotechnology-based solutions to combat MP pollution. One such initiative includes incorporating Ballast Water Treatment Systems (BWTSs) filtration chambers in vessels, as previously suggested.[76] This would prevent MPs from being further spread during ballasting procedures. However, the utilization of BWTS has several drawbacks, including unsustainability from both economic and environmental perspectives. For example, factors such as the use of UV, particularly in high turbidity conditions, and maintenance

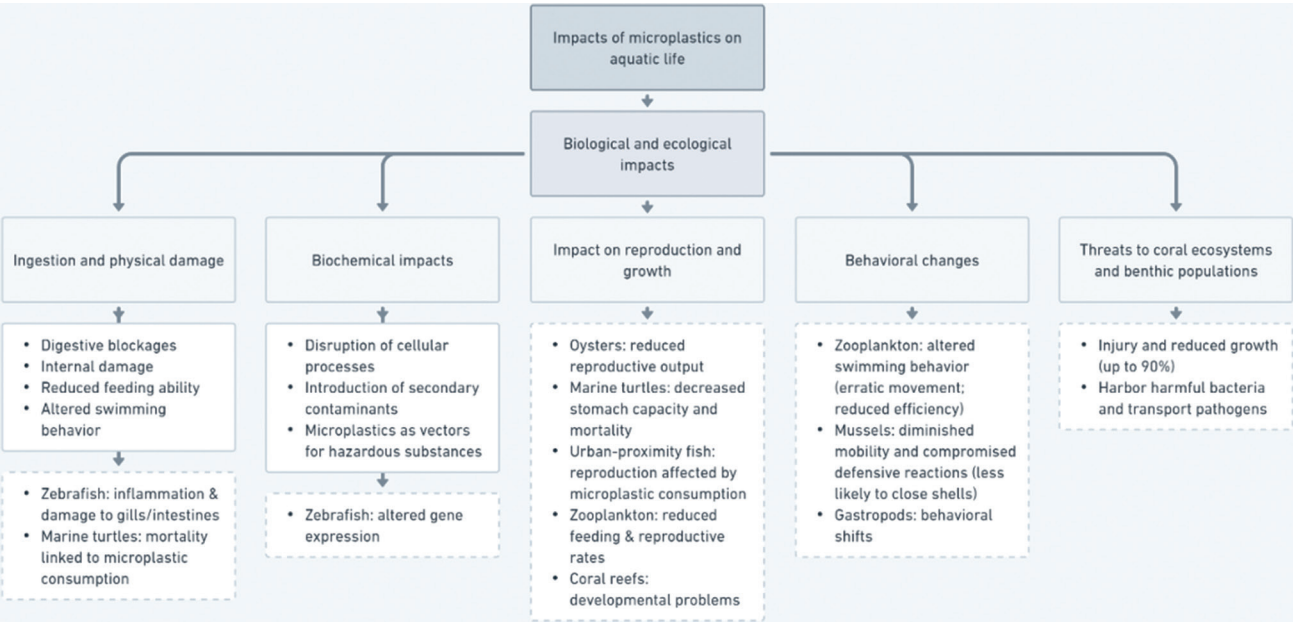

Figure 2. Comprehensive overview of microplastic (MP) impacts on aquatic life. The flowchart summarizes various MPs' effects on marine organisms (solid square), detailing specific consequences and citing relevant research examples (dashed square). Flowchart created by the authors.

Table 2. Experimental studies quantifying MP effects on zooplankton feeding behavior

Study	Species/ System (most impacted)	MP type consumed/ tested	Particle size (μm)	Concentration	Exposure duration	Feeding effect	Quantitative change
Cole *et al.*[69]	*Centropages typicus* (copepod)	Fluorescent PS beads	7.3	0, 4,000, 7,000, 11,000, 25,000 particles/mL	24 h	Significantly decreased algal ingestion rate in a dose–response relationship when concentrations of MPs increased (>4,000 particles/mL)	Not specified
Scherer *et al.*[70]	*D. magna*	Fluorescent PS spheres	1, 10, 90	3, 30, 300, 3,000 particles/mL; for 90 μm, the highest tested concentration was 300 particles/mL	2 min for *D. magna* (as short-term experiments with a concentration of 100 particles/mL)	Concentration- and size-dependent ingestion; *D. magna* excludes 90 μm; co-exposure to natural particles (e.g., algae, sand, and leaf) reduces ingestion and enhances egestion	Up to 6,180 particles/h ingested
Malinowski *et al.*[71]	*Daphnia dentifera*	Fluorescent PE microspheres	27–32	Various concentrations: • Low: 2.38×10^{-8} mg/L • Medium: 0.023 mg/L • High: 162 mg/L	24 h	Significantly reduced algal consumption (gut algae) at high concentrations (grazing capacity declined)	Lower gut algae content at high MP exposure; effect consistent with reduced ingestion. (% coverage, assessed by fluorescence)
	Arctodiaptomus dorsalis					No significant difference (decrease at medium (p=0.011) and high (p=0.003) concentrations compared to Control 1)	Not specified, but a notable decrease compared to the control
Yin *et al.*[72]	*D. magna* and *S. kingi*	PE	32–38	0, 0.4, 2, and 10 mg/L	21 days	Reduced grazing capacity and reproductive impairment due to increasing levels of the ingested MP, while no significant effects on feeding behavior were observed in *S. kingi*	*D. magna*: significantly reduced reproductive capacity, including a decline in the number of neonates and their body size. (quantitative values not detailed). The parameters in all treatments rapidly declined on day 13
Montoya *et al.*[73]	Marine microbial and phytoplankton communities (pelagic mesocosms)	Mixture of PS (1.04–1.09 g/cm^3), PE (0.89–0.95 g/cm^3), PP (0.85–0.92 g/cm^3), PVC (1.16–1.41 g/cm^3), and PET (1.34–1.41 g/cm^3)	20–1,000	100 pieces/L (20 per polymer)	NA (not a zooplankton feeding test)	MPs indirectly increased phytoplankton biomass and benefited photosynthetic efficiency via shifts in bacterial and phytoplankton assemblages and NH_4^+cycling (ecosystem functional response, but not a zooplankton grazing assay)	Enhanced chlorophyll a biomass (R^2=0.33, P<0.01), NH_4^+ (R^2=0.27, P<0.01), and photosynthetic efficiency (R^2=0.31, p<0.05)
Köster and Paffenhöfer[74]	*E. pileatus* (calanoid copepod) and *D. gegenbauri* (doliolid)	Nylon microfibers	Width=10 μm; length = ~300 μm (mean 336 μm, with rare up to 1.45 mm)	5.7–9.0 fibers/mL (similar to diatom *R. alata*)	• *E. pileatus*: 18 h (initial), then 6.0–6.1 h • *D. gegenbauri*: 6.0–6.1 h • Both at 20°C on a plankton wheel in 960 mL bottles (5 individuals/bottle)	• At~7 fibers/mL, no significant effect on diatom clearance • Fiber clearance *by D. gegenbauri* was greater than that of *E. pileatus,* while the ingestion of their food (*R. alata,* diatom) was 10 times more than the ingestion of fibers	Clearance rate of *E. pileatus* for *R. alata* (21.4 mL/individual/h), compared to (13.1 mL/individual/h) for fibers; in contrast, *D. gegenbauri* had a higher clearance rate for fibers (27.2 mL/individual/h) than that for *R. alata* (18.7 mL/individual/h). In addition, the number of fibers per pellet was 3.5 for copepods and 3–16 for doliolids

Abbreviations: *D. gegenbauri*: *Dolioletta gegenbauri*; *D. magna*: *Daphnia magna*; *E. pileatus*: *Eucalanus pileatus*; MP: Microplastic; PE: Polyethylene; PET: Polyethylene terephthalate; PP: Polypropylene; PS: Polystyrene; PVC: Polyvinyl chloride; *R. alata*: *Rhizosolenia alata*, *S. kingi*: *Scapholeberis kingi*.

costs are considered significant factors in energy consumption.[77,78] Moreover, carbon dioxide emissions that can be generated from BWTSs[79] and persistent toxic chemicals, such as the formation of disinfection by-products, are further environmental challenges.[80] These observations emphasize the dual nature of the solutions needed to alleviate the consequences of MP pollution in our oceans, encompassing natural adaptations and human-driven interventions.

2.3. Environmental impacts of MP contamination

2.3.1. Influence on water quality

Marine water quality is fundamental for maintaining marine biodiversity and habitat well-being. MPs have been shown to harm various elements of water purity, leading to increased water cloudiness and hindering light penetration crucial for aquatic plant life, such as influencing the process of microalgal photosynthesis. Moreover, MPs play a role in introducing pollutants into marine waters.[81-83] Intriguingly, previous studies by Liu *et al*. and Pestana *et al*.[84,85] have linked MPs to the proliferation of harmful algal blooms. In a broader context, a study by Hale *et al*.[52] highlighted the compounded threats of MPs to marine life and its food chains, from zooplankton to finfish.

2.3.2. Sediment quality deterioration

The omnipresence of MPs in marine sediments raises alarms due to sediments' importance in marine ecosystems. Previous studies by Kane and Clare, Barrett *et al*.[86,87] have detailed the widespread occurrence and retention of MPs in marine sediments. Delving into the repercussions for bottom-dwelling organisms, MPs' negative impacts were discussed.[56,88] Another study, Waldschläger *et al*.[89] further pointed out potential geophysical changes induced by MPs.

2.3.3. Disruption of nutrient cycles

For marine ecosystems, nutrient cycling is vital. It has been discussed how MPs can adversely affect nutrient dynamics by disrupting the nutrient cycles within the plant–soil system.[90,91] For example, MPs have been found to have a direct and/or indirect impact on the essential nutrients, such as magnesium and potassium, necessary for chlorophyll synthesis in plants.[90] MPs disrupt the plant–soil nutrient dynamics by altering soil nutrient availability, enzyme activities, and functional microbial communities, compromising the natural nutrient cycles essential for sustainable agriculture and land use.[91] Moreover, another study by Gerstenbacher *et al*.[92] has provided insights into the effects of MPs on seagrass and aquatic nutrient balances. MPs impede light and gas exchange, increasing toxin concentrations and disrupting metabolic processes. It has been reported that specific MPs, such as polyurethane foam and polylactic acid, can enhance nitrification and denitrification processes. Moreover, polyvinyl chloride (PVC) inhibited both these processes, highlighting the differential impacts of MPs on sedimentary nitrogen cycling.[93]

2.3.4. Persistence and potential irreversibility

The long-lasting nature of MPs poses persistent challenges. The studies by Amelia *et al*.[55] and Ma *et al*.[94] emphasized the enduring threats of MPs, especially their toxicological effects. Global perspectives by Ziani *et al*.[51] and Yang *et al*.[95] highlighted the near-impossible removal of MPs. Pourebrahimi and Pirooz[96] foresaw long-term ecological shifts due to MP pollution. MPs, resulting from the degradation of larger plastic materials, have become pervasive pollutants in marine environments, where their ability to adsorb and transfer other harmful pollutants poses significant challenges to their effective removal and management.

2.3.5. Bioaccumulation and transfer of MPs in the food chain

The prevalent presence of MPs in marine ecosystems has severe implications for bioaccumulation and their movement through food webs. Organisms such as plankton, foundational to marine food webs, are particularly vulnerable.[54,59] Li *et al*.[88] have detailed the dangers of MP transfers to higher trophic organisms. At the end of many marine food chains, humans also face risks from MP consumption via seafood.[66]

2.4. Pollutants associated with MPs and their impact

In addition to their intrinsic dangers, MPs are a significant problem due to their propensity to serve as carriers for various environmental contaminants. MPs are inclined to bind with diverse toxins within aquatic systems, from heavy metals and persistent organic pollutants to harmful microbes. Such relationships amplify the ecosystem risks of MPs, enabling the transfer of these toxins into marine life and, subsequently, apex predators, including humans. Addressing these dual threats requires an in-depth understanding of the relationship between MPs and the myriad pollutants they may carry. This section elucidates this intricate relationship, considering the modes of attachment, ecological implications, and potential health consequences.[55,95,97]

2.4.1. Introduction to the concept of MPs as pollutant vectors

MPs, abundant within marine ecosystems, mainly result from the breakdown of larger plastic items. Their persistent nature and expansive surface area bolster their potential

to adsorb toxins.[59,95,98] Agboola and Benson[99] detailed the critical interactions between MPs and organic pollutants, emphasizing the significance of physisorption and chemisorption. Tragically, these pollutants might alter their bioactivity when attached to MPs, introducing enhanced risks for marine organisms.[100] As MPs navigate marine environments, they scatter these pollutants, potentially extending the reach of these toxins.[54] Recognizing MPs as carriers of these pollutants is pivotal for comprehensive risk assessment and informed remediation tactics.

2.4.2. Types of pollutants associated with MPs

The relationship between MPs and pollutants has gained significant attention due to its amplifying effect on ecological consequences. MPs, especially PVC and PP, can adsorb heavy metals such as lead, Cu, and Cd, emphasizing the potential environmental risks. Moreover, persistent organic pollutants present long-lasting challenges for marine environments, with MPs depicted as carriers of these pollutants.[17,98,101]

2.4.3. Mechanisms of association

The relationship between pollutants and MPs entails complex physicochemical interactions, predominantly governed by adsorption and desorption processes. Agboola and Benson[99] distinguished physisorption and chemisorption as the main drivers behind these interactions. Factors such as MP properties, pollutant type, and surrounding environmental conditions, including pH and salinity, influence these interactions, for example, influencing As adsorption on MPs.[75] The large surface of MPs provides numerous binding sites, further enhancing their pollutant-carrying capacity.[98]

2.4.4. Bioavailability and trophic transfer

Analyzing the relationship between pollutants and MPs is critical to understanding their marine ecosystem implications. Once attached to MPs, pollutants can infiltrate aquatic food chains, leading to bioaccumulation and ecotoxicological impacts on marine organisms. This underscores their potential adverse effects on human health through dietary exposure, with varied toxin accumulations due to differential ingestion rates among marine species.[54,88,102] The tendency of hydrophobic toxins to prefer specific MPs and become bioavailable post-ingestion poses substantial threats.[98] Recognizing the risks, research by Agboola and Benson[99] suggested enhanced bioavailability of MP-bound pollutants than those freely present. Costa *et al.*[103] documented evidence of these pollutants even in brief food chains, highlighting the bioaccumulation risks in top predators.

2.4.5. Ecological and health risks

The intertwining of MPs and pollutants poses multifaceted ecological and health challenges. Adverse effects on marine organisms due to toxins such as organic pollutants and heavy metals are evident,[17,64] ranging from oxidative stress to developmental irregularities. The risk of toxin magnification across food chains is particularly emphasized by Bhuyan.[102] From a human health perspective, toxin exposure through seafood ingestion is concerning. Research has demonstrated potential health impacts of MPs, from hormonal imbalances to DNA damage.[65,102]

2.5. Human health implications of MP contamination

The pervasive presence of MPs in marine ecosystems has invoked heightened scrutiny due to the potential health risks for humans. These minute fragments originate from the disintegration of larger plastic pieces. They are integrated into numerous trophic levels, presenting potential channels for human contact primarily through seafood consumption and inhalation of airborne MPs.

Current studies have continually illustrated the health risks associated with such exposures. Evidence suggests that MP consumption might lead to cellular anomalies, including endocrine system disruptions.[104] Moreover, MPs serve as carriers for various pollutants, further exacerbating health dangers and even posing risks of disease transmission.[55]

2.5.1. Introduction to the human health context

Since MPs are ubiquitous in the marine environment, assessing their potential entry into the human diet is crucial. As has been outlined in an earlier study,[17] MPs can invade various marine segments, resulting in their accumulation in organisms that humans consume. Furthermore, a study by Chen *et al.*[105] revealed that besides seafood, humans could also encounter MPs by inhaling airborne particles or through water consumption, highlighting the importance of expansive research.

2.5.2. Routes of exposure

Humans primarily encounter MPs via three routes: consumption, inhalation, and, to a lesser degree, direct skin contact. Seafood, especially from significant fishing regions such as China, bottled water, and atmospheric MPs originating from urban areas are potential sources of exposure.[17,102,104] Kiran *et al.*[17] pointed out the inhalation risk of atmospheric MPs from urban areas. Skin absorption from MPs in cosmetics and personal care products is another channel that warrants further exploration.[95] Meanwhile, nanoplastics may enter through physical piercing and endocytosis/phagocytosis.[17]

2.5.3. Bioaccumulation and toxicology

Bioaccumulation refers to a living organism's gradual concentration of substances, such as MPs and associated pollutants. MPs can accumulate in human tissues and act as transporters of organic chemicals, indicating potential health risks when these chemicals are ingested[99,104]. The toxins binding to MPs might enhance their availability in the body, leading to heightened adverse health reactions, including endocrine system disturbances.[106]

2.5.4. Endocrine disruption and other biological effects

The binding propensity of MPs to various contaminants has raised concerns about their physiological impact on humans. MPs can transport chemicals that disrupt the endocrine system, leading to potential hormonal imbalances. Certain plastic additives can also induce cellular stress and inflammation, potentially compromising cellular well-being.[107,108]

2.5.5. Public health perspective

MPs' widespread environmental presence highlights potential community health dangers, including their ability to transport marine pollutants and the associated risk of disease transmission, primarily through seafood consumption. Therefore, ensuring water quality, especially in urban aquatic systems, is paramount.[55,100]

The pervasive impacts of MPs extend beyond biological disruptions in marine organisms to broader environmental, ecological, and human health challenges. MPs alter nutrient cycling, destabilize food webs, and accumulate as pollutants in aquatic habitats, amplifying risks to biodiversity and ecosystem functioning, particularly in vulnerable regions such as the Arabian Gulf. Furthermore, their role as vectors for harmful substances, such as heavy metals and endocrine disruptors, adds another layer of ecological and public health complexity. Addressing these interconnected challenges requires a detailed understanding of MPs' environmental pathways and impacts, which are explored in the following sections.

These widespread impacts of MPs on marine ecosystems underscore the urgent need for innovative solutions, such as AI-driven detection and bioremediation strategies, to mitigate their effects, particularly in vulnerable regions such as the Arabian Gulf.

3. Traditional techniques for MP detection and identification

Before utilizing methods for counting and distinguishing MPs, a range of preparatory steps is typically undertaken. The preparation of MP samples is influenced by their environmental origin, such as marine, terrestrial, and atmospheric contexts[109]. Standard procedures, including sampling, density separation, filtration, sieving, digestion, and visual categorization, are applied across different sample types to isolate MPs from other particulate matter in the Arabian Gulf.[44,110]

Additional procedures are incorporated based on the distinct characteristics of the sample under investigation. For example, atmospheric MPs can be collected passively from environmental degradation or via an air pump directing the air toward a sensor. The critical step post-collection involves separating MPs from organic materials to reduce analysis disruptions.

In marine contexts, MPs are usually collected through pumping systems or with a Manta trawl, a specialized net for aquatic sampling. MPs within the 1–5 mm range are typically examined through direct observation or microscopic techniques, contingent on operator expertise.[111] Due to these requirements, automating the identification and quantification of MPs to facilitate environmental risk evaluations presents challenges. Therefore, enhancing MP detection focuses on shortening analysis time, maintaining the integrity of MP samples, implementing on-site real-time assessments, and advancing automated identification technologies.[112]

Optical imaging methods are prevalent to detect MPs, as they influence light in various ways, including reflection, absorption, transmission, diffraction, scattering, and creating interference, which are determined by their optical attributes. The following subsections discuss the main optical imaging techniques.

3.1. Microscopy methods

Microscopic imaging provides essential details on MPs' morphological structure and surface texture. The selection of microscopy techniques is contingent on MP size: Optical microscopy for MPs under 1 mm, stereomicroscopy for MPs between 0.1 and 1 mm, and scanning electron microscopy for MPs smaller than 0.1 mm, despite its low throughput. Polarized light optical microscopy is utilized to identify MPs in wastewater by leveraging the anisotropic optical properties of specific polymers such as PE, PP, and PET.[113]

3.2. Spectroscopic analysis

Spectroscopic analysis is critical for the nondestructive, precise, and accurate chemical characterization of MPs, distinguishing them based on spectral signatures. FTIR and Raman spectroscopy can reveal MP chemical makeup and structure. However, Raman spectroscopy

distinguishes itself by providing higher spatial resolution. The micro-FTIR and micro-Raman spectroscopies enable the identification of smaller MPs with specific detection capabilities for various polymers. Challenges include specific sample preparation to avoid fluorescence in Raman spectroscopy and the requirement for dehydrated and regularly shaped samples for practical FTIR analysis.[114]

3.3. Thermal analysis

Techniques such as differential scanning calorimetry and thermogravimetric analysis (TGA) assess physical and chemical properties based on thermal stability. These are considered destructive and require skilled operation. They are helpful for bulk samples and often complement spectroscopic methods. TGA, combined with other analytical methods such as FTIR, enhances the specificity of MP material identification.[115] Table 3 summarizes commonly used analytical techniques for MP identification and characterization, highlighting their size detection limits, cost, and analysis speed.[116-121]

In summary, the identification and analysis of MPs involve a combination of microscopy for morphological assessment and spectroscopy for chemical characterization, each with specific applications and limitations. Thermal analysis provides additional physical and chemical data, while alternative methods such as fluorescence staining offer the potential for simpler identification, albeit with their challenges. The following section focuses on AI and bioremediation technologies as promising and highly applicable approaches for researchers studying the Arabian Gulf.

4. Artificial intelligence and bio-remediation technologies

4.1. Introduction to artificial intelligence

At its core, AI is the domain of computer science that endeavors to emulate human intelligence processes through the design and development of algorithms. These algorithms let machines carry out activities that traditionally necessitate human intellect, such as visual perception, speech recognition, decision-making, and language translation. The following four distinct phases have marked the evolution of AI. It started with the early foundations phase, in which the seeds of AI were sown in the 1940s and 1950s. Alan Turing, a pioneering computer scientist, introduced the Turing test as a criterion of intelligence, suggesting that a machine could be considered "intelligent" if it could imitate a human to the point of being indistinguishable from one. This was followed by the knowledge-based systems phase in the 1970s, which witnessed the rise of expert systems, attempting to mimic the decision-making of human experts by encoding knowledge in rule-based systems.[122] The machine learning phase gained momentum in the late 1980s and 1990s, and the focus shifted to developing algorithms that could learn from data. The machine learning subfield enabled computers to improve task performance through experience.[123] The deep learning phase and the recent renaissance in AI, particularly in the 2010s, have been powered by advances in neural networks and deep learning. Inspired by the human brain's architecture, these systems have significant advancements in image and speech recognition, as demonstrated by the notable success gained by Goodfellow *et al.*[124] in 2016.

4.2. Challenges of artificial intelligence in marine MP applications

Despite rapid progress, applying AI to marine MPs faces two immediate hurdles. First, data standardization, where models trained on FTIR/Raman spectroscopy and microscopy data require large, well-labeled, standardized datasets with consistent metadata (polymer, size class, morphology, weathering state, additives, and imaging/spectral settings). Lack of shared schemas and benchmark splits leads to overfitting and irreproducible

Table 3. Comparative summary of microplastic analytical techniques

Technique	Size detection limit (μm)	Cost	Analysis speed	Reference
Optical microscopy	≥1,000	Low	Fast	116
Stereomicroscopy	100–1,000	Moderate	Moderate	117
Scanning electron microscopy	<100	High	Slow	118
Polarized light optical microscopy	50–1,000	Moderate	Moderate	119
Fourier-transform infrared spectroscopy	10–20	High	Moderate	116
Raman spectroscopy	~1	High	Slow	120
Differential scanning calorimetry	Bulk sample	Moderate	Moderate	121
Thermogravimetric analysis	Bulk sample	Moderate	Moderate	121

results. We recommend Gulf-wide templates for sample preparation, spectral/image formats, and labels, as well as interlaboratory ring trials and model cards with uncertainty calibration. Second, generalization, where domain shift—caused by the Arabian Gulf's high salinity, temperature, biofouling, oxidation, and distinct polymer use—can degrade accuracy for models trained elsewhere. Transfer learning, domain adaptation (e.g., feature alignment), self-supervised pretraining, and synthetic data augmentation can mitigate shift, but require external validation on Gulf field samples and stress-testing across salinity/temperature gradients. Practical guardrails include holding out Gulf test sets, reporting calibration error, and publishing inference latency to ensure edge/boat-side deployability.

4.3. Promising artificial intelligence application domains in MP research

4.3.1. MP detection and classification

MPs from diverse everyday products, with varied chemical structures and shapes, can be visualized through scanning electron microscopy and other advanced microscopy methods,[125] making these methods suitable for utilizing recent advancements in AI applications for images.

Image segmentation techniques distinguish specific MP images from background visuals and other particles. While automated identification and classification techniques have excelled in medical imaging, applying these methods to MP imaging remains challenging due to the nuances in size class distribution, which is highly sensitive. Several studies have been conducted on MP detection and identification. For example, a combination of holographic imaging and transfer learning using convolutional neural networks (CNNs) has been explored and shown to improve the results.[126]

In a 2019 study, Mukhanov *et al.*[127] employed ImageJ software to convert red, green, and blue (RGB) images into binary formats, enabling the classification of MPs into four morphological categories—rounded, irregular, elongated, and fibers—using a combination of infrared spectrometry and Raman spectroscopy integrated with a hyperspectral imaging system. Similarly, Serranti *et al.*[128] utilized multivariate image analysis and designed analytical techniques to identify the type and morphology of plastics. Although these advanced imaging methods have achieved accurate classification, their widespread application is limited by high costs and accessibility challenges. Meanwhile, Gauci *et al.*[129] applied a least-squares approach to assessing MP size and surface textures from samples collected in Malta in the Central Mediterranean. They further analyzed color metrics by calculating mean square error across RGB channels. While these techniques demonstrate efficiency in tasks such as edge detection and area estimation, they rely heavily on pre-configured algorithms and subjective human interpretation. As a result, there remains a pressing need for integrative and standardized methodologies, leveraging advancements in AI to enhance MP detection and classification accuracy.

In the study by Shi *et al.*,[130] scanning electron microscopy was utilized to capture images of MPs from everyday products (Figure 3). A deep learning method was employed to quantify and categorize MPs using a hand-labeled dataset containing 237 images of MP particles (fragments or beads) sized between 50 μm and 1 mm and fibers approximately 10 μm in diameter. For quantification, the U-Net and MultiResUNet deep learning models were used for semantic segmentation. Both models surpassed traditional computer vision methods, achieving a high average Jaccard index above 0.75. In another study, Ronneberger *et al.*[131] merged the U-Net with object-aware pixel embedding to further quantify densely packed and intertwined fibers. A modified VGG16 neural network was used for categorizing by shape, achieving a remarkable 98.33% accuracy. New images can be segmented and categorized accurately using these trained models in seconds, a more efficient and cost-effective process than manual methods. As datasets expand, this approach could aid in identifying and measuring MPs in environmental samples in subsequent studies.

Recent studies have shown that 1D-CNNs enhance Raman/FTIR classification under noise/weathering;[132] U-Net-family models deliver pixel-accurate masks for sizing;[133] Faster/Mask R-CNN support high-throughput detection in brightfield and UV;[134,135] and holography/phone-microscopy enables rapid, low-cost screening. These findings underscore the need for Gulf-specific datasets and external validation.

4.3.2. MP quantification

Quantifying MPs is essential for tracking their progression and predicting their actions. Traditionally, this task has been both time-consuming and reliant on costly instruments. Several studies have introduced deep learning-based architectures designed to automatically enumerate and categorize MP particles, ranging from 1–5 mm, captured in photos from digital cameras or smartphones with a resolution of 16 megapixels or more. They employed several algorithms, such as the U-Net neural networks,[131] which are designed for object detection and classification.

The quantification of plastics from images falls under object detection.[136] In object detection, not only is the object identified, but its position within the image is also determined using a bounding box. Notable deep

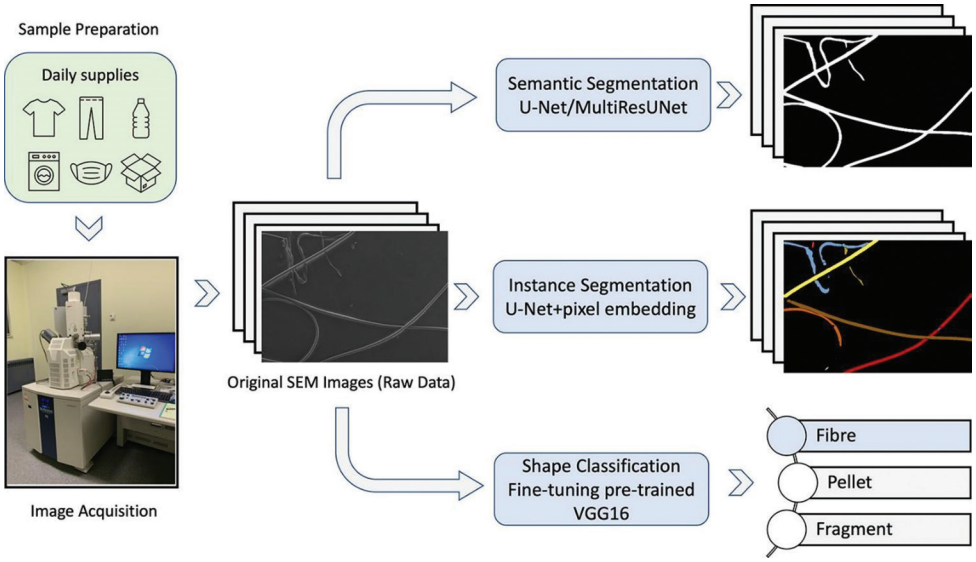

Figure 3. Segmentation models for microplastic image analysis. Adapted from Shi *et al.*[130]

learning architectures that utilize bounding boxes include algorithms such as Fast Region-based CNNs (RCNN),[137] You Only Look Once,[138] and Single Shot MultiBox Detector.[139] These methods excel in scenarios where the primary objective is determining the object's location and frequency in an image.

However, for MP classification, pinpointing the exact pixels of the particle is crucial, especially for size estimation. This requirement makes object instance segmentation or semantic segmentation techniques more appropriate, as they detect the object and categorize each pixel according to its corresponding object class. Some prominent deep learning architectures for this purpose include Fully CNN,[140] Mask-RCNN,[141] and U-Net.[131]

A particular study has demonstrated AI applications in both quantifying and classifying MPs.[142] In that research, the initial phase of the proposed framework utilized the U-Net neural network for segmenting particles within images. Once these particles were singled out, the subsequent phase employed the VGG16 neural network to categorize them into three primary types: fragments, pellets, and lines. These categories were chosen due to their prevalence within the specified size range, as described in Figure 4.

4.3.3. MP monitoring

Achieving effective MP monitoring is a pivotal long-term objective to grasp the impact and progression of MP contamination comprehensively. Despite its importance, current research in this field is notably demanding in terms of time and effort. Present monitoring methods involve collecting, processing, and manually examining vast sample quantities, but these methodologies lack uniformity and standardization. It is essential to understand the movement patterns of MPs to improve monitoring effectiveness, allowing for optimizing the placement and application of monitoring instruments. There is a growing interest in establishing high-throughput and automated monitoring systems to streamline the analysis of MP distribution on a grand scale. One promising approach is employing models to study MP behaviors, providing deeper insights into their distribution, origins, endpoints, and movement trajectories. For example, modeling has demonstrated its potential in pinpointing optimal global locations for effective plastic waste collection.

Though modeling offers insights into certain MP behaviors, it is grounded in tangible data concerning MPs' observed and measured attributes. The complexity within model equations is imperative to truly encapsulate the intricate dynamic forces that steer inertial particle movement. Machine learning and deep learning models can address these numerous challenges that involve vast data, thereby optimizing efficiency.[143] Specifically, image-centric machine learning has been pivotal in material science, assisting in analyzing extensive image sets to decipher the correlation between material structures and their properties.[144]

4.3.4. MP source tracking

In the context of MPs, pinpointing the source of pollution becomes essential, whether it stems from industrial activities, consumer goods, or waste disposal methods. Given the intricate nature of MP dispersal, which is

shaped by elements such as aquatic flows, wind directions, and human interventions, there is a pressing need for sophisticated analysis methods. Through machine learning, scientists can identify potential origins of MP emissions and anticipate areas of future buildup. This knowledge guides precise remediation actions and policy decisions to curb additional contamination. Wu *et al.*[145] employed random forest, multilabel decision trees, and support vector machines, which are all supervised machine learning algorithms, to determine the origins of the contaminants by analyzing data such as physicochemical properties.

4.3.5. MP data aggregation

A pressing issue arises from the vast and varied types of data, making data preprocessing challenging. Preprocessing the enormous variety of MP imagery, especially regarding data scaling, can be difficult when preparing it for use with deep CNN algorithms. Depending on the specific deep CNN algorithm used, it is essential to rescale the extensive MP imagery datasets, which come in various ranges, units, and scales, to ensure they match the required standardization and prerequisites. As illustrated in Figure 5, this preprocessing stage constitutes a critical component of the overall machine learning workflow for the MP analysis platform. The sheer volume of this data adds to the complexity, making it a significant hurdle in the automated processing of high-volume imagery.

5. MP biodegradation

MP contamination can be controlled or even eliminated in specific circumstances through biodegradation. Biodegradation is a natural process by which organic compounds in the environment are broken down and converted to simpler compounds, mineralized, and redistributed back to the environment.[146] It not only applies to organic compounds but also to some inorganic complexes, such as macroplastics and MPs. Biodegradation of MPs involves fragmentation into smaller sizes and, eventually, mineralization, a process entirely driven by microorganisms.[147] It occurs almost everywhere in the biosphere, including the soil rhizosphere, aquatic environments, and landfills.[148] There is growing exploration of microbial degradation as a promising, eco-friendly method for removing MPs from the environment.

The typical microorganisms associated with the biodegradation of MPs include bacteria, fungi, and algae.[149] These microorganisms vary in their mode of MP degradation and the type of polymers they degrade, as shown in Table 4.[150-158] The fungal class, for example, has been reported as a common candidate for bioremediation

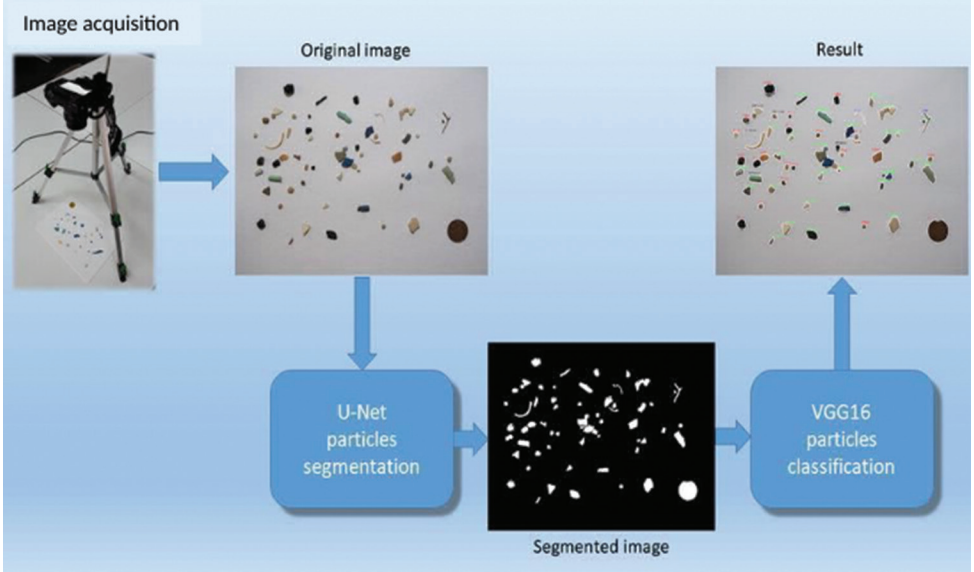

Figure 4. An example model showcases the quantification and classification of three primary MP types. Adapted with permission from Lorenzo-Navarro *et al.*[142] Copyright 2020, Elsevier.

Figure 5. The primary machine learning workflow for developing the microplastic analysis platform. Image created by the authors.

Table 4. Examples of bacteria, fungi, and algae in the biodegradation of plastics

Biodegrading microorganism	Example	Type of plastic	Reference
Bacteria	*Staphylococcus aureus*	PE	150
	Bacillus gottheilii	PE, PP, PET, and PS	151
	Bacillus subtilis	PE	152
	Pseudomonas aeruginosa	PE	153
Fungi	*Penicillium* species	PHB	153
	Pestalotiopsis microspora	PUR	153
	Zalerion maritimum	PE	154
	Aspergillus species	PE	155
Algae	*Anabaena spiroides*	PE	156
	Spirulina species	PE and PP	157
	Phaeodactylum tricornutum	PET	156
	Chlamydomonas reinhardtii	PET	158

Abbreviations: PE: Polyethylene; PET: Polyethylene terephthalate; PHB: Poly-3-hydroxybutyric acid; PP: Polypropylene; PS: Polystyrene; PUR: Polyester polyurethane.

in almost every ecosystem due to its diverse environmental adaptability as well as the capacity to secrete a wide range of enzymes and amino acids, such as manganese peroxidase, laccase, aspartate, histidine, serine, and lignin peroxidase, that can degrade macroplastics and MPs until mineralization.[159] According to Ameen *et al.*,[160] some fungal mycelia discharge extracellular enzymes that aid in breaking down plastics into small pieces (oligomers, dimers, and monomers), which are subsequently absorbed by the fungi and mineralized with the help of internal enzymes. The success of fungi in the degradation of plastics has also been associated with producing numerous polysaccharides and proteins that enable them to attach to plastic surfaces and secrete extracellular enzymes that help disintegrate the plastics.[159] The common fungi that have been used in the biodegradation of plastics include *Penicillium* species, *Pestalotiopsis microspore, Zalerion maritimum, Aspergillus* species, *Phanerochaete chrysosporium*, *Trametes versicolor,* and white rot fungi. These fungal species' degradation ability varies with the type of plastics and the duration taken to break down the plastics. For example, *Penicillium* species and *Z. maritimum* have been reported to break down the PE MPs, whereas *Aspergillus* species can break down the high-density PE plastics.[161]

Apart from fungi, bacteria are also known to play a significant role in the degradation of plastics in the environment.[151] Like fungi, bacteria also secrete both intracellular and extracellular enzymes that aid in the degradation of plastics. These enzymes include hydrolases, xylanase, depolymerases, protease, and chitinase.[159] The commonly used bacteria for MP biodegradation belong to the genera *Bacillus*, *Rhodococcus*, *Escherichia,* and *Pseudomonas.*[151] *Bacillus* species are the most researched bacteria in bioremediation, with different species showing variations in their degradation efficiencies. For example, *Bacillus cereus* has been shown to degrade PE, PET, and PS plastics, leading to weight losses of 1.6%, 6.6%, and 7.4%, respectively. Meanwhile, *Bacillus gottheilii* has been reported to degrade the same polymers, leading to weight losses of 6.2%, 3%, and 5.8%, respectively. *Bacillus subtilis,* on the other hand, has been reported to degrade high-impact PS, resulting in 23% weight loss. Other bacterial species, for example, *Pseudomonas aeruginosa* and *Penicillium simplicissimum,* have also been reported to degrade PE plastics, resulting in 20% and 7.7% weight loss, respectively.[162] Studies have also shown that different bacterial species can be combined to have a synergistic effect on MP degradation. A significant example is the combination of *Actinobacteria* and *Firmicutes,* which led to the degradation of low-density PE plastics by 60% in 3 weeks.[163]

Algae are also categorized as microorganisms that are capable of degrading plastic materials. These microorganisms produce toxins that effectively break down polymeric materials.[164] Like fungi and bacteria, microalgae species degrade different MPs at varying rates. For example, *Anabena spirodes* takes 45 days to degrade 8.18% of PE plastics. Other microalgae associated with the degradation of plastics include *Spirulina* species, *Phaeodactylum tricornutum*, *Chlamydomonas reinhardtii*, *Cryptomonas* species, and *Phormidium lucidum* (Table 4).[159]

Irrespective of the microorganisms involved, the biodegradation of MPs occurs through a sequence of steps, starting with biofilm formation, deterioration, fragmentation, assimilation, and mineralization (Figure 6). Biofilm formation occurs on the surface of the plastic, where microbes attach to the surface, reducing the hydrophobicity of the plastic[165]. Deterioration of the plastic occurs due to biofilm formation and the release of extracellular enzymes or toxins by microorganisms, leading to the fragmentation of plastics into monomers, oligomers, or dimers[166]. Assimilation involves taking up fragmented plastic molecules by microorganisms, converting them to soluble organic compounds with the help of intracellular enzymes. The last process of converting MPs to carbon dioxide, water, and methane is mineralization.[159]

Environmental factors and plastic properties drive the efficacy of MP biodegradation. Environmental factors such

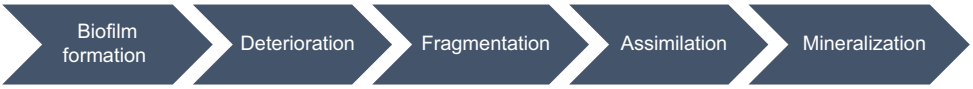

Figure 6. Illustration of the steps in microplastic biodegradation. Image created by the authors.

as oxygen level, pH, sunlight, and temperature directly or indirectly affect biodegrading microorganisms' growth, enzymatic production, and performance.[29] The abiotic environmental factors also affect the plastic decomposition rate as they affect these compounds' chemical composition. For example, a study by Gutiérrez-Silva *et al.*[167] showed that an increase in UV light and moisture led to an increased hydrolysis rate of poly (butylene adipate-co-terephthalate)-thermoplastic starch blends and, consequently, the rate of polymer biodegradation. Another study by Katarzyna Świderek,[168] showed that biodegradation of PET is directly affected by pH levels, as acidic conditions (pH 5) induced the hydrolysis of the two ester bonds forming bis-(hydroxyethyl) terephthalate, whereas only one ester bond was hydrolyzed in neutral and alkaline conditions (pH 7 and 9). Plastic properties such as molecular weight, crystallinity, shape, and size affect the polymer deposition rate. Polymers with high molecular weight, such as high-density PE, decompose gradually compared to low-density PE.[159] Other factors, such as crystallinity and the composition of co-polymers, affect the degradation rate as they determine plastic microbial accessibility and water.[169]

In the Arabian Gulf, extreme environmental conditions such as high salinity and elevated temperatures (>30°C) may limit the effectiveness of many plastic-degrading microorganisms. For example, halophilic bacteria such as *Halomonas profundus* and *Marinobacter hydrocarbonoclasticus* have shown plastic-degrading potential in saline environments, whereas thermophilic species such as *Thermobifida fusca* and engineered *Clostridium thermocellum* have demonstrated efficient PET degradation under elevated temperatures.[168,170] These findings suggest that the selection of native or adapted halo- and thermotolerant strains, as well as the development of engineered enzymes, is critical for effective biodegradation under Gulf conditions. Recent advances in protein engineering have enabled the development of thermostable PET hydrolases such as IsPETase and Cut190 variants, which retain high catalytic efficiency under elevated temperatures typical of the Gulf environment.[171,172] Direct evolution and computational enzyme design are further enhancing the substrate range and stability of these enzymes, opening new opportunities for scalable bioremediation strategies tailored to extreme marine ecosystems.

6. Conclusion

The widespread presence of MPs in marine environments poses a complex environmental and health issue. Beyond direct physiological effects, MPs may disrupt marine ecosystems, including reproduction in marine organisms and, consequently, food-web dynamics. Furthermore, consuming seafood contaminated with MPs may pose health risks to consumers. A multifaceted approach, including thorough research, is needed to address this problem. In addition to proactive legislative actions to reduce plastic waste, developing AI-powered technologies will improve monitoring and detection.

To implement this agenda, we propose a staged roadmap linking standards, shared data, validated AI, and field-tested bioremediation to policy uptake. Short-term actions establish common protocols and a regional repository; medium-term efforts deploy pilots and low-cost sensing; long-term measures embed AI- and nature-based solutions into coastal management and plastics policy. Measurable targets—including a 50% reduction in coastal MP concentrations within 10 years, repository growth to >1 million labeled spectra/images, and region-wide monitoring coverage—provide accountability while fostering international collaboration and academic–industry consortia.

Addressing MPs with particular emphasis on cutting back on single-use plastic bags is a global steady movement to control the contamination of ecosystems. While limited policies directly target primary MPs (e.g., bans on microbeads), interventions such as bans, fees, and taxes on plastic bags have gained traction globally. Many European nations have implemented widespread tariffs for plastic bags, greatly decreasing consumption. As effective efforts of Gulf nations to protect local, including marine environments, the UAE, through the Ministry of Climate Change and Environment, plans to implement a full ban on single-use plastics on January 1, 2026.[173] Similarly, the efforts on MPs in Saudi Arabia's marine environments, including the Arabian Gulf Sea, have been emphasized in a number of relevant national and international reports. According to the Minister of Environment, Water, and Agriculture, Saudi Arabia has joined the Alliance to End Plastic Waste in the Ocean and the World Ocean Council on a global scale.[174] As sustainable innovation is promoted locally in Saudi Arabia, plastic has been recycled in road construction to improve

quality and lower costs.[175] While significant progress has been made through these initiatives, enforcement issues and unequal implementation remain challenges, especially at the national level. Although its efforts are mainly concentrated on more general environmental projects, Saudi Arabia has been making progress in combating plastic pollution. For example, the Saudi Green Initiative prioritizes environmental sustainability, aiming to preserve 30% of Saudi Arabia's land and marine regions by 2030. This initiative includes the national efforts that indirectly support the reduction of plastic waste and pollution in marine environments, such as waste management and afforestation projects. Second, innovative solutions such as cleaning robots have been implemented in Saudi Arabia to reduce plastic waste along coastlines. Red Sea Global, a developer of regenerative tourism destinations, leads programs to promote clean beaches and sustainable practices.[176] Such coastal cleanliness and sustainability efforts also support Saudi Arabia's broader Vision 2030 objectives for developing a sustainable tourism sector.[177] Third, recent life-cycle assessment evidence from Saudi Arabia indicates that advanced waste management strategies, including pyrolysis and mechanical recycling, can lessen the environmental impact of plastic waste.[178] These strategies seek to reduce dependency on landfills and produce high-quality recycled products, emphasizing a transition toward a circular economy concept.[169,178] Public awareness and responsible consumption can also play vital roles in mitigating this growing environmental challenge.

These national and regional initiatives align with general global perspectives that highlight advanced 2D nanomaterial-based treatment solutions and the crucial role of atmospheric transport and deposition as primary routes for MP exposure, underscoring the necessity for comprehensive, cross-media mitigation strategies.[179,180]

Acknowledgments

None.

Funding

None.

Conflict of interest

The authors declare they have no competing interests.

Author contributions

Conceptualization: Amani Almaabadi, Hany M. Almotairy
Visualization: All authors
Writing–original draft: All authors
Writing–review & editing: Amani Almaabadi, Mona Alshahrani, Hany M. Almotairy

Consent for publication

Not applicable.

Availability of data

Not applicable.

Further disclosure

During the preparation of this work, the authors used Grammarly and ChatGPT to improve language clarity. The authors reviewed and edited all content to ensure accuracy and take full responsibility for the final manuscript.

References

1. Carpenter EJ, Smith Jr. KL. Plastics on the Sargasso sea surface. *Science*. 1972;175(4027):1240-1241.

   doi: 10.1126/science.175.4027.1240

2. Zhou C, Bi R, Su C, Liu W, Wang T. The emerging issue of microplastics in marine environment: A bibliometric analysis from 2004 to 2020. *Mar Pollut Bull*. 2022;179:113712.

   doi: 10.1016/j.marpolbul.2022.113712

3. Wang YZ, Revie RW, Shehata MT, Parkins RN, Krist K. Initiation of environment induced cracking in pipeline steel: Microstructural correlations. *ASME*. 1998;40221:529-542.

   doi: 10.1115/IPC1998-2061

4. Thompson RC, Olsen Y, Mitchell RP, *et al*. Lost at sea: Where is all the plastic?. *Science*. 2004;304(5672):838.

   doi: 10.1126/science.1094559

5. Catarino AI, Kramm J, Voelker C, Henry TB, Everaert G. Risk posed by microplastics: Scientific evidence and public perception. *Curr Opin Green Sustainable Chem*. 2021;29:100467.

   doi: 10.1016/j.cogsc.2021.100467

6. Arthur C, Baker J, Bamford H. *Proceedings of the International Research Workshop on the Occurrence, Effects, and Fate of Microplastic Marine Debris*. NOAA Marine Debris Program; 2009. Available from: https://marinedebris.noaa.gov/proceedings-international-research-workshop-microplastic-marine-debris [Last accessed on 2025 Dec 24].

7. Jenner LC, Rotchell JM, Bennett RT, Cowen M, Tentzeris V, Sadofsky LR. Detection of microplastics in human lung tissue using μFTIR spectroscopy. *Sci Total Environ*. 2022;831:154907.

   doi: 10.1016/j.scitotenv.2022.154907

8. Kim D, Mo K, Kim M, Cui F. Occurrence and sources of micro-plastics in various water bodies, sediments, and fishes in Ansan, South Korea. *Environ Sci Pollut Res Int*. 2023;30(22):62579-62589.

   doi: 10.1007/s11356-023-26562-9

9. Gunawan NR, Tessman M, Zhen D, *et al*. Biodegradation of renewable polyurethane foams in marine environments occurs through depolymerization by marine microorganisms. *Sci Total Environ*. 2022;850:158761.

doi: 10.1016/j.scitotenv.2022.158761

10. Danso D, Chow J, Streit WR. Plastics: Environmental and biotechnological perspectives on microbial degradation. *Appl Environ Microbiol.* 2019;85:e01095-19.

doi: 10.1128/AEM.01095-19

11. Hussain I, Ganiyu SA, Alasiri H, Alhooshani K. A state-of-the-art review on waste plastics-derived aviation fuel: Unveiling the heterogeneous catalytic systems and techno-economy feasibility of catalytic pyrolysis. *Energy Convers Manag.* 2022;274:116433.

doi: 10.1016/j.enconman.2022.116433

12. Jahirul MI, Rasul MG, Schaller D, Khan MMK, Hasan MM, Hazrat MA. Transport fuel from waste plastics pyrolysis–A review on technologies, challenges and opportunities. *Energy Convers Manag.* 2022;258:115451.

doi: 10.1016/j.enconman.2022.115451

13. Napper IE, Thompson RC. Plastic debris in the marine environment: History and future challenges. *Glob Chall.* 2020;4(6):1900081.

doi: 10.1002/gch2.201900081

14. Geyer R. Production, use, and fate of synthetic polymers. In: *Plastic Waste and Recycling.* United States: Academic Press; 2020. p. 13-32.

doi: 10.1016/B978-0-12-817880-5.00002-5

15. Shen M, Huang W, Chen M, Song B, Zeng G, Zhang Y. (Micro) plastic crisis: Un-ignorable contribution to global greenhouse gas emissions and climate change. *J Clean Prod.* 2020;254:120138.

doi: 10.1016/j.jclepro.2020.120138

16. Chen J, Wang W, Liu H, Xu X, Xia J. A review on the occurrence, distribution, characteristics, and analysis methods of microplastic pollution in ecosystems. *Environ Pollut Bioavail*. 2021;33(1):227-246.

doi: 10.1080/26395940.2021.1960198

17. Kiran BR, Kopperi H, Venkata Mohan S. Micro/nano-plastics occurrence, identification, risk analysis and mitigation: Challenges and perspectives. *Rev Environ Sci Biotechnol*. 2022;21(1):169-203.

doi: 10.1007/s11157-021-09609-6

18. Koelmans AA, Redondo-Hasselerharm PE, Nor NHM, de Ruijter VN, Mintenig SM, Kooi M. Risk assessment of microplastic particles. *Nat Rev Mater.* 2022;7(2):138-152.

doi: 10.1038/s41578-021-00411-y

19. Pakhomova S, Zhdanov I, van Bavel B. Polymer type identification of marine plastic litter using a miniature near-infrared spectrometer (MicroNIR). *Appl Sci (Basel).* 2020;10(23):8707.

doi: 10.3390/app10238707

20. Joos L, De Tender C. Soil under stress: The importance of soil life and how it is influenced by (micro) plastic pollution. *Comput Struct Biotechnol J.* 2022;20:1554-1566.

doi: 10.1016/j.csbj.2022.03.041

21. Born MP, Brüll C, Schüttrumpf H. Implications of a new test facility for fragmentation investigations on virgin (Micro) plastics. *Environ Sci Technol.* 2023;57(28):10393-10403.

doi: 10.1021/acs.est.3c02189

22. Jakubowicz I, Enebro J, Yarahmadi N. Challenges in the search for nanoplastics in the environment-A critical review from the polymer science perspective. *Polym Test*. 2021;93:106953.

doi: 10.1016/j.polymertesting.2020.106953

23. Hidayaturrahman H, Lee TG. A study on characteristics of microplastic in wastewater of South Korea: Identification, quantification, and fate of microplastics during treatment process. *Mar Pollut Bull.* 2019;146:696-702.

doi: 10.1016/j.marpolbul.2019.06.071

24. Anagnosti L, Varvaresou A, Pavlou P, Protopapa E, Carayanni V. Worldwide actions against plastic pollution from microbeads and microplastics in cosmetics focusing on European policies. Has the issue been handled effectively?. *Mar Pollut Bull.* 2021;162:111883.

doi: 10.1016/j.marpolbul.2020.111883

25. Hwang J, Choi D, Han S, Jung SY, Choi J, Hong J. Potential toxicity of polystyrene microplastic particles. *Sci Rep.* 2020;10(1):7391.

doi: 10.1038/s41598-020-64464-9

26. Tadsuwan K, Babel S. Microplastic abundance and removal via an ultrafiltration system coupled to a conventional municipal wastewater treatment plant in Thailand. *J Environ Chem Eng.* 2022;10(2):107142.

doi: 10.1016/j.jece.2022.107142

27. Zheng Y, Zhu J, Li J, Li G, Shi, H. Burrowing invertebrates induce fragmentation of mariculture Styrofoam floats and formation of microplastics. *J Hazard Mater.* 2023;447:130764.

doi: 10.1016/j.jhazmat.2023.130764

28. Song YK, Hong SH, Eo S, Han GM, Shim WJ. Rapid production of micro-and nanoplastics by fragmentation of expanded polystyrene exposed to sunlight. *Environ Sci Technol*. 2020;54(18):11191-11200.

doi: 10.1021/acs.est.0c02288

29. Lin Z, Jin T, Zou T, *et al*. Current progress on plastic/microplastic degradation: Fact influences and mechanism.

Environ Pollut. 2022;304:119159.

doi: 10.1016/j.envpol.2022.119159

30. Zhang D, Liu X, Huang W, *et al*. Microplastic pollution in deep-sea sediments and organisms of the Western Pacific Ocean. *Environ Pollut.* 2020;259:113948.

doi: 10.1016/j.envpol.2020.113948

31. Li J, Gao F, Zhang D, Cao W, Zhao C. Zonal distribution characteristics of microplastics in the Southern Indian Ocean and the influence of Ocean current. *J Mar Sci Eng.* 2022;10(2):10.3390/jmse10020290.

doi: 10.3390/jmse10020290

32. Hansen J, Hildebrandt L, Zimmermann T, El Gareb F, Fischer EK. Pröfrock D. Quantification and characterization of microplastics in surface water samples from the Northeast Atlantic Ocean using laser direct infrared imaging. *Mar Pollut Bull.* 2023;190:114880.

doi: 10.1016/j.marpolbul.2023.114880

33. Vaughan GO, Al-Mansoori N, Burt JA. The Arabian gulf. In: *World Seas: An Environmental Evaluation*. Vol. 2. United States: Academic Press; 2019. p. 1-23.

doi: 10.1016/b978-0-08-100853-9.00001-4

34. Hereher ME. Assessment of climate change impacts on sea surface temperatures and sea level rise-The Arabian Gulf. *Climate (Basel).* 2020;8(4):50.

doi: 10.3390/cli8040050

35. Mohamed ARM, Abood AN. Current status of Iraqi artisanal marine fisheries in Northwest of the Arabian Gulf of Iraq. *Arch Agr Environ Sci.* 2020;5(4):457-464.

doi: 10.26832/24566632.2020.050404

36. Guieu C, Al Azhar M, Aumont O, *et al*. Major impact of dust deposition on the productivity of the Arabian Sea. *Geophys Res Lett.* 2019;46(12):6736-6744.

doi: 10.1029/2019GL082770

37. Ibrahim HD, Xue P, Eltahir EA. Multiple salinity equilibria and resilience of Persian/Arabian Gulf basin salinity to brine discharge. *Front Mar Sci.* 2020;7:573.

doi: 10.3389/fmars.2020.00573.

38. Abayomi OA, Range P, Al-Ghouti MA, Obbard JP, Almeer SH, Ben-Hamadou R. Microplastics in coastal environments of the Arabian Gulf. *Mar Pollut Bull.* 2017;124(1):181-188.

doi: 10.1016/j.marpolbul.2017.07.011

39. Naji A, Nuri M, Vethaak AD. Microplastics contamination in molluscs from the northern part of the Persian Gulf. *Environ Pollut.* 2018;235:113-120.

doi: 10.1016/j.envpol.2017.12.046

40. Akhbarizadeh R, Moore F, Keshavarzi B. Investigating microplastics bioaccumulation and biomagnification in seafood from the Persian Gulf: A threat to human health?. *FAC Part A.* 2019;36(11):1696-1708.

doi: 10.1080/19440049.2019.1649473

41. Saeed T, Al-Jandal N, Al-Mutairi A, Taqi H. Microplastics in Kuwait marine environment: Results of first survey. *Mar Pollut Bull.* 2020;152:110880.

doi: 10.1016/j.marpolbul.2019.110880

42. Jahromi FA, Keshavarzi B, Moore F, *et al*. Source and risk assessment of heavy metals and microplastics in bivalves and coastal sediments of the Northern Persian Gulf, Hormogzan Province. *Environ Res.* 2021;196:110963.

doi: 10.1016/j.envres.2021.110963

43. Al Hammadi M, Knuteson S, Kanan S, Samara F. Microplastic pollution in oyster bed ecosystems: An assessment of the northern shores of the United Arab Emirates. *Environ Adv.* 2022;8:100214.

doi: 10.1016/j.envadv.2022.100214

44. Ali HJA, Al-Thukair AA, Pulikkoden AK, Chanbasha B. Microplastic contaminants in the sediment of the East Coast of Saudi Arabia. London: IntechOpen; 2023.

doi: 10.5772/intechopen.109019

45. Saudi Arabia General Authority for Statistics (SAGASTAT). Marine Fishery and Aquaculture Publication; 2023. Available from: https://www.stats.gov.sa/en/search?q=%22marine+fishery+and+aquaculture+publication %22 [Last accessed on 2025 Dec 24].

46. Al-Salem SM, Uddin S, Lyons B. Evidence of microplastics (MP) in gut content of major consumed marine fish species in the State of Kuwait (of the Arabian/Persian Gulf). *Mar Pollut Bull.* 2020;154:111052.

doi: 10.1016/j.marpolbul.2020.111052

47. Baalkhuyur FM, Qurban MA, Panickan P, Duarte CM. Microplastics in fishes of commercial and ecological importance from the Western Arabian Gulf. *Mar Pollut Bull.* 2020;152:110920.

doi: 10.1016/j.marpolbul.2020.110920

48. Al-Thawadi S. Microplastics and nanoplastics in aquatic environments: Challenges and threats to aquatic organisms. *Arabian J Sci Eng.* 2020;45(6):4419-4440.

doi: 10.1007/s13369-020-04402-z

49. Gurjar UR, Xavier KM, Shukla SP, Deshmukhe G, Jaiswar AK, Nayak BB. Incidence of microplastics in gastrointestinal tract of golden anchovy (*Coilia dussumieri*) from north east coast of Arabian Sea: The ecological perspective. *Mar Pollut Bull.* 2021;169:112518.

doi: 10.1016/j.marpolbul.2021.112518

50. Lamichhane G, Acharya A, Marahatha R, *et al*. Microplastics in environment: Global concern, challenges, and controlling measures. *Int J Environ Sci Technol (Tehran)*. 2023;20(4):4673-4694.

doi: 10.1007/s13762-022-04261-1

51. Ziani K, Ioniță-Mîndrican CB, Mititelu M, *et al*. Microplastics: A real global threat for environment and food safety: A state of the art review. *Nutrients*. 2023;15(3): 617.

doi: 10.3390/nu15030617

52. Hale RC, Seeley ME, La Guardia MJ, Mai L, Zeng EY. A global perspective on microplastics. *J Geophys Res Oceans*. 2020;125(1):e2018JC014719.

doi: 10.1029/2018JC014719

53. Mason VG, Skov MW, Hiddink JG, Walton M. Microplastics alter multiple biological processes of marine benthic fauna. *Sci Total Environ.* 2022;845:157362.

doi: 10.1016/j.scitotenv.2022.157362

54. Nanthini Devi K, Raju P, Santhanam P, Perumal P. Impacts of microplastics on marine organisms: Present perspectives and the way forward. *Egypt J Aquat Res.* 2022;48(3):205-209.

doi: 10.1016/j.ejar.2022.03.001

55. Amelia TSM, Khalik WMA, Ong MC, Shao YT, Pan HJ, Bhubalan K. Marine microplastics as vectors of major ocean pollutants and its hazards to the marine ecosystem and humans. *Prog Earth Planet Sci.* 2021;8(1):1-26.

doi: 10.1186/s40645-020-00405-4

56. Issac MN, Kandasubramanian B. Effect of microplastics in water and aquatic systems. *Environ Sci Pollut Res Int.* 2021;28:19544-19562.

doi: 10.1007/11356-021-13184-2

57. Habib RZ, Thiemann T. Microplastic in commercial fish in the Mediterranean sea, the red sea and the Arabian gulf. Part 1: The Mediterranean sea. *J Water Resour Prot.* 2021;13(8):563-587.

doi: 10.4236/jwarp.2022.146025

58. Huang CH, Chu TW, Kuo CH, Hong MC, Chen YY, Chen B. Effects of microplastics on reproduction and growth of freshwater live feeds Daphnia magna. *Fishes.* 2022;7(4):181.

doi: 10.3390/fishes7040181

59. Gola D, Tyagi PK, Arya A, *et al*. The impact of microplastics on marine environment: A review. *ENMM*. 2021;16:100552.

doi: 10.1016/j.enmm.2021.100552

60. Van Colen C, Vanhove B, Diem A, Moens T. Does microplastic ingestion by zooplankton affect predator-prey interactions? An experimental study on Larviphagy. *Environ Pollut.* 2020;256:113479.

doi: 10.1016/j.envpol.2019.113479

61. Uguen M, Nicastro KR, Zardi GI, *et al*. Microplastic leachates disrupt the chemotactic and chemokinetic behaviours of an ecosystem engineer (*Mytilus edulis*). *Chemosphere.* 2022;306:135425.

doi: 10.1016/j.chemosphere.2022.135425

62. Rodrigues CC, Salla RF, Rocha TL. Bioaccumulation and ecotoxicological impact of micro (nano) plastics in aquatic and land snails: Historical review, current research and emerging trends. *J Hazard Mater.* 2023;444:130382.

doi: 10.1016/j.jhazmat.2022.130382

63. Baechler BR, Stienbarger CD, Horn DA, *et al*. Microplastic occurrence and effects in commercially harvested North American finfish and shellfish: current knowledge and future directions. *Limnol Oceanogr Lett.* 2020;5(1):113-136.

doi: 10.1002/lol2.10122

64. Corinaldesi C, Canensi S, Dell'Anno A, *et al*. Multiple impacts of microplastics can threaten marine habitat-forming species. *Commun Biol.* 2021;4(1):431.

doi: 10.1038/s42003-021-01961-1

65. Morrison M, Trevisan R, Ranasinghe P, *et al*. A growing crisis for one health: Impacts of plastic pollution across layers of biological function. *Front Mar Sci.* 2022;9:980705.

doi: 10.3389/fmars.2022.980705

66. Yu RS, Singh S. Microplastic pollution: Threats and impacts on global marine ecosystems. *Sustainability.* 2023;15(17):13252.

doi: 10.3390/su151713252

67. Chen CF, Ju YR, Lim YC, Wang MH, Chen CW, Dong CD. Microplastics in coastal farmed oyster (*Crassostrea angulata*) shells: Abundance, characteristics, and diversity. *Mar Pollut Bull.* 2023;194:115228.

doi: 10.1016/j.marpolbul.2023.115228

68. Onyena AP, Aniche DC, Ogbolu BO, Rakib MRJ, Uddin J, Walker TR. Governance strategies for mitigating microplastic pollution in the marine environment: A review. *Microplastics*. 2022;1(1):15-46.

doi: 10.3390/microplastics1010003

69. Cole M, Lindeque P, Fileman E, *et al*. Microplastic ingestion by zooplankton. *Environ Sci Technol*. 2013;47(12):6646-6655.

doi: 10.1021/es400663f

70. Scherer C, Brennholt N, Reifferscheid G, Wagner M. Feeding type and development drive the ingestion of microplastics by freshwater invertebrates. *Sci Rep.* 2017;7(1):17006.

doi: 10.1038/s41598-017-17191-7

71. Malinowski CR, Searle CL, Schaber J, Höök TO. Microplastics impact simple aquatic food web dynamics through reduced zooplankton feeding and potentially releasing algae from consumer control. *Sci Total Environ.* 2023;904:166691.

doi: 10.1016/j.scitotenv.2023.166691

72. Yin J, Duan C, Zhou F, *et al*. Microplastics affect interspecific interactions between *Cladoceran* species in the absence and presence of predators by triggering asymmetric individual responses. *Water Res.* 2023;248:120877.

doi: 10.1016/j.watres.2023.120877

73. Montoya D, Rastelli E, Casotti R, *et al*. Microplastics alter the functioning of marine microbial ecosystems. *Ecol Evol.* 2024;14(11):e70041.

doi: 10.1002/ece3.70041

74. Köster M, Paffenhöfer G. Feeding of marine zooplankton on microplastic fibers. *Arch Environ Contam Toxicol.* 2022;83(2):129-141.

doi: 10.1007/s00244-022-00948-1

75. Sharma S, Bhardwaj A, Thakur M, Saini A. Understanding microplastic pollution of marine ecosystem: A review. *Environ Sci Pollut Res Int.* 2023;31:41402-41445.

doi: 10.1007/s11356-023-28314-1

76. Naik RK, Chakraborty P, D'Costa PM, Anilkumar N, Mishra RK, Fernandes VA simple technique to mitigate microplastic pollution and its mobility (via ballast water) in the global ocean. *Environ Pollut.* 2021;283:117070.

doi: 10.1016/j.envpol.2021.117070

77. Mahmud SM, Chuah LF, Nik WM, Abu Bakar A, Musa MA. Retrofitting ballast water treatment system: A container ship case study. *Chem Eng Trans*. 2024;110:367-372.

doi: 10.3303/CET24110062

78. Thach ND, Van Hung P. Development of UV reactor controller in ballast water treatment system to minimize the biological threat on marine environment. *J Sea Res*. 2024;198:102465.

doi: 10.1016/j.seares.2023.102465

79. Ejder E, Ceylan BO, Celik MS, Arslanoğlu Y. Sustainability in maritime transport: Selecting ballast water treatment for a bulk carrier. *Mar Environ Res.* 2024;198:106511.

doi: 10.1016/j.marenvres.2024.106511

80. Zhang H, Xue J, Wang Q, Yuan L, Wu H. Formation of halogenated disinfection by-products during ballast water chlorination. *ESWRT*. 2022;8(3):648-656.

doi: 10.1039/D1EW00674F

81. Yang L, Ma C. Toward a better understanding of microalgal photosynthesis in medium polluted with microplastics: A study of the radiative properties of microplastic particles. *Front Bioeng Biotechnol.* 2023;11:1193033.

doi: 10.3389/fbioe.2023.1193033

82. Kye H, Kim J, Ju S, Lee J, Lim C, Yoon, Y. Microplastics in water systems: A review of their impacts on the environment and their potential hazards. *Heliyon*. 2023;9(3):e14359.

doi: 10.1016/heliyon.2023.e14359

83. Ricciardi M, Pironti C, Motta O, Miele Y, Proto A, Montano L. Microplastics in the aquatic environment: Occurrence, persistence, analysis, and human exposure. *Water*, 2021;13(7):973.

doi: 10.3390/w13070973

84. Liu H, Sun K, Liu X, *et al*. Spatial and temporal distributions of microplastics and their macroscopic relationship with algal blooms in Chaohu Lake, China. *J Contam Hydrol.* 2022;248:104028.

doi: 10.1016/j.jconhyd.2022.104028

85. Pestana CJ, Moura DS, Capelo-Neto J, *et al*. Potentially poisonous plastic particles: microplastics as a vector for cyanobacterial toxins microcystin-LR and microcystin-LF. *Environ Sci Technol*. 2021;55(23):15940-15949.

doi: 10.1021/acs.est.1c05796

86. Kane IA, Clare MA. Dispersion, accumulation, and the ultimate fate of microplastics in deep-marine environments: A review and future directions. *Front Earth Sci (Lausanne)*. 2019;7:80.

doi: 10.3389/feart.2019.00080

87. Barrett J, Chase Z, Zhang J, *et al.* Microplastic pollution in deep-sea sediments from the Great Australian Bight. *Front Mar Sci.* 2020;7:808.

doi: 10.3389/fmars.2020.576170

88. Li Y, Sun Y, Li J, Tang R, Miu Y, Ma, X. Research on the influence of microplastics on marine life. *IOP Conf Ser Earth Environ Sci.* 2021;631:012006.

doi: 10.1088/1755-1315/631/1/012006

89. Waldschläger K, Brückner MZ, Almroth BC, *et al*. Learning from natural sediments to tackle microplastics challenges: A multidisciplinary perspective. *Earth Sci Rev.* 2022;228:104021.

doi: 10.1016/j.earscirev.2022.104021

90. Yu H, Qi W, Cao X, *et al*. Microplastic residues in wetland ecosystems: Do they truly threaten the plant-microbe-soil system?. *Environ Int.* 2021;156:106708.

doi: 10.1016/j.envint.2021.106708

91. Salam M, Zheng H, Liu Y, *et al.* Effects of micro (nano) plastics on soil nutrient cycling: State of the knowledge. *J Environ Manage.* 2023;344:118437.

doi: 10.1016/j.jenvman.2023.118437

92. Gerstenbacher CM, Finzi AC, Rotjan RD, Novak AB. A review of microplastic impacts on Seagrasses, epiphytes, and associated sediment communities. *Environ Pollut.* 2022;303:119108.

doi: 10.1016/j.envpol.2022.119108

93. Seeley ME, Song B, Passie R, Hale RC. Microplastics affect

sedimentary microbial communities and nitrogen cycling. *Nat Commun.* 2020;11(1):2372.

doi: 10.1038/s41467-020-16235-3

94. Ma H, Pu S, Liu S, Bai Y, Mandal S, Xing B. Microplastics in aquatic environments: Toxicity to trigger ecological consequences. *Environ Pollut.* 2020;261:114089.

doi: 10.1016/j.envpol.2020.114089

95. Yang H, Chen G, Wang J. Microplastics in the marine environment: Sources, fates, impacts and microbial degradation. *Toxics*. 2021;9(2):41.

doi: 10.3390/toxics9020041

96. Pourebrahimi S, Pirooz M. Microplastic pollution in the marine environment: A review. *J Hazard Mater Adv.* 2023;10:100327.

doi: 10.1016/j.hazadv.2023.100327

97. Alfaro-Núñez A, Astorga D, Cáceres-Farías L, *et al*. Microplastic pollution in seawater and marine organisms across the Tropical Eastern Pacific and Galápagos. *Sci Rep.* 2021;11(1):6424.

doi: 10.1038/s41598-021-85939-3

98. Lionetto F, Corcione CE. An overview of the sorption studies of contaminants on poly (Ethylene Terephthalate) microplastics in the marine environment. *J Mar Sci Eng.* 2021;9(4):445.

doi: 10.3390/jmse9040445

99. Agboola OD, Benson NU. Physisorption and chemisorption mechanisms influencing micro (nano) plastics-organic chemical contaminants interactions: A review. *Front Environ Sci.* 2021;9:167.

doi: 10.3389/fenvs.2021.678574

100. He B, Liu A, Duan H, Wijesiri B, Goonetilleke A. Risk associated with microplastics in urban aquatic environments: A critical review. *J Hazard Mater.* 2022;439:129587.

doi: 10.1016/j.jhazmat.2022.129587

101. Gao F, Li J, Sun C, *et al*. Study on the capability and characteristics of heavy metals enriched on MPs in marine environment. *Mar Pollut Bull.* 2019;144:61-67.

doi: 10.1016/j.marpolbul.2019.04.039

102. Bhuyan MS. Effects of microplastics on fish and in human health. *Front Environ Sci.* 2022;10:250.

doi: 10.3389/fenvs.2022.827289

103. Costa E, Piazza V, Lavorano S, Faimali M, Garaventa F, Gambardella C. Trophic transfer of microplastics from copepods to jellyfish in the marine environment. *Front Environ Sci.* 2020;8:571732.

doi: 10.3389/fenvs.2020.571732

104. Li Y, Tao L, Wang Q, Wang F, Li G, Song M. Potential health impact of microplastics: A review of environmental distribution, human exposure, and toxic effects. *Environ Health.* 2023;1(4):249-257.

doi: 10.1021/envhealth.3c00052

105. Chen J, Wu J, Sherrell PC, *et al*. How to build a microplastics-free environment: Strategies for microplastics degradation and plastics recycling. *Adv Sci (Weinh).* 2022;9(6):2103764.

doi: 10.1002/advs.202103764

106. Menéndez-Pedriza A, Jaumot J. Interaction of environmental pollutants with microplastics: A critical review of sorption factors, bioaccumulation and ecotoxicological effects. *Toxics*. 2020;8(2):40.

doi: 10.3390/toxics8020040

107. Amran NH, Zaid SSM, Mokhtar MH, Manaf LA, Othman S. Exposure to microplastics during early developmental stage: Review of current evidence. *Toxics.* 2022;10(10):597.

doi: 10.3390/toxics10100597

108. Campanale C, Massarelli C, Savino I, Locaputo V, Uricchio VF. A detailed review study on potential effects of microplastics and additives of concern on human health. *Int J Environ Res Public Health.* 2020;17(4):1212.

doi: 10.3390/ijerph17041212

109. Munyaneza J, Jia Q, Qaraah FA, Hossain MF, Wu C, Zhen H, Xiu G. A review of atmospheric microplastics pollution: In-depth sighting of sources, analytical methods, physiognomies, transport and risks. *Sci Total Environ.* 2022;822:153339.

doi: 10.1016/j.scitotenv.2022.153339

110. Rani M, Ducoli S, Depero L, *et al*. A complete guide to extraction methods of microplastics from complex environmental matrices. *Molecules*. 2023;28(15):5710.

doi: 10.3390/molecules28155710

111. Cutroneo L, Reboa A, Besio G, *et al*. Microplastics in seawater: Sampling strategies, laboratory methodologies, and identification techniques applied to the port environment. *Environ Sci Pollut Res Int.* 2020;27:8938-8952.

doi: 10.1007/s11356-020-07783-8

112. Liu Z, Wang W, Liu X. Automated characterization and identification of microplastics through spectroscopy and chemical imaging in combination with chemometric: Latest developments and future prospects. *Trends Analyt Chem.* 2023;160:116956.

doi: 10.1016/j.trac.2023.116956

113. Mariano S, Tacconi S, Fidaleo M, Rossi M, Dini L. Micro and nanoplastics identification: Classic methods and innovative detection techniques. *Front Toxicol.* 2021;3:636640.

doi: 10.3389/ftox.2021.636640

114. Fries E, Dekiff JH, Willmeyer J, Nuelle MT, Ebert M, Remy D. Identification of polymer types and additives in marine microplastic particles using pyrolysis-GC/MS and scanning electron microscopy. *Environ Sci.* 2013;15(10):1949-1956.

doi: 10.1039/C3EM00214D

115. Yu J, Wang P, Ni F, *et al*. Characterization of microplastics in environment by thermal gravimetric analysis coupled with Fourier transform infrared spectroscopy. *Mar Pollut Bull.* 2019;145:153-160.

doi: 10.1016/j.marpolbul.2019.05.037

116. Hidalgo-Ruz V, Gutow L, Thompson RC, Thiel M. Microplastics in the marine environment: A review of the methods used for identification and quantification. *Environ Sci Technol.* 2012;46(6):3060-3075.

doi: 10.1021/es2031505

117. Song YK, Hong SH, Jang M, *et al*. A comparison of microscopic and spectroscopic identification methods for analysis of microplastics in environmental samples. *Mar Pollut Bull.* 2015;93(1-2):202-209.

doi: 10.1016/j.marpolbul.2015.01.015

118. Ivleva NP, Wiesheu AC, Niessner R. Microplastic in aquatic ecosystems. *Angew Chem Int Ed Engl.* 2017;56(7):1720-1739.

doi: 10.1002/anie.201606957

119. Prata JC. Microplastics in wastewater: State of the knowledge on sources, fate, and solutions. *Mar Pollut Bull.* 2018;129(1):262-265.

doi: 10.1016/j.marpolbul.2018.02.046

120. Araujo CF, Nolasco MM, Ribeiro AMP, Ribeiro-Claro PJA. Identification of microplastics using Raman spectroscopy: Latest developments and future prospects. *Water Res.* 2018;142:426-440.

doi: 10.1016/j.watres.2018.05.060

121. Crawford CB, Quinn B. *Microplastic Pollutants*. Netherlands: Elsevier Limited; 2016.

doi: 10.1016/C2015-0-04315-5

122. Russell SJ, Norvig P. *Artificial Intelligence a Modern Approach*. London. Saudi Green Initiative. 2016 Web resource. Saudi vision 2030; 2010. https://www.vision2030.gov.sa/en/explore/projects/saudi-green-initiative [Last accessed on 2026 Jan 27].

123. Murphy KP. *Machine Learning: A Probabilistic Perspective*. United States: MIT Press; 2012. Available from: https://mitpress.mit.edu/9780262018029/machine-learning [Last accessed on 2026 Jan 27].

124. Goodfellow I, Bengio Y, Courville A. Deep *Learning*. United States: MIT Press; 2016. Available from: https://mitpress.mit.edu/9780262035613/deep-learning [Last accessed on 2026 Jan 27].

125. Bianco V, Pirone D, Memmolo P, Merola F, Ferraro P. Identification of microplastics based on the fractal properties of their holographic fingerprint. *ACS Photonics*. 2021;8(7):2148-2157.

doi: 10.1021/acsphotonics.1c00591

126. Zhu Y, Yeung C.H, Lam EY. Digital holographic imaging and classification of microplastics using deep transfer learning. *Applied Optics*. 2021;60(4):A38-A47.

doi: 10.1364/AO.403366

127. Mukhanov VS, Litvinyuk DA, Sakhon EG, Bagaev AV, Veerasingam S, Venkatachalapathy, R. A new method for analyzing microplastic particle size distribution in marine environmental samples. *Ecol Montenegrina.* 2019;23:77-86.

doi: 10.37828/em.2019.23.10

128. Serranti S, Palmieri R, Bonifazi G, Cózar A. Characterization of microplastic litter from oceans by an innovative approach based on hyperspectral imaging. *Waste Manag.* 2018;76:117-125.

doi: 10.1016/j.wasman.2018.03.003

129. Gauci A, Deidun A, Montebello J, Abela J, Galgani, F. Automating the characterisation of beach microplastics through the application of image analyses. *Coast Manage.* 2019;182:104950.

doi: 10.1016/j.ocecoaman.2019.104950

130. Shi B, Patel M, Yu D, *et al*. Automatic quantification and classification of microplastics in scanning electron micrographs via deep learning. *Sci Total Environ.* 2022;825:153903.

doi: 10.1016/j.scitotenv.2022.153903

131. Ronneberger O, Fischer P, Brox T. U-Net: Convolutional networks for biomedical image segmentation. In: Navab N, Hornegger J, Wells W, Frangi A. (eds). *Medical Image Computing and Computer-Assisted Intervention*. Lecture Notes in Computer Science. Cham: Springer; 2015. p. 234-241.

doi: 10.1007/978-3-319-24574-4_28

132. Zhang W, Feng W, Cai Z, Wang H, Yan Q, Wang Q. A deep one-dimensional convolutional neural network for microplastics classification using Raman spectroscopy. *Vib Spectrosc.* 2023;124:103487.

doi: 10.1016/j.vibspec.2022.103487

133. Li H, Xu S, Teng J, Jiang X, Fan L. Deep learning assisted ATR-FTIR and Raman spectroscopy fusion technology for microplastic identification. *Microchem J.* 2025;212:113224.

doi: 10.1016/j.microc.2025.113224

134. Han XL, Jiang NJ, Hata T, Choi J, Du YJ, Wang YJ. Deep learning based approach for automated characterization of large marine microplastic particles. *Mar Environ Res.* 2023;183:105829.

doi: 10.1016/j.marenvres.2022.105829

135. Thammasanya T, Patiam S, Rodcharoen E, Chotikarn, P. A new approach to classifying polymer type of microplastics based on Faster-RCNN-FPN and spectroscopic imagery under ultraviolet light. *Sci Rep.* 2024;14:3529.

doi: 10.1038/s41598-024-53251-5

136. Liu Y, Sun P, Wergeles N, Shang Y. A Survey and performance evaluation of deep learning methods for small object detection. *Expert Syst Appl.* 2021;172:114602.

doi: 10.1016/j.eswa.2021.114602

137. Girshick R. Fast R-CNN. In: *Proceedings of the IEEE International Conference on Computer Vision.* Santiago, Chile. 2015. p. 1440-1448.

doi: 10.1109/ICCV.2015.169

138. Redmon J, Divvala S, Girshick R, Farhadi A. You only look once: Unified, real-time object detection. In: *Proceedings of the IEEE Conference on Computer Vision and Pattern Recognition*. 2016. p. 779-788.

doi: 10.1109/CVPR.2016.91

139. Liu W, Anguelov D, Erhan D, *et al*. SSD: Single Shot MultiBox detector. In: *Computer Vision–ECCV 2016: 14th European Conference, Amsterdam, the Netherlands,* 2016. p. 21-37.

doi: 10.1007/978-3-319-46448-0_2

140. Long J, Shelhamer E, Darrell T. Fully Convolutional Networks for Semantic Segmentation. In: *Proceedings of the IEEE conference on Computer Vision and Pattern Recognition.* 2015. p. 3431-3440.

doi: 10.48550/arXiv.1411.4038

141. He K, Gkioxari G, Dollár P. Girshick R. "Mask R-CNN". In: *IEEE International Conference on Computer Vision (ICCV)*, Venice, Italy. 2017. p. 2980.

doi: 10.1109/ICCV.2017.322

142. Lorenzo-Navarro J, Castrillón-Santana M, Sánchez-Nielsen E, *et al*. Deep learning approach for automatic microplastics counting and classification. *Sci Total Environ.* 2021;765:142728.

doi: 10.1016/j.scitotenv.2020.142728

143. Frère L, Paul-Pont I, Moreau J, *et al*. A semi-automated Raman micro-spectroscopy method for morphological and chemical characterizations of microplastic litter. *Mar Pollut Bull.* 2016;113(1-2):461-468.

doi: 10.1016/j.marpolbul.2016.10.051

144. Zhang L, Shao S. Image-based machine learning for materials science. *J Appl Phys*. 2022:132(10):7381.

doi: 10.1063/5.0087381

145. Wu P, Wang B, Lu Y, et al. Machine Learning-Assisted Insights into Sources and Fate of Microplastics in Wastewater Treatment Plants. *ACS ES&T Water*. 2023; 4(3): 1107-1118.

doi: 10.1021/acsestwater.3c00386.

146. Joutey NT, Bahafid W, Sayel H, El Ghachtouli N. Biodegradation: Involved microorganisms and genetically engineered microorganisms. *InTech eBooks*. 2013;1:289-320.

doi: 10.5772/56194

147. Arpia AA, Chen WH, Ubando AT, Naqvi SR, Culaba AB. Microplastic degradation as a sustainable concurrent approach for producing biofuel and obliterating hazardous environmental effects: A state-of-the-art review. *J Hazard Mater.* 2021;418:126381.

doi: 10.1016/j.jhazmat.2021.126381

148. Pan Y, Gao SH, Ge C, *et al*. Removing microplastics from aquatic environments: A critical review. *Environ Sci Ecotechnol.* 2022;13:100222.

doi: 10.1016/j.ese.2022.100222

149. Pathak VM. Review on the current status of polymer degradation: A microbial approach. *Bioresour Bioprocess.* 2017;4(1):1-31.

doi: 10.1186/s40643-017-0145-9

150. Thomas BT, Olanrewaju-Kehinde DSK, Popoola OD. James ES. Degradation of plastic and polythene materials by some selected microorganisms isolated from soil. *World Appl Sci J*. 2015;33(12):1888-1891.

151. Auta HS, Emenike CU, Fauziah SH. Screening of *Bacillus* strains isolated from mangrove ecosystems in Peninsular Malaysia for microplastic degradation. *Environ Pollut.* 2017;231:1552-1559.

doi: 10.1016/j.envpol.2017.09.043

152. Shahnawaz M, Sangale MK. Ade AB. Rhizosphere of Avicennia marina (Forsk.) Vierh. as a landmark for polythene degrading bacteria. *Environ Sci Pollut Res Int.* 2016; 23: 14621-14635.

doi: 10.1007/s11356-016-6542-3.

153. Kale SK, Deshmukh AG, Dudhare MS. Patil VB. Microbial degradation of plastic: A review. *J Biochem Technol.* 2015;6(2):952-961.

154. Kumari A, Rajput VD, Mandzhieva SS, et al. Microplastic pollution: an emerging threat to terrestrial plants and insights into its remediation strategies. *Plants.* 2022; 11(3): 340. doi: 10.3390/plants11030340.

155. Nasrabadi AE, Ramavandi B, Bonyadi Z. Recent progress in biodegradation of microplastics by *Aspergillus* sp. in aquatic environments. *Colloid Interface Sci Commun.* 2023;57:100754.

doi: 10.1016/j.colcom.2023.100754

156. Barone GD, Ferizović D, Biundo A, Lindblad P. Hints at the applicability of microalgae and cyanobacteria for the biodegradation of plastics. *Sustainability.* 2020;12(24):10449.

doi: 10.3390/su122410449

157. Hadiyanto H, Khoironi A, Dianratri I, Suherman S, Muhammad F, Vaidyanathan S. Interactions between polyethylene and polypropylene microplastics and *Spirulina* sp. microalgae in aquatic systems. *Heliyon*. 2021;7(8):e07676.

doi: 10.1016/j.heliyon.2021.e07676

158. Di Rocco G, Taunt HN, Berto M, *et al*. A PETase enzyme synthesised in the chloroplast of the microalga *Chlamydomonas reinhardtii* is active against post-consumer plastics. *Sci Rep.* 2023;13(1):10028.

doi: 10.1038/s41598-023-37227-5

159. Bacha A, Nabi I, Zaheer M, Jin W, Yang L. Biodegradation of macro-and micro-plastics in environment: A review on mechanism, toxicity, and future perspectives. *Sci Total Environ.* 2023;858:160108.

doi: 10.1016/j.scitotenv.2022.160108

160. Ameen F, Moslem M, Hadi S, Al-Sabri AE. Biodegradation of low-density polyethylene (LDPE) by Mangrove fungi from the red sea coast. *Prog Rubber Plast Recycl Technol*. 2015;31(2):125-143.

doi: 10.1177/147776061503100204

161. Devi RS, Kannan VR, Nivas D, Kannan K, Chandru S, Antony AR. Biodegradation of HDPE by *Aspergillus* spp. from marine ecosystem of Gulf of Mannar, India. *Mar Pollut Bull.* 2015;96(1-2):32-40.

doi: 10.1016/j.marpolbul.2015.05.050

162. Sowmya HV, Ramalingappa B, Krishnappa M, Thippeswamy B. Degradation of polyethylene by *Penicillium simplicissimum* isolated from local dumpsite of Shivamogga district. *Environ Dev Sustain.* 2015;17:731-745.

doi: 10.1007/s10668-014-9571-4

163. Lwanga EH, Thapa B, Yang X, *et al*. Decay of low-density polyethylene by bacteria extracted from earthworm's guts: A potential for soil restoration. *Sci Total Environ.* 2018;624:753-757.

doi: 10.1016/j.scitotenv.2017.12.144

164. Chia WY, Tang DYY, Khoo KS, Lup ANK, Chew KW. Nature's fight against plastic pollution: Algae for plastic biodegradation and bioplastics production. *Environ Sci Ecotechnol.* 2020;4:100065.

doi: 10.1016/j.ese.2020.100065

165. Urbanek AK, Rymowicz W, Mirończuk AM. Degradation of plastics and plastic-degrading bacteria in cold marine habitats. *Appl Microbiol Biotechnol.* 2018;102:7669-7678.

doi: 10.1007/00253-018-9195-y

166. Álvarez-Barragán J, Domínguez-Malfavón L, Vargas-Suárez M, González-Hernández R, Aguilar-Osorio G, Loza-Tavera H. Biodegradative activities of selected environmental fungi on a polyester polyurethane varnish and polyether polyurethane foams. *Appl Environ Microbiol.* 2016;82(17):5225-5235.

doi: 10.1128/aem.01344-16

167. Gutiérrez-Silva K, Capezza AJ, Gil-Castell O, Badia-Valiente JD. UV-C and UV-C/H2O-Induced abiotic degradation of films of commercial PBAT/TPS blends. *Polymers*. 2025;17(9):1173.

doi: 10.3390/polym17091173

168. Świderek K, Velasco-Lozano S, Galmés MÀ, *et al*. Mechanistic studies of a lipase unveil effect of pH on hydrolysis products of small PET modules. *Nat Commun*. 2023;14(1):3556.

doi: 10.1038/s41467-023-39201-1

169. Lambert S, Wagner M. Environmental performance of bio-based and biodegradable plastics: The road ahead. *Chem Soc Rev.* 2017;46(22):6855-6871.

doi: 10.1039/c7cs00149e

170. Krumov N, Atanasova N, Boyadzhieva I, *et al*. New halophilic community degrades plastics: A metagenomic study. *Fermentation*. 2025;11(4):227.

doi: 10.3390/fermentation11040227

171. Yan F, Wei R, Cui Q, Bornscheuer UT. Liu YJ. Thermophilic whole-cell degradation of polyethylene terephthalate using engineered *Clostridium thermocellum*. *Microb Biotechnol.* 2021;14(2):374-385.

doi: 10.1111/1751-7915.13580

172. Tournier V, Topham CM, Gilles A,et al. An engineered PET depolymerase to break down and recycle plastic bottles. *Nature*. 2020; 580(7802): 216-219.

doi: 10.1038/s41586-020-2149-4.

173. Dhali SL, Parida D, Kumar B, Bala K. Recent trends in microbial and enzymatic plastic degradation: A solution for plastic pollution predicaments. *Biotechnol Sustain Mater.* 2024;1(1):11.

doi: 10.1186/s44316-024-00011-0

174. Husain Z. *UAE's Plan to Ban Single-use Plastics by 2026: Everything You Need to Know*. Gulf News; 2025. Available from: https://gulfnews.com/living-in-uae/ask-us/uaes-plan-to-ban-single-use-plastics-by-2026-everything-you-need-to-know-1.500272559 [Last accessed on 2025 Oct 01].

175. Ministry of Environment, Water and Agriculture (MEWA). *Saudi Arabia Commits to Supporting Global Environmental Initiatives to Combat Marine Pollution*. NAAMA Electronic Services System Portal for the Environment, Water and Agricultural Sectors; 2025. Available from: https://www.mewa.gov.sa/en/mediacenter/news/pages/ennews249.aspx [Last accessed on 2025 Nov 11].

176. Riyadh Municipality. *Environmental Protection in KSA*. Riyadh: Riyadh Municipality (Gov.); 2025. Available from:

https://www.alriyadh.gov.sa/en/content/environmental-protection [Last accessed on 2025 Sep 29].

177. AlNemer AM. Examining the Kingdom of Saudi Arabia's tourism sector and assessing its potential contributions in achieving the Kingdom's Vision 2030. In: *ProQuest Dissertations and Theses*. [Doctoral dissertation, Pepperdine University]; 2024. p. 31331279. Available from: https://www.proquest.com/openview/74b33515b81431419be19685746c14b7/1?pq-origsite=gscholar&cbl=18750&diss=y [Last accessed on 2026 Jan 27].

178. Almadhi A, Abdelhadi A, Alyamani, R. Moving from linear to circular economy in Saudi Arabia: Life-cycle assessment on plastic waste management. *Sustainability.* 2023;15(13):10450.

doi: 10.3390/su151310450

179. Das TK, Basak S, Ganguly S. 2D nanomaterial for microplastic removal: A critical review. *Chem Eng J.* 2024;492:152451.

doi: 10.1016/j.cej.2024.152451

180. O'Brien S, Rauert C, Ribeiro F, *et al*. There's something in the air: a review of sources, prevalence and behavior of microplastics in the atmosphere. *Sci Total Environ*. 2023;874:162193.

doi: 10.1016/j.scitotenv.2023.162193

ACCSCIENCE PUBLISHING

Explora: Environment and Resource

REVIEW ARTICLE

Integrating algal consortia into domestic wastewater biorefineries: Mechanisms, efficiency, and circular economy perspectives

Sarah Khan, Anwesha Mondal, Shremayi Chatterjee, and Santanu Paul*

Department of Botany, Laboratory of Cell and Molecular Biology, University of Calcutta, Kolkata, West Bengal, India

Abstract

Urbanization is occurring on a large scale at an unprecedented pace. In this context, algal consortia represent a sustainable and environmentally friendly solution for domestic wastewater remediation. This review focuses on mixed algal consortia as a treatment approach for domestic wastewater containing organic and inorganic pollutants, including nitrogen, phosphorus, heavy metals, and other chemicals. These consortia demonstrate enhanced pollutant removal efficiencies through synergistic biosorption, bioaccumulation, and biodegradation mediated by multiple algal species. Indeed, algal biomass can be valorized in biorefineries to produce a range of resources, including biofuels, biopolymers, and organic phyco-fertilizers, thereby advancing the circular bioeconomy. Overall, this review positions algal consortia as a potentially low-cost platform that integrates wastewater remediation with bioresource recovery, promoting the transformation of urban ecosystems toward a greener, more resilient future.

Keywords: Algal consortia; Phycoremediation; Domestic wastewater; Biorefinery; Circular bioeconomy; Biosorption; Bioaccumulation; Sustainable wastewater treatment

***Corresponding author:**
Santanu Paul
(spbot@caluniv.ac.in)

Citation: Khan S, Mondal A, Chatterjee S, Paul S. Integrating algal consortia into domestic wastewater biorefineries: Mechanisms, efficiency, and circular economy perspectives. *Explora Environ Resour.* 2026;3(1):025460078. doi: 10.36922/EER025460078

Received: November 12, 2025

Revised: January 9, 2026

Accepted: January 22, 2026

Published online: February 20, 2026

1. Introduction

Algal consortia are complex living communities in which multiple algal species coexist and interact to enhance efficiency across processes, including wastewater treatment, biomass processing, bioenergy production, farming, and medical biotechnology.[1] Algae are adaptable photoautotrophic organisms that grow rapidly, sequester carbon dioxide, take up nutrients, and release valuable bioactive compounds, making them significant ecological resources for sustainability and environmental management.[2,3] Compared to monocultures, algal consortia exhibit improved nutrient removal potential, stability, and environment-responsive characteristics.[4] Phycoremediation uses micro- or macroalgae to remove or transform pollutants, such as toxic chemicals, from wastewater.[5] Heavy organic loads in municipalities generate nutrient-rich wastewater that is discharged into water bodies either untreated or only partially treated. Furthermore, the microalgal consortium used to treat wastewater is advantageous because it sequesters carbon and removes nutrients while generating high biomass.[6] Microalgal consortia can be applied to municipal wastewater and industrial effluents, and to certain waste-derived streams (e.g., leachates), under aerobic or anaerobic process configurations. Numerous studies

have examined the feasibility of using microalgae for wastewater treatment, including their use for nitrogen and phosphorus removal from effluents, commonly recognized as a driver of eutrophication when discharged into aquatic ecosystems.[7] Common wastewater treatment techniques are energy-intensive and not cost-effective in developing countries.[8] This review aims to shed light on the role of algal consortia in domestic wastewater remediation, the mechanisms of pollutant removal, and their potential integration into a circular bioeconomy framework. Furthermore, the paper offers suggestions for future research on the challenges that limit the deployment of algal consortia systems at scale and provides recommendations on their efficacy and sustainability.

2. Composition of domestic wastewater and algal systems for wastewater treatment

Domestic wastewater refers to household and residential wastewater (i.e., wastewater generated from toilets, kitchens, bathrooms, and floor drains in houses and similar residential buildings). Because domestic wastewater contains varying concentrations of carbon, nitrogen, and phosphorus, its organic and nutrient loads can be substantial. Several studies have explored the capacity and advantages of microalgal growth for treating wastewater from various sources and have reported on its potential and benefits.[9] Microalgal cultivation on sewage wastewater can enhance the removal efficiencies of nitrogen, carbon, and phosphorus, as well as pollutants, with lower environmental impacts (Figure 1). Globally, microalgal cultivation is being promoted as a sustainable alternative nutrient source, as the long-term application of chemical fertilizers is increasingly recognized as unsustainable and a contributor to land pollution.[10] Wastewater characterization typically includes measurements of physicochemical and biological parameters, including biochemical oxygen demand, chemical oxygen demand, dissolved oxygen, total solids, total suspended solids, total dissolved solids, total ammonium, total nitrate, soluble phosphorus, total phosphorus, total iron, total chlorine, total magnesium, total calcium, surface-active agents, electrical conductivity, pH, turbidity, total coliform, and heavy metals (Table 1). With regard to chemicals, sewage and domestic wastewater contain inorganic (30%) and organic (70%) substances, as well as various gases.[11] Organic compounds consist mainly of proteins, carbohydrates, and lipids that are indicators of human dietary habits. Inorganic materials include acids, bases, chlorides, trace elements, and toxic compounds. Various biotic and abiotic constituents and pollutants are present in home wastewater, including biodegradable organic materials and other organic matter.[12] Algal coexistence within consortia can generate both cooperative and competitive interactions[13]; metabolite exchange and other cross-feeding processes can increase biomass productivity and pollutant removal efficiency, improving system stability.[14] The effectiveness of algal consortia has been demonstrated across multiple wastewater types, and these systems may be more adaptable to changing environmental conditions (Table 2).

3. Mechanisms of domestic wastewater remediation by algal consortia

Understanding the mechanisms of nutrient removal by microalgae is essential for designing effective wastewater

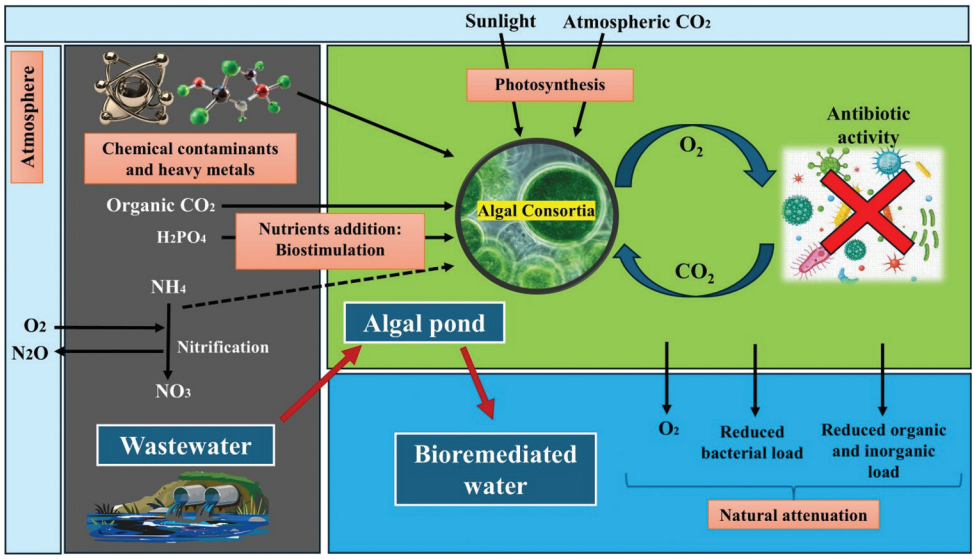

Figure 1. The schematic presentation of algal consortia being used as a bioremediation agent. Image created by the authors.

Table 1. Physico-chemical characteristics of domestic wastewater and their permissible standard limits

Physico-chemical and biological analysis parameters	Unit	Permissible standard limits	References
pH	-	6.0–9.0	4,8,15
Nitrate	mg/L	89.0–99.2	
Biochemical oxygen demand	mg/O_2/L	90.0–99.0	
Chemical oxygen demand	mg/O_2/L	85.0–99.8	
Total solids	gSS/M^3	83.0–97.0	
Total Kjeldahl nitrogen	gN/m^3	85.0–97.0	
Total carbon	gC/m^3	93.2–99.0	
Total phosphate	gP/m^3	86.0–98.0	
Phosphate	mg/L	85.0–98.0	

treatment systems. Suspended-cell cultivation-based systems have been predominantly used to treat domestic wastewater.[17] In immobilized-cell systems, microalgal cells are entrapped within a polymeric matrix, and substrates diffuse into and out of the matrix through its pores.[18] Integration of these systems with biopolymers has been reported to improve biomass yield, photosynthetic pigment production, and lipid accumulation. Organic substances present in wastewater during phycoremediation are converted into algal biomass through metabolic pathways that degrade carbohydrates, proteins, lipids, and other bioactive components (Table 3).[10] Microalgae use various remediation pathways, which can be classified into three main types: Biosorption, bioaccumulation, and biodegradation (Figures 2 and 3).[19]

Table 2. Reports of microalgal consortia and their effective removal efficiencies in organic wastewater

Sl. No	Algal consortia	Source	Wastewater parameter	Days	Efficiency (%)	References
1.	*Chlorella sorokiniana*, *Chlorella vulgaris*, *Scenedesmus obliquus*	Meat processing wastewater	COD	7 days	91	4
			TN		67	
			TP (PO_4^{3-})		69	
2.	*Chlorella saccharophila*, *Chlamydomonas pseudococcus*, *Scenedesmus* spp., *Neochloris oleoabundans*	Dairy wastewater	OD	7 days	82.60	4
			COD		88.90	
			TSS		88.25	
			TDS		77.23	
			TKN		98.33	
			Nitrogen (NH_4^+)		99.61	
			Nitrogen (NO_3^-)		96.97	
			Phosphorus (PO_4^{3-})		93.02	
3.	*Chlorella vulgaris*, *Chlorella protothecoides*	Municipal Wastewater	TN	7 days	35.4	4
			TP		74.4	
			TOC		22.2	
			COD		60.0	
			Orthophosphate		87.0	
4.	*Chlorella* spp., *Scenedesmus* spp., *Sphaerocystis* spp., *Arthrospira* spp.	Domestic wastewater	Phosphorus (PO_4^{3-})	7 days	53–100	4
			Nitrogen (NH_4^+)		39	
5.	*Phormidium* spp., *Chlorella pyrenoidosa*	Municipal wastewater	COD	7 days	53±2	4
			TAN		81±3	
			TP		75±2	
			Nitrogen (NO_3^-)		87±5	
6.	*Nostoc muscorum*, *Anabaena subcylindrica*	Sewage wastewater	Phosphorus (PO_4^{3-})	8 days	20.8–95	8
			Nitrogen (NO_3^-)		19.6–80	
			Nitrogen (NH_4^+)		20.9–96	
7.	*Chlorella* spp., *Merismopedia* spp., *Closteriopsis* spp., *Scenedesmus* spp.	Municipal wastewater	TP	-	98.28	4
			Nitrogen (NH_4^+)		88.23	
			Nitrogen (NO_3^-)		86.55	
			COD		82.45	
8.	*Oscillatoria pseudogeminata*, *O. proteus*, *O. trichoides*, and *Lyngbya ceylanica*	Dairy wastewater	pH	-	-	16

(Cont'd...)

Table 2. ***(Continued)***

Sl. No	Algal consortia	Source	Wastewater parameter	Days	Efficiency (%)	References
			Color			
			Odor			
			TDS			
			COD			
			BOD			
9.	Mixed algae culture of *Microspora* spp., *Navicula* spp., *Lyngbya* spp., *Cladophora* spp., *Spirogyra* spp., and *Rhizoclonium* spp.	Sewage wastewater	COD	8 days	683.6 mg/O_2/L	8
			BOD		389.8 mg/O_2/L	
			TSS		891.9 gSS/m^3	
			TDS		4,546.2 g/m^3	
			TP		20.9 mg/L	
			Nitrogen (NO_3^-)		11.7 mg/L	
			Phosphorus (PO_4^{3-})		9.4 mg/L	
			Sulfate ion		53.5 mg/L	
			Chloride ion		51.5 mg/L	
10.	*Ulothrix zonata*, *Ulothrix aequalis*, *Rhizoclonium hieroglyphicum*, and *Oedogonium* spp.	Dairy manure wastewater	TN	7 days	62	10
			TP		70	

Abbreviations: BOD: Biochemical oxygen demand; COD: Chemical oxygen demand; NH_4^+: Ammonium ion; NO_3^-: Nitrate ion; OD: Dissolved oxygen; PO_4^{3-}: Phosphate ion; TDS: Total dissolved solids; TKN: Total Kjeldahl nitrogen; TN: Total nitrogen; TOC: Total organic carbon; TP: Total phosphorus; TSS: Total suspended solids.

Table 3. Mechanisms of nutrient uptake into the algal biomass

Nutrients	Mechanisms of uptake into the algal biomass	References
Dissolved carbon dioxide	Integration into the Calvin cycle	20
Organic carbon	Integration into the respiratory metabolism pathways	21
Nitrogen	Fixation into ammonia, followed by conversion into amino acids	22
Nitrates and nitrites	Reduction into ammonium, followed by conversion into amino acids	23
Ammonium	Direct conversion into amino acids	24
Phosphorus	Phosphorylation and chemical precipitation	25

3.1. Biosorption

Biosorption is one of the earliest and most rapid mechanisms by which algal consortia remove contaminants from domestic wastewater. This process is largely physicochemical and occurs at the cell surface, without requiring metabolic energy. The outer wall of microalgae is rich in functional groups, such as hydroxyl, carboxyl, amino, phosphate, and sulfate moieties, that provide multiple binding sites for dissolved pollutants.[26] Through electrostatic attraction, ion exchange, complexation, and van der Waals forces, contaminants, including nutrients, heavy metals, dyes, and organic molecules, can be passively immobilized onto the algal surface.[27] A key characteristic of biosorption is its speed, as pollutant binding occurs almost immediately upon contact with the algal biomass. This makes biosorption particularly effective during the initial stages of wastewater treatment, especially under fluctuating or high pollutant loads.[28] In algal consortia, the diversity of cell wall compositions among species further enhances biosorption capacity by providing a broader range of binding sites than monocultures. The other major advantage of biosorption is that it does not rely on active metabolism, allowing both living and non-living algal biomass to participate in pollutant removal. This feature is especially beneficial in unfavorable environmental conditions, where algal growth may be limited. However, biosorption also has inherent limitations. The process is reversible, and changes in pH, ionic strength, or competing ions may lead to desorption of bound pollutants. Moreover, biosorption alone does not transform contaminants, but merely transfers them from the aqueous phase to the biomass, necessitating careful handling or downstream processing of the spent algal material.[29]

3.2. Bioaccumulation

Bioaccumulation is the active uptake and internalization of pollutants into algal cells and is therefore metabolically driven. Unlike biosorption, this mechanism requires living cells and energy-dependent transport systems. Pollutants first cross the cell membrane via diffusion, facilitated transport, or active transport, and are subsequently compartmentalized within cellular

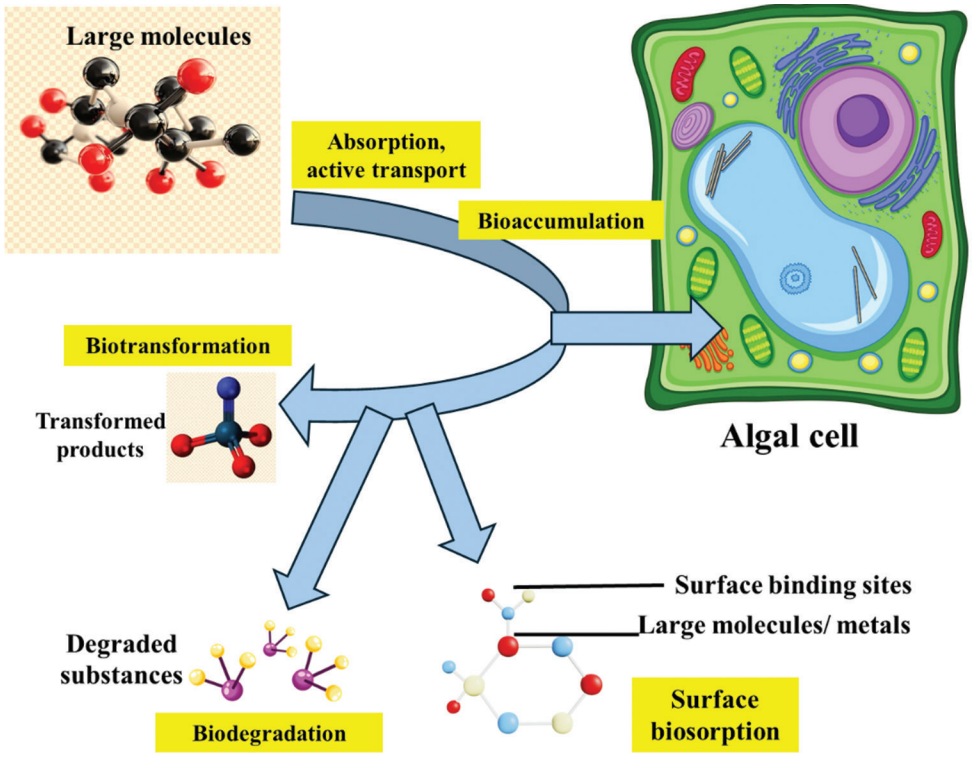

Figure 2. Mechanistic events during algal remediation. Image created by the authors.

organelles, such as vacuoles, chloroplasts, or the cytoplasm.[30] One defining feature of bioaccumulation is its selectivity, and algal cells regulate nutrient and certain contaminant uptake based on physiological demand and environmental stress. In domestic wastewater systems, bioaccumulation plays a critical role in the assimilation of nitrogen, phosphorus, and trace metals, which are incorporated into cellular components, including proteins, nucleic acids, and pigments. Exposure to toxic elements often induces oxidative stress, leading to the activation of antioxidant enzymes and metal-chelating molecules, thereby enabling detoxification while maintaining cellular function.[31]

The principal advantage of bioaccumulation lies in its ability to permanently remove pollutants from wastewater through intracellular sequestration and metabolic assimilation. In algal consortia, species-specific uptake capacities complement each other, resulting in enhanced overall remediation efficiency. This mechanism is constrained by algal growth rates and physiological tolerance thresholds. Excessive pollutant concentrations may inhibit cellular metabolism, reduce photosynthetic efficiency, or lead to cell death. In addition, bioaccumulation is inherently slower than biosorption, as it depends on active growth and cellular adaptation.[32]

3.3. Biodegradation

Biodegradation is the most complex and transformative mechanism of wastewater remediation by algal consortia. In this process, organic pollutants are enzymatically broken down into simpler, less toxic molecules that can be further metabolized or released as end products, such as carbon dioxide, water, or inorganic ions. Microalgae secrete a range of enzymes, including oxidoreductases, hydrolases, and oxygenases, that play a central role in degrading complex organic compounds, such as hydrocarbons, pharmaceuticals, and dyes.[33] A distinguishing characteristic of biodegradation is its integrative nature, as it often occurs alongside biosorption and bioaccumulation. Pollutants initially adsorbed to the cell surface or internalized into the cell may subsequently undergo enzymatic transformation. In algal consortia, interspecies interactions further enhance biodegradation, as different species contribute complementary enzymatic capabilities, creating a more robust and versatile degradation network.[9]

The major advantage of biodegradation is its capacity to detoxify pollutants rather than merely immobilizing them. This makes it particularly valuable for long-term wastewater treatment and environmental safety. Biodegradation is sensitive to environmental conditions such as light availability, oxygen concentration, pH, and temperature. The process is also slower compared to

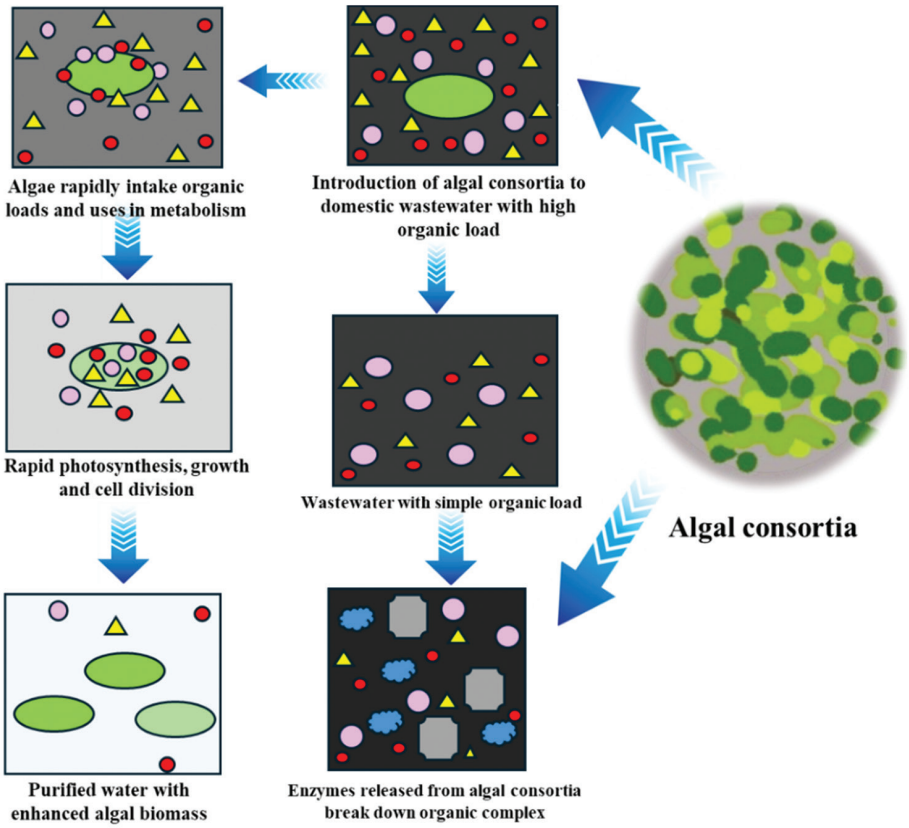

Figure 3. Holistic mechanism of using algal consortia in domestic wastewater treatment. Image created by the authors.

biosorption and may be inhibited by highly recalcitrant or toxic compounds. In addition, incomplete degradation can sometimes lead to the formation of intermediate byproducts, which may pose environmental risks if not fully mineralized.[34]

4. Efficiency comparison: Algal consortia versus monocultures

Microalgae are used to remove nutrients and contaminants from various types of domestic wastewaters. Because of environmental and nutrient-level variations, as well as contamination, it is challenging to maintain a continuous, stable monoculture throughout the entire operational cycle. Controlling pollutant concentrations, biomass production, and process stability in wastewater during treatment is difficult to achieve with monocultures. In contrast, the contributions of microalgal consortia surpass those of single-species systems in pollutant removal, biomass production, and process stability.[13] The biggest advantage of consortia is their metabolic diversity and functional complementarity (Figure 4). Different algal species have different nutrient uptake rates, growth rates, and pollutant tolerance. Together, these species have synergistic

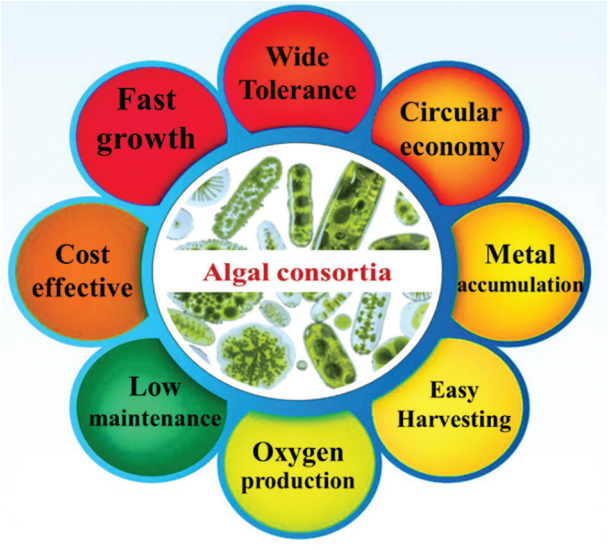

Figure 4. Advantages of using algal consortia. Image created by the authors.

interactions while simultaneously removing various contaminants, nitrogen, phosphorus, carbon compounds, and heavy metals. Mixed-algal systems are therefore capable of performing complex degradation processes that are

commonly inefficient in monocultures. Algal consortia are often more resilient to fluctuations in light, temperature, and pH, reducing the risk of invasion or culture collapse. This ecological stability can translate into more reliable biomass yield and temperature performance.[9] On the other hand, monocultures are susceptible to rapid collapse, for example, due to environmental stressors or biological activity. The heterogeneous physiological requirements and photosynthetic efficiencies of algal species enable consortia to use resources more effectively than individual species.[35] These collaborative exchanges can involve metabolites, signaling compounds, and growth-promoting substances, enabling greater nutrient removal and biomass accumulation. The most frequently used systems are naturally occurring prokaryotic and eukaryotic in aquatic settings or engineered for purpose-optimized performance.[10]

It is important to note that reported removal efficiencies across studies are strongly influenced by experimental design and operating conditions. Variations in wastewater composition, reactor configuration, light availability, hydraulic retention time, and cultivation scale make direct comparison of efficiency values challenging. Numerous high removal rates reported under laboratory conditions are achieved using synthetic or well-controlled wastewater, which may not fully reflect the complexity of real domestic effluents. Consequently, efficiency metrics should be interpreted within their experimental context rather than as universally comparable benchmarks. Recognizing these limitations is essential when assessing the scalability and reproducibility of algal consortia-based systems for practical wastewater treatment applications.

When comparing algal consortia with monocultures, the most meaningful difference lies not in, but how in quickly nutrients are removed under ideal conditions, but how reliably the system performs over time. Monocultures can show high removal efficiencies in controlled environments; however, their performance often becomes unstable when wastewater composition, light intensity, or temperature varies. In contrast, the algal consortia tend to buffer these variations because different species contribute complementary metabolic and physiological functions. When one species is stressed or temporarily underperforms, others can continue to sustain nutrient uptake and biomass production. This ecological balance reduces the risk of culture collapse and helps maintain the consistent removal of organic components. Consequently, for domestic wastewater treatment where influent quality is inherently variable, long-term stability, adaptability, and operational reliability become more relevant performance indicators than short-term peak efficiencies, making algal consortia a more practical choice than monocultures.

Figure 5. Different applications of biomass from algal consortia. Image created by the authors.

5. Valorization of biomass from algal consortia: The algal biorefinery approach

A biorefinery is a facility that uses algal biomass to produce bioenergy and value-added products. Waste-to-worth is the idea of using microalgae not only to capture nutrients from water bodies, but also to convert nutrient-rich algal biomass into useful products, thereby stimulating a circular bioeconomy.[36] On the other hand, there is a platform that develops sustainable technologies and could go one step beyond the "trash-to-cash" idea by producing industrially important renewable chemicals or minerals. In this section, details of several microalgae-derived biomass for valorization are discussed (Figure 5).

5.1. Feedstock potential of algal biomass

Algal biomass is referred to as a 3G feedstock because it has higher biomass productivity than plant-based lignocellulosic biomass. Previous studies focused on biodiesel production, but reported limitations, including low yield and high production cost.[37] Recently, research has focused on using algal biomass as a feedstock for multiple biobased products due to its high carbohydrate and protein content. A study reported that microalgal biomass mostly contains ash (5–17%), crude protein (18–46%), carbohydrates (18–46%), and crude lipid (12–48%) along with the embedded energy content of 19–27 MJ kg^{-1}.[38] Algae are a rich source of metabolically active compounds, including amino acids, carotenoids, lipids, fatty acids of dietary value, polysaccharides, and proteins.

Recent studies have identified antibacterial, antioxidant, anti-inflammatory, antitumor, and antiviral properties, in addition to the well-established finding that algal biomass itself serves as a dietary and nutrient source for food and feed standards.[39] Although algal carotenoids are secondary pigments, they possess therapeutic properties. The nutritional value of algal metabolites is notable, as they can replace animal protein and lipid sources in the aquaculture industry. *Arthrospira* and *Chlorella* are well known for their very high protein content, ranging from 50% to 70% of their dry weight, along with essential fatty acids, antioxidants, and micronutrients crucial for the health of livestock and fish.[27] Algal species have evolved carbon-concentrating mechanisms and can thrive in complex waste streams and polluted environments, making them promising bio-factories for biorefinery approaches. Algal fuels, including both liquid fuels (biodiesel and bioethanol) and gaseous fuels (biomethane, biogas), are renowned in global energy markets as a promising alternative to conventional fossil fuels.[40] The remarkable activities of algal biomass have upsurged its value in the global market, which has demanded intensive research on cultivation and valorization methods to attain a sustainable supply chain.

5.2. Biodiesel

Algal oleochemicals are a sustainable environmental solution for producing green energy (biodiesel) that integrates carbon dioxide sequestration and waste minimization through a biorefinery approach. Lipids, being low-value compounds, are used to produce a byproduct or for bioremediation, although biodiesel recovery is the primary target.[41] It is a liquid fuel derived from algal lipids and valorized through various conversion technologies such as transesterification and thermochemical conversion.[42,43] *Chlorella* spp. is among the most commercially used algae for biodiesel production and has been genetically modified in a few cases for enhanced lipid yield and carbon capture.[44] As a carbon-neutral fuel, algal biodiesel can effectively replace conventional fuels, thereby reducing harmful greenhouse gases in the atmosphere. Bioenergy supply chains could be improved by new and emerging technological platforms that process feedstock biomass into one or more forms of energy in a closed-loop system. In this way, algal biomass could be used to produce algal fuels and serve as a potential candidate in the green energy sector with biorefining value.[38]

5.3. Biohydrogen

Biohydrogen is a promising renewable energy carrier because it produces no direct carbon dioxide emissions at the point of use. After lipid recovery, delipidified microalgae residue (DMR) remains a rich source of carbohydrates and proteins, serving as an organic substrate for various hydrogen-producing microbes. DMRs undergo a harsh oil-extraction process and are therefore expected to be directly converted to hydrogen or other fuels after standard pre-treatment procedures.[41] Wieczorek *et al.*[45] investigated the potential of *Chlorella vulgaris* for the production of biohydrogen, wherein enzymatic pre-treatment of dry biomass (10 g volatile solids [VS] L^{-1}) resulted in sevenfold higher biohydrogen production (135 ± 3.11 mL hydrogen g^{-1} VS) than corresponding untreated biomass (19 ± 2.94 mL hydrogen g^{-1} VS). On the other hand, microalgal species such as *Chlamydomonas reinhardtii* can produce hydrogen in the presence of light due to the enzymatic activity of chloroplast [Fe]-hydrogenase.[46] Due to its high energy content (120 kJ g^{-1}) and sustainability, biohydrogen can be used as a "classic fuel" to support our energy infrastructure and to replace the current fossil-based fuels.

5.4. Biomethane

Biomethane, one of the major constituents of biogas, is produced by anaerobic digestion of organic wastes. Biogas generation from organic waste depends on the feedstock's carbon-to-nitrogen ratio. DMR has a high carbon-to-nitrogen ratio and is well-suited to methanogenic microbes for producing methane-rich biogas. Various algal species, such as *Nannochloropsis salina* and *C. variabilis*, have been applied.[47] Biomethane has a high calorific value and can enhance the biorefinery process. Biogas contains 70% methane, which can be used for cooking, heating, and lighting. It is a promising value-added product of microalgae biorefinery.[41,48]

5.5. Bioethanol

Bioethanol is considered a sustainable fuel because it is non-toxic and produced efficiently from renewable feedstocks. Delipidified biomass is a byproduct of algal industries. It acts as a potential source for bioethanol production. Enzymatic hydrolysis of raw or pre-treated DMR has yielded sugar at 37–43% (w/w). Bioethanol yield from DMR after saccharification and fermentation has been reported by various researchers, ranging from 0.14 to 0.26 g/g DMR.[45,49-52]

5.6. Biopolymers

DMR is an excellent source of biopolymers, such as polyhydroxybutyrate (PHB) and polyhydroxyalkanoates, which are important for their biodegradability, chemical diversity, biocompatibility, and production from renewable carbon resources.[53] Numerous strains, particularly cyanobacteria such as *Anabaena* spp., *Synechocystis* spp.,

and *Synechococcus* spp., can accumulate PHBs when cultivated in wastewater with PHB content ranging from 2.4% to 7.4% dry cell weight.[19] Furthermore, the biomass itself can serve as a source for developing starch-based bioplastics or as a reinforcing agent to enhance the properties of existing bioplastics through blending.

5.7. Algal metabolites

According to the Food and Agriculture Organization, algal proteins have high nutritional value and are competitive as food and feed ingredients.[54] Research has shown that marine algal polysaccharides have immense potential as a source of industrially viable and novel products. Polysaccharides are used worldwide as nutraceuticals, cosmeceuticals, pharmaceuticals, drug-delivery vehicles, fertilizers, and aquafeed.[55] Microalgae are sustainable sources of essential oils with large amounts of long-chain n-3 polyunsaturated fatty acids, omega-3 fatty acids, docosahexaenoic acid, and eicosapentaenoic acid, and moderate percentages of monounsaturated fatty acids and lesser amounts of saturated fatty acids. Vegan diets are low in vitamins, so algal foods are a source of folate, Vitamin B12, and niacin. *Chlorella pyrenoidosa* and *Arthrospira platensis* are largely cultured for the purpose of commercial Vitamin B.[56] Algae are rich in carotenoids; for example, *Dunaliella salina* and *A. platensis* have high carotenoid levels. Algal carotenoids act synergistically to prevent cellular damage in cancer patients, reduce cardiovascular disease risk, and lower blood cholesterol, and are used as antioxidants.[57]

5.8. Organic phyco-fertilizers

Algal biomass acts as an effective source of biofertilizer for food crops. Besides increasing the micronutrient availability in the soil, mainly iron, copper, zinc, and manganese, algal consortia can also enhance their organic-carbon content. This increase in soil quality is accompanied by higher grain yields and product quality, as the grains are more nutritious. For instance, Ferreira *et al.*[58] achieved significant improvement in root length and GI of some seed types (tomato, watercress, cucumber, soybean, wheat, and barley seeds) after application of the biomass of a microalgal consortium composed of *Tetradesmus obliquus*, *Chlorella protothecoides*, *C. vulgaris*, and *Synechocystis* spp. at 0.5 g/L. Microalgae utilization in sustainable agriculture is likely to be one of the most important applications of microalgal biomass in the short term, particularly for biomass cultivated from domestic wastewater in wastewater treatment and agriculture, and will also improve the economic feasibility of microalgal production and downstream processing.[59,60]

While algal consortia offer the dual benefits of wastewater remediation and biomass valorization, they also entail inherent trade-offs. High pollutant removal efficiency can sometimes lead to changes in biomass composition, such as altered lipid, carbohydrate, or protein content, which may affect the quality and yield of downstream products, such as biofuels, biopolymers, and fertilizers. Conversely, optimizing biomass for specific biorefinery applications may slightly compromise nutrient uptake or treatment performance. Understanding and balancing these interactions is crucial to designing consortia that effectively support circular bioeconomy frameworks without significantly sacrificing either remediation efficiency or product suitability.

6. Environmental and socioeconomic implications

Beyond nutrient removal, such systems contribute to environmental sustainability by reducing organic load, lowering greenhouse gas emissions through carbon sequestration, and enabling the recovery of water, nutrients, and biomass within a circular economy framework. From a socioeconomic perspective, algal consortia offer opportunities for decentralized, low-energy wastewater treatment, particularly in resource-limited regions, while simultaneously generating numerous value-added products. By linking wastewater remediation with resource recovery and local economic benefits, this approach aligns environmental protection with social and economic sustainability, making it a viable strategy for long-term urban and peri-urban water management.

Sustainability, based on the effective integration of product recovery and waste management, is a key element of the future bioeconomy, which relies on sustainable biological feedstocks and biotechnology methods for valorization, looped through biorefineries.[61] Microalgal biomass incorporation into bioprocesses increases carbon utilization and supports a sustainability-integrated, low-carbon economy. Growing algae in carbon dioxide-rich habitats reduces greenhouse gas emissions and produces renewable feedstocks for various purposes.[13] The fermentative valorization of algal biomass yields biorenewable resources that produce biofuels, such as hydrogen and methane, as well as renewable short-chain fatty acids. These may be used as biopolymer molecules to produce stable solids, such as biopolymers and carbon fixation, or as eco-compliant plastics for waste materials without the consumption of chemical substances. Algae possess the metabolic versatility to transform a single biomass into several value-added products.[62] Algal biomass is a valuable raw material for food, feed, and

fuel production, where renewability is a key requirement in sustainable sectors. Integrated algal processing can enable zero-waste, carbon-neutral technologies and lower reliance on synthetic metabolites and land-based crops.[5,13] In addition, algae are contributing to environmental remediation in their generation of renewable fuels with no sulfur, their removal of complex waste products, and storage of atmospheric and industrial carbon dioxide. Most fundamentally, algae may provide promising solutions to environmental challenges by generating clean, zero-sulfur, carbon-neutral renewable fuels and, eventually, by degrading complex waste streams and reducing the effects of a changing world by sequestering atmospheric carbon dioxide and industrial carbon dioxide emissions.[63] Algal biotechnologies integrated into wastewater treatment and bioresource recovery systems form the backbone of such a comprehensive solution—a model which combines environmental restoration, climate intervention, and socioeconomic progress, characteristics of a truly sustainable circular bioeconomy.

7. Challenges and limitations

While algal consortia have shown great potential for wastewater remediation and bioenergy production, they still pose numerous concerns surrounding their application. Growth optimization, biomass harvesting, and process scalability are major bottlenecks that prevent the implementation of cost-effective, energy-efficient approaches. Stable algal growth under variable wastewater conditions requires a balance among various physical, chemical, and biological parameters, including nutrient composition, light intensity, and hydraulic retention time.[64,65] Challenges remain in tuning these parameters for large-scale cultivation. Engineering synthetic or semi-synthetic algal consortia is an emerging approach to improve pollutant degradation efficiency.[66] Communities with at least one genetically altered strain would enable targeted changes in specific metabolic pathways that are required for nitrogen, phosphorus, or heavy metal removal. Yet, bioengineered systems require robust regulation and long-term ecological monitoring to ensure environmental safety and stability. A significant limitation also resides in the heterogeneity and complexity of wastewater composition. There is very little metabolic flexibility for one type of algal species to degrade or assimilate all types of contaminants. Therefore, selecting strains for consortium formation is important. Certain pollutants may block photosynthesis or inhibit enzyme activity, reducing remediation efficiency.[67] Furthermore, most efforts have taken place in laboratory environments; therefore, applying laboratory parameters to field-scale systems is limited by environmental variability, microbial contamination, and variable lighting or nutrient availability. Economic and technological limitations also exist for commercial algal cultivation. High operational costs, energy-intensive harvesting systems, and the use of costly chemical solvents for recovery pose the primary challenges. Efficient extraction of value-added metabolites from algal biomass requires cost-effective, environmentally friendly, and productive solvents.[68]

Despite promising laboratory- and pilot-scale outcomes, comprehensive life-cycle assessment and techno-economic analysis of algal consortia-based wastewater treatment systems remain limited. Most available studies focus on short-term performance metrics, while long-term operational stability, energy balance, and cost efficiency under real wastewater conditions are rarely evaluated. The scarcity of full-scale case studies further restricts direct assessment of economic feasibility and environmental trade-offs. Addressing these gaps through integrated life-cycle assessment-techno-economic analysis frameworks and extended field-scale investigations will be essential for translating algal consortia from experimental systems to reliable wastewater treatment technologies. Accordingly, the sustainability and cost-effectiveness of algal consortia should be viewed as potential outcomes rather than established attributes. While existing studies suggest promising environmental benefits and resource recovery opportunities, these advantages are strongly dependent on system design, operational scale, and local conditions. A cautious interpretation is therefore necessary until economic and systems-level assessments become widely available.

8. Future prospects and conclusion

Growing algal consortia in nutrient-rich domestic wastewater provides an environmentally sustainable solution for pollutant removal and waste disposal, generating usable biomass. Not only are environmental problems addressed, but valuable goods such as biofuels, biofertilizers, and organic soil boosters are also harvested. As algal consortia grow, their synergistic metabolic functions enable them to increase nutrient uptake and remove contaminants more efficiently compared to a single species. These cooperative communities convert wastewater into a living resource and provide environmental resilience. In the future, promising prospects include creating algal consortia that integrate species with complementary traits, such as metal-binding properties and nitrogen- or carbon-assimilation capabilities. This is important for understanding how these microorganisms interact with one another, how they conduct metabolic exchanges, and how they can also balance in common environments. Globally, the use of algal products is on the rise, as they

are widely used in nutrition, pharmaceuticals, energy, and agriculture. Algae are a highly suited biological solution for a waste-to-value-oriented next generation, equipped with the rapid expansion, carbon dioxide fixing, and valuable metabolite formation needed for exploitation. Advances in genetics, metabolic engineering, and process design enable us to more effectively extract pollutants, maximize biomass production, and recover energy and materials from waste streams. Microalgae also show promise as a pre-treatment step in wastewater treatment; they reduce the organic load and suspended solids before traditional treatment is required. Such systems can be embedded in existing infrastructure, making them environmentally friendly and cost-effective for water management. From a broader perspective, success in algal consortia will require sustained participation of researchers, engineers, and policymakers. Innovatively developed together and brought into the open with sufficient awareness, these living systems may pave the way for sustainable resource use.

This review demonstrates that algal consortia provide a stable and adaptable option for domestic wastewater treatment, largely because the coexistence of multiple algal species allows key remediation functions to be shared and sustained under variable conditions. Through the combined action of surface interactions, intracellular uptake, and enzymatic transformation, algal consortia can remove major nutrient loads and associated contaminants more consistently than single-species systems. At the same time, the biomass produced during treatment is a usable resource rather than residual waste, with demonstrated potential to be converted into bioenergy, biofertilizers, and other value-added products. Taken together, these features position algal consortia not simply as a treatment technology, but as a practical link between wastewater management and resource recovery, where environmental remediation and material reuse can be addressed within the same operational framework.

Acknowledgments

The authors acknowledge the institutional support from CAS Phase VII, DBT-BUILDER, and DST-FIST Level II, Department of Botany, University of Calcutta.

Funding

This work was supported by grants from the University Grants Commission, India (A.M. Fellow ID: 191620246470, Dec 2019) and CSIR-HRDG (S.C. Fellow ID: 09/0028(17403)/2024-EMR-I).

Conflict of interest

The authors declare that they have no competing interests.

Author contributions

Conceptualization: Anwesha Mondal
Visualization: Santanu Paul
Writing–original draft: Sarah Khan
Writing–review & editing: Anwesha Mondal, Shremayi Chatterjee

Ethics approval and consent to participate

Not applicable.

Consent for publication

Not applicable.

Availability of data

Not applicable.

References

1. Hena S, Fatimah S, Tabassum S. Cultivation of algae consortium in a dairy farm wastewater for biodiesel production. *Water Res Ind*. 2015;10:1-14.

   doi: 10.1016/j.wri.2015.02.002

2. Mondal A, Mukherjee A, Pal R. Phycosynthesis of nanoiron particles and their applications- a review. *Biocatal Agric Biotechnol*. 2024a;55:102986.

   doi: 10.1016/j.bcab.2023.102986.

3. Mondal A, Paul S, Pal R, Paul S. Nano iron loaded algal biomass: For better yield, amino acid and iron content in rice-a 'nano-phycofertilizer'. *Algal Res.* 2024b;81:103573.

   doi: 10.1016/j.algal.2024.103573

4. Gururani P, Bhatnagar P, Kumar V, Vlaskin MS, Grigorenko AV. Algal consortia: A novel and integrated approach for wastewater treatment. *Water.* 2022;14(22):3784.

   doi: 10.3390/w14223784

5. Dey I, Mondal A, Pal R. Algae-based systems for removal of emerging pollutants from sewage sludge. *Biotechnol Rem Emer Poll Wastew Sys.* 2025a:109-133.

   doi: 10.1007/978-981-96-3945-8_5

6. Dey I, Mondal A, Satpati GG, Pal R. Tannery wastewater remediation potential of cyanobacteria and algae with nutrient recovery, ecological monitoring and biomass valorization: A circular economy. *Nex Chem Eng.* 2025b;1:100009.

   doi: 10.1016/j.nxcen.2025.100009

7. Cai T, Park SY, Li Y. Nutrient recovery from wastewater streams by microalgae: Status and prospects. *Renew Sustain Energy Rev.* 2013;19:360-369.

   doi: 10.1016/j.rser.2012.11.030

8. Ahmad F, Khan AU, Yasar A. Comparative phycoremediation

of sewage water by various species of algae. *Proc Pak Acad Sci.* 2013;50(2):131-139.

9. Moondra N, Jariwala ND, Christian RA. Role of phycoremediation in domestic wastewater treatment. *Water Conserv Manag.* 2021;5(2):66-70.

   doi: 10.26480/wcm.02.2021.66.70

10. Gonçalves AL, Pires JC, Simões M. A review on the use of microalgal consortia for wastewater treatment. *Algal Res.* 2017;24:403-415.

    doi: 10.1016/j.algal.2016.11.008

11. Koul B, Yadav D, Singh S, Kumar M, Song M. Insights into the domestic wastewater treatment (DWWT) regimes: A review. *Water.* 2022;14(21):3542.

    doi: 10.3390/w14213542

12. Manasa RL, Mehta A. Wastewater: Sources of pollutants and its remediation. In *Environmental Biotechnology*. Vol. 2. Berlin: Springer; 2020. p. 197-219.

    doi: 10.1007/978-3-030-38196-7_9

13. Dey I, Mukherjee C, Pal R. Impact of tannery wastewater treatment plant effluent on phytoplankton community of receiving stream heading to the Indian Sundarbans. *Inland Water Biol.* 2024;17(1):71-81.

    doi: 10.1134/S199508292401019X

14. Thakur TK, Barya MP, Dutta J, *et al*. Integrated phytobial remediation of dissolved pollutants from domestic wastewater through constructed wetlands: An interactive macrophyte-microbe-based green and low-cost decontamination technology with prospective resource recovery. *Water*. 2023;15(22):3877.

    doi: 10.3390/w15223877

15. Mahapatra DM, Chanakya HN, Ramachandra TV. Bioremediation and lipid synthesis through mixotrophic algal consortia in municipal wastewater. *Bioresour Technol.* 2014;168:142-150.

    doi: 10.1016/j.biortech.2014.03.130

16. Chahal S, Bhandari R. Cyanobacterial phycoremediation: A sustainable approach to dairy wastewater management. *Environ Technol.* 2025;46:3077-3089.

    doi: 10.1080/09593330.2025.2453947

17. Cheng J, Qiu Y, Huang R, Yang W, Zhou J, Cen K. Biodiesel production from wet microalgae by using graphene oxide as solid acid catalyst. *Bioresour Technol*. 2016;221:344-349.

    doi: 10.1016/j.biortech.2016.09.064

18. Cheah YT, Chan DJC. A methodological review on the characterization of microalgal biofilm and its extracellular polymeric substances. *J Appl Microbiol*. 2022;132(5):3490-3514.

    doi: 10.1111/jam.15455

19. Diankristanti PA, Ng IS. Marine microalgae for bioremediation and waste-to-worth valorization: Recent progress and prospects. *Blue Biotechnol.* 2024;1(1):10.

    doi: 10.1186/s44315-024-00010-w

20. Li P, Wang D, Hu Z, *et al*. Insight into the potential mechanism of bicarbonate assimilation promoted by mixotrophic in CO_2 absorption and microalgae conversion system. *Chemos*. 2024;349:140903.

    doi: 10.1016/j.chemosphere.2023.140903

21. Neilson AH, Lewin RA. The uptake and utilization of organic carbon by algae: An essay in comparative biochemistry. *Phycol.* 1974;13(3):227-264.

    doi: 10.2216/i0031-8884-13-3-227.1

22. Kumar A, Bera S. Revisiting nitrogen utilization in algae: A review on the process of regulation and assimilation. *Biores Technol Rep.* 2020;12:100584.

    doi: 10.1016/j.biteb.2020.100584

23. Vega JM, Menacho A, León J. Nitrate assimilation by microalgae. *Trends Photochem Photobiol*. 1991;2:69-111.

24. Taylor MW, Barr NG, Grant CM, Rees TAV. Changes in amino acid composition of Ulva intestinalis (Chlorophyceae) following addition of ammonium or nitrate. *Phycol* 2006;45(3):270-276.

    doi: 10.2216/05-15.1

25. Larsdotter K, Jansen JLC, Dalhammar G. Biologically mediated phosphorus precipitation in wastewater treatment with microalgae. *Environ Technol.* 2007;28(9):953-960.

    doi: 10.1080/09593332808618855

26. Banerjee S, Lahiri R, Choudhury AK, *et al*. Unraveling the potential of cyanobacteria as food and investigating its production and nutritional properties. *Biocatal Agric Biotechnol*. 2024;62:103421.

    doi: 10.1016/j.bcab.2024.103421

27. Chen Z, Osman AI, Rooney DW, Oh WD, Yap PS. Remediation of heavy metals in polluted water by immobilized algae: Current applications and future perspectives. *Sustain*. 2023;15(6):5128.

    doi: 10.3390/su15065128.

28. Zabochnicka-Świątek M, Krzywonos M. Potentials of biosorption and bioaccumulation processes for heavy metal removal. *Pol J Environ Studies*. 2014:23(2):551-561.

29. Bilal M, Rasheed T, Sosa-Hernández JE, Raza A, Nabeel F, Iqbal HM. Biosorption: An interplay between marine algae and potentially toxic elements-a review. *Mar Drugs*. 2018;16(2):65.

    doi: 10.3390/md16020065

30. Doshi H, Seth C, Ray A, Kothari IL. Bioaccumulation of heavy metals by green algae. *Curr Microbiol.* 2008;56(3):246-255.

    doi: 10.1007/s00284-007-9070-z

31. Ali AY, Idris AM, Eltayeb MA, El-Zahhar AA, Ashraf IM. Bioaccumulation and health risk assessment of toxic metals in red algae in Sudanese Red Sea coast. *Tox Rev.* 2021;40(4):1327-1337.

doi: 10.1080/15569543.2019.1697886

32. Flouty R, Estephane G. Bioaccumulation and biosorption of copper and lead by a unicellular algae *Chlamydomonas reinhardtii* in single and binary metal systems: A comparative study. *J Environ Manage*. 2012;111:106-114.

doi: 10.1016/j.jenvman.2012.06.042

33. Mathew MM, Khatana K, Vats V, *et al*. Biological approaches integrating algae and bacteria for the degradation of wastewater contaminants-a review. *Front Microbiol.* 2022;12:801051.

doi: 10.3389/fmicb.2021.801051

34. Wang M, Zhang W, He T, Rong L, Yang Q. Degradation of polycyclic aromatic hydrocarbons in aquatic environments by a symbiotic system consisting of algae and bacteria: Green and sustainable technology. *Arc Microbiol.* 2024;206(1):10.

doi: 10.1007/s00203-023-03734-2

35. Mugnai S, Derossi N, Hendlin Y. Algae communication conspecific and interspecific: The concepts of phycosphere and algal-bacteria consortia in a photobioreactor (PBR). *Plant Signal Behav.* 2023;18(1):2148371.

doi: 10.1080/15592324.2022.2148371

36. Shukla M, Kumar S. Algal biorefineries for biofuels and other value-added products. In: *Biorefining of Biomass to Biofuels.* Berlin: Springer; 2017. p. 305-341.

doi: 10.1007/978-3-319-67678-4_14

37. Mishra VK, Goswami R. A review of production, properties and advantages of biodiesel. *Biofuels*. 2018;9(2):273-289.

doi: 10.1080/17597269.2017.1336350

38. Kumar AN, Yoon JJ, Kumar G, Kim SH. Biotechnological valorization of algal biomass: An overview. *Syst Microbiol Bioman.* 2021;1(2):131-141.

doi: 10.1007/s43393-020-00012-w

39. Wu JY, Tso R, Teo HS, Haldar S. The utility of algae as sources of high value nutritional ingredients, particularly for alternative/complementary proteins to improve human health. *Front Nut.* 2023;10:1277343.

doi: 10.3389/fnut.2023.1277343

40. John SU, Onu CE, Ezechukwu CMJ, Nwokedi IC, Onyenanu CN. Multi-product biorefineries for biofuels and value-added products: Advances and future perspectives. *Acad Green Ener*. 2025;2(1):1-39.

doi: 10.20935/AcadEnergy7605

41. Sarma S, Sharma S, Rudakiya D, *et al*. Valorization of microalgae biomass into bioproducts promoting circular bioeconomy: A holistic approach of bioremediation and biorefinery. *3 Biotech.* 2021;11(8):378.

doi: 10.1007/s13205-021-02911-8

42. Elliott DC. Review of recent reports on process technology for thermochemical conversion of whole algae to liquid fuels. *Algal Res.* 2016;13:255-263.

doi: 10.1016/j.algal.2015.12.002

43. Zhou Y, Hu C. Catalytic thermochemical conversion of algae and upgrading of algal oil for the production of high-grade liquid fuel: A review. *Catalysts.* 2020;10(2):145.

doi: 10.3390/catal10020145

44. Chi NTL, Duc PA, Mathimani T, Pugazhendhi A. Evaluating the potential of green alga *Chlorella* sp. For high biomass and lipid production in biodiesel viewpoint. *Biocatal Agric Biotechnol*. 2019;17:184-188.

doi: 10.1016/j.bcab.2018.11.011

45. Wieczorek N, Kucuker MA, Kuchta K. Fermentative hydrogen and methane production from microalgal biomass (*Chlorella vulgaris*) in a two-stage combined process. *Appl Energy.* 2014;132:108-117.

doi: 10.1016/j.apenergy.2014.07.003

46. Wang Y, Yang H, Zhang X, Han F, Tu W, Yang W. Microalgal hydrogen production. *Small Met.* 2020;4(3):1900514.

doi: 10.1002/smtd.201900514

47. Naaz F, Bhattacharya A, Pant KK, Malik A. Investigations on energy efficiency of biomethane/biocrude production from pilot scale wastewater grown algal biomass. *Appl Energy.* 2019;254:113656.

doi: 10.1016/j.apenergy.2019.113656

48. Zhu L, Li Z, Hiltunen E. Theoretical assessment of biomethane production from algal residues after biodiesel production. *Energy Environ.* 2018;7(1):273.

doi: 10.1002/wene.273

49. Cheng HH, Whang LM, Wu SH. Enhanced bioenergy recovery from oil-extracted microalgae residues via twoidues H2/CH4 or H2/butanol anaerobic fermentation. *Biotechnol J.* 2016;11(3):375-383.

doi: 10.1002/biot.201500285

50. Goo BG, Baek G, Choi DJ, *et al*. Characterization of a renewable extracellular polysaccharide from defatted microalgae *Dunaliella tertiolecta*. *Biores Technol.* 2013;129:343-350.

doi: 10.1016/j.biortech.2012.11.077

51. Lam MK, Tan IS, Lee KT. Utilizing lipid-extracted microalgae biomass residues for maltodextrin production. *Chem Eng.* 2014;235:224-230.

doi: 10.1016/j.cej.2013.09.023

52. Mirsiaghi M, Reardon KF. Conversion of lipid-extracted

Nannochloropsis salina biomass into fermentable sugars. *Algal Res.* 2015;8:145-152.

doi: 10.1016/j.algal.2015.01.013

53. Vicente D, Proença DN, Morais PV. The role of bacterial polyhydroalkanoate (PHA) in a sustainable future: A review on the biological diversity. *Int J Environ Res Public Health.* 2023;20(4):2959.

doi: 10.3390/ijerph20042959

54. Koyande AK, Show PL, Guo R, Tang B, Ogino C, Chang JS. Bio-processing of algal bio-refinery: A review on current advances and future perspectives. *Bioengineered.* 2019;10(1):574-592.

doi: 10.1080/21655979.2019.1679697

55. Benalaya I, Alves G, Lopes J, Silva LR. A review of natural polysaccharides: Sources, characteristics, properties, food, and pharmaceutical applications. *Int J Mol Sci.* 2024;25(2):1322.

doi: 10.3390/ijms25021322

56. Durdakova M, Kolackova M, Ridoskova A, *et al*. Exploring the potential nutritional benefits of *Arthrospira* maxima and *Chlorella vulgaris*: A focus on vitamin B_{12}, amino acids, and micronutrients. *Food Chem.* 2024;452:139434.

doi: 10.1016/j.foodchem.2024.139434

57. Uma VS, Usmani Z, Sharma M, *et al*. Valorization of algal biomass to value-added metabolites: Emerging trends and opportunities. *Phytochem Rev.* 2023;22(4):1015-1040.

doi: 10.1007/s11101-022-09805-4

58. Ferreira A, Bastos CR, Marques-Dos-Santos C, Acién-Fernández FG, Gouveia L. Algaeculture for agriculture: From past to future. *Front Agron*. 2023;5:1064041.

doi: 10.3389/fagro.2023.1064041

59. Sabnam S, Mondal A, Paul S. Advancing seed priming with algal extracts: A review of mechanistic roles in seed germination and plant growth. *Explor Environ Res.* 2025;2(2):025120025.

doi: 10.36922/EER025120025

60. Mondal A, Sabnam S, Paul S. Sirocladium kumaoense derived iron nanoparticles as a biopriming agent for enhanced early growth of rice seedlings. *J Appl Phycol*. 2025;37:1-15.

doi: 10.1007/s10811-025-03680-0

61. Maina S, Kachrimanidou V, Koutinas A. A roadmap towards a circular and sustainable bioeconomy through waste valorization. *Curr Opin Green Sustain*. 2017;8:18-23.

doi: 10.1016/j.cogsc.2017.07.007

62. Leong YK, Chang JS. Bioprocessing for production and applications of bioplastics from algae. In: *Biomass Biofuels Biochem*. Netherlands: Elsevier; 2022. p. 105-132.

doi: 10.1016/B978-0-323-96142-4.00008-7

63. Ghosh D, Hossain S. Role of sustainable bioenergy and green fuels in building climate-resilient futures. *In: Climate Resilience: Impact of Quantum Computing and Artificial Intelligence on Urban Planing.* Berlin: Springer; 2025. p. 257-274.

doi: 10.1007/978-3-032-06791-3_13

64. Rani S, Gunjyal N, Ojha CSP, Singh RP. Review of challenges for algae-based wastewater treatment: Strain selection wastewater characteristics abiotic and biotic factors. *J Hazard Toxic Radioact Waste.* 2021;25(2):03120004.

doi: 10.1061/(ASCE)HZ.2153-5515.0000578

65. Malik R, Saleem S, Basharat M, Bhatti MF, Sheikh Z. Effect of hydraulic retention time on wastewater treatment and microalgal growth at low light intensity. *Algal Res.* 2024;80:103545.

doi: 10.1016/j.algal.2024.103545

66. Zhang TY, Hu HY, Wu YH, *et al*. Promising solutions to solve the bottlenecks in the large-scale cultivation of microalgae for biomass/bioenergy production. *Renew Sustain Energy Rev.* 2016;60:1602-1614.

doi: 10.1016/j.rser.2016.02.008

67. Petsas AS, Vagi MC. Effects on the photosynthetic activity of algae after exposure to various organic and inorganic pollutants. In: *Chlorophy*. London: InTechOpen; 2017. p. 37.

doi: 10.5772/67991

68. Monfet E, Unc A. Defining wastewaters used for cultivation of algae. *Algal Res.* 2017;24:520-526.

doi: 10.1016/j.algal.2016.12.008

ACCSCIENCE PUBLISHING

Explora: Environment and Resource

PERSPECTIVE ARTICLE

Biological carbon sequestration in constructed wetlands: A nature-based strategy for climate mitigation and wastewater treatment

Basundhara Lenka* and **Dipta Gosh**

Department of Biotechnology, School of Biotechnology, Kalinga Institute of Industrial Technology, Bhubaneswar, Odisha, India

Abstract

Constructed wetlands are engineered ecosystems composed of substrates, vegetation, and microorganisms that serve as a sustainable alternative for wastewater treatment. Despite their benefits, greenhouse gas emissions continue to pose a challenge. Consequently, increasing research efforts focus on developing cleaner strategies to reduce overall global warming potential while enhancing carbon sequestration. This perspective outlines the current status of carbon sequestration and wastewater treatment, highlighting the close coupling between pollutant removal and carbon cycling. It also describes existing limitations and explores future prospects.

Keywords: Carbon sequestration; Constructed wetlands; Greenhouse gas emissions; Pollutants; Wastewater treatment

***Corresponding author:**
Basundhara Lenka
(lenkabasundhara@gmail.com)

Citation: Lenka B, Gosh D. Biological carbon sequestration in constructed wetlands: A nature-based strategy for climate mitigation and wastewater treatment. *Explora Environ Resour*. 2026;3(1):025480082. doi: 10.36922/EER025480082

Received: November 29, 2025

Revised: January 02, 2026

Accepted: January 05, 2026

Published online: January 26, 2026

1. Introduction

Wetlands are found across diverse landscapes and may contain either permanent or temporary shallow water. Their soils, substrates, and biological communities are specially adapted to flooding and waterlogging, which promotes the development of anaerobic conditions.[1] Wetlands occupy approximately 5–8% of the Earth's land surface. They typically consist of freshwater, soil, vegetation such as macrophytes and microphytes, and diverse microbial communities.[2]

Wetlands are generally classified into two categories: Natural wetlands and constructed (man-made) wetlands. The most widely used classification systems categorize wetlands into five types: marine (coastal wetlands), estuarine (including mangrove swamps, deltas, and tidal marshes), lacustrine (associated with lakes), riverine (along rivers and streams), and palustrine (bogs and swamps). These divisions are based on hydrological, ecological, biological, and environmental characteristics.[2]

Wetland vegetation plays a key role in wastewater treatment, as plants can directly absorb nutrients from the water, thereby enhancing the overall efficiency of contaminant removal. Natural wetlands—such as wet grasslands, mangroves, and salt marshes—are characterized by static or flowing water, and their soils are rich in carbon (C), functioning as major C sinks. These ecosystems also serve as hotspots for biogeochemical cycling of C.[3] The C sequestration rate of wetlands, expressed as the amount of C stored per

hectare per year, ranks just below that of forests and is comparable to agroecosystems.[4] In coastal wetlands, frequent tidal inundation alters the environment and slows the decomposition of plant organic matter, which can enhance long-term C retention; however, site-specific hydrodynamics can also limit soil C density.[5] Studies have shown that methane (CH_4) fluxes from natural wetlands (15.6–49.5 mg CH_4/m^2/day) are substantially higher than those observed in disturbed wetlands (−1.4–4.0 mg CH_4/m^2/day).[4] Despite these emissions, natural wetlands remain prominent C sequesters, underscoring the importance of their protection in the context of a growing global population.

In contrast, constructed wetlands (CWs) are engineered systems designed to harness natural processes involving soils, vegetation, and associated microbial communities for wastewater treatment.[6] For instance, vertical flow CWs equipped with gravel substrates achieve less than 50% removal of emerging organic contaminants, including acesulfame, carbamazepine, benzotriazole, and naproxen.[7] Similarly, Muduli *et al.*[8] reported that a baffled horizontal subsurface-flow CW efficiently removed the following contaminants: Chemical oxygen (O_2) demand (COD; 68.1%), total suspended solids (86.5%), total phosphorus (64.8%), total nitrogen (N) (78.25%), and NH_4^+–N (95.2%). CWs generally exhibit shorter C accumulation periods and lower soil C density compared with coastal wetlands. However, due to the high net primary productivity of wetland plants and the continuous input of organic matter and nutrients from wastewater, CWs achieve high C sequestration rates in soil, resulting in considerable C storage potential.[5]

As roots release C and N, they stimulate microbial activity in the soil. These interactions often lead wetlands to function as C sinks, where C storage exceeds C release. The root zone, or rhizosphere, is defined as the soil region influenced by hydraulic, chemical, and microbial processes associated with roots and has been shown to enhance immobilization of contaminants.[9] CWs are recognized as crucial systems for wastewater treatment, where the influx of diverse pollutants often creates redox gradient that can increase CH_4 emissions, and under certain conditions, promote N_2O production, thereby contributing to global warming.[10]

Research on wetlands primarily focuses on their ecological functions, conservation, biodiversity, water quality improvement, nutrient cycling, and ecosystem restoration. This perspective highlights the critical role of CWs as platforms for both wastewater treatment and biological C sequestration. However, their net climate benefit is constrained by greenhouse gas (GHG) emissions, particularly N_2O and CH_4. Addressing these trade-offs through essential design and management measures is necessary to maximize climate mitigation while ensuring the primary treatment function remains intact.

2. CW designs and their functional variants

CWs are established according to specific guidelines to function as buffer zones, protecting aquatic ecosystems and nearby species from both point and non-point source pollution.[11] CWs for C sequestration are primarily classified into free-water-surface flow and subsurface-flow systems. A hybrid system can also be created by combining these two designs. The classification of these wetlands generally depends on the water flow path and the type of vegetation planted.[12] Floating treatment wetlands replicate natural floating islands using buoyant platforms planted with emergent vegetation.[13]

In surface flow CWs, water moves through open channels with diverse vegetation, where factors such as depth, plant types, and flow velocity influence C storage and treatment efficiency.[14] Subsurface flow CWs include horizontal and vertical systems. In horizontal subsurface flow wetlands, wastewater flows beneath the substrate through porous media, passing through O_2-rich and anoxic zones that enhance pollutant removal.[12] Vertical subsurface flow CWs use gravel or sand beds with intermittent batch feeding; "fill-and-drain" operations improve contact between wastewater and microbes, increasing purification efficiency.[1] Vertical subsurface flow CWs are widely applied for domestic, dairy, landfill leachate, and food processing wastewater, requiring less space than horizontal systems. Variants include vertical upflow and downflow configurations.[12,13] While effective, vertical systems face challenges such as clogging under high wastewater loads.

3. Wetland ecosystems as carbon sinks and sources

Wetlands serve as major hotspots for C sequestration. Water saturation creates anoxic conditions that slow decomposition and lead to the accumulation of total soil C. However, alterations in evapotranspiration and precipitation patterns can significantly influence C cycling in CWs.[15] C sequestration is further mediated by vegetation through photosynthesis, in which atmospheric carbon dioxide (CO_2) is converted into glucose and subsequently transformed into complex compounds such as cellulose and lignin, which are deposited in plant tissues. Thus, it is essential to understand the potential of C sequestration in CWs while simultaneously addressing C emissions.[4]

Some studies report that wetlands acquire 200 times more C in soils than in vegetation. C can accumulate rapidly as organic matter, while anoxic conditions

slow decomposition, increasing C residence time and reducing C losses through mineralization. The potential of C sequestration through wetland restoration has been estimated at approximately 0.4 ton C/ha/year over a 50-year period, based on direct system measurements.[2] CH_4 emissions in CWs occur through three primary pathways: Molecular diffusion, ebullition, and plant-mediated transport through aerenchyma. Among these, plant-mediated release is the dominant process, accounting for approximately 70% of total CH_4 emissions. Ebullition contributes nearly three times more flux than diffusion. Plant transport occurs either by diffusion or by faster convective processes, which deliver O_2 to the roots while venting microbial byproducts to the atmosphere.[16] Figure 1 provides an overview of C sequestration in CWs.

During CH_4 transport in CWs, oxidation can occur through either anaerobic or aerobic pathways, influencing overall fluxes. Aerobic oxidation, carried out by methanotrophic bacteria, converts CH_4 into CO_2 at zones where CH_4 and O_2 overlap, including the water–air interface, substrate–air interface, rhizosphere, and internal plant tissues,[17] depending on O_2 availability.[18] This process is regarded as the principal CH_4 sink in wetland systems and is capable of oxidizing more than 50% of CH_4 production in CWs.[19]

Anaerobic oxidation of methane (AOM) refers to the microbial oxidation of CH_4 in the absence of oxygen, utilizing alternative electron acceptors such as sulfate (sulfate-reduction-dependent AOM), metal oxides like Fe^{3+} and Mn^{4+}, and nitrite or nitrate (nitrite-dependent AOM), as well as through direct interspecies electron transfer.[20,21] Although often overlooked, AOM is increasingly recognized as an important CH_4 sink. For instance, Guerrero-Cruz *et al.*[21] demonstrated that AOM reduced CH_4 emissions by more than 50% in freshwater wetlands. It is also estimated that wetlands are significant C sinks, sequestering around 830 Tg C/year.

Since CWs have been shown to sequester more C than natural wetlands, it is essential for researchers to investigate the factors influencing C storage in these systems, particularly those that can reduce CH_4 emissions. Ma *et al.*[22] demonstrated that CWs act as both C sources and sinks, thereby contributing to the global warming potential. For example, in most intact wetlands (about 67%) where CH_4 fluxes remain low, the initial surge of CH_4 released during wetland establishment is offset over time by continuous CO_2 uptake, resulting in a net CO_2-equivalent C sink. By contrast, intact wetlands with high CH_4 fluxes act as net C sources, although their cumulative source strength increases only modestly over a 500-year timescale.

Similarly, CH_4 emissions at the Lankheet CW varied with temperature and vegetation density, averaging 7.8 mg/m²/h at 15°C and increasing to 24.5 mg/m²/h at 24°C. When expressed as CO_2 equivalents, the wetland still functions as a net CO_2 sink under current conditions, with an annual sequestration rate of 0.27–2.4 kg/m²/year. This represents 12–67% of the C fixed in plant biomass.[23]

To ensure maximum societal, environmental, and economic benefits, comprehensive management plans tailored to different CW types and functions should be developed, accounting for both their ecological services and cost-saving potential.

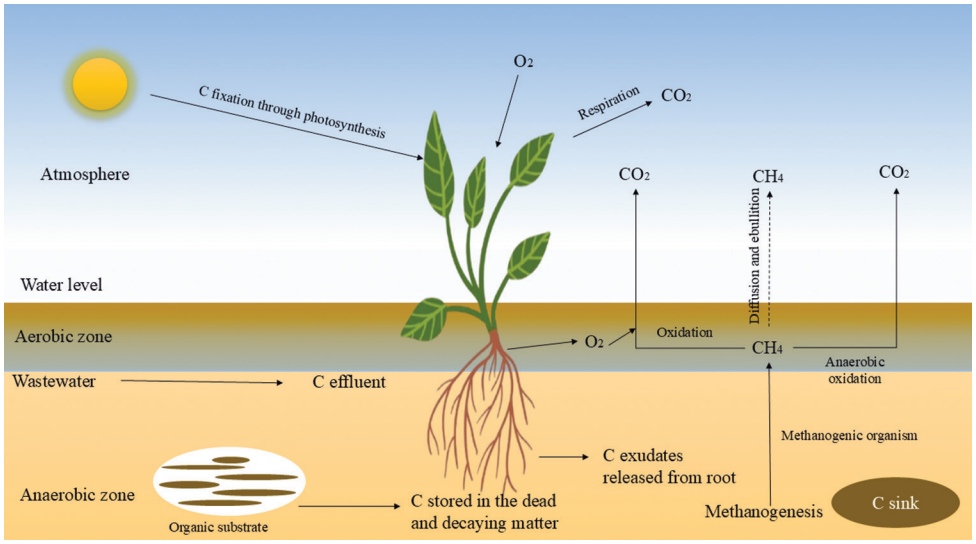

Figure 1. Overview of carbon (C) sequestration in constructed wetlands. Image created by authors using Microsoft powerpoint (version 2019).

4. Dynamics of CWs in wastewater treatment

CWs have emerged as a versatile, nature-based technology for wastewater treatment. Recent advances include hybrid configurations for enhanced N removal, targeted removal of specific contaminants, reactive media for phosphorus retention, characterization of microbial communities, and hydraulic modeling.[24] Growing demand for NH_4^+–N removal has accelerated the adoption of hybrid CWs, which demonstrate superior performance compared to single-unit systems. CWs have been applied not only to municipal sewage but also to industrial effluents from tanneries, wineries, composting facilities, and aquaculture. Researchers have highlighted the effectiveness of CWs in removing emerging pollutants, such as linear alkylbenzenesulfonates and pharmaceutical or personal care products, underscoring them as a sustainable, nature-based solution for diverse wastewater streams.[1]

For instance, Li *et al.*[25] reported that phytoremediation in CWs is regarded as an effective secondary wastewater treatment approach for pharmaceutical contaminants, particularly within decentralized systems. Their study examined rhizosphere dynamics and the associated microbial communities, demonstrating that the removal of pharmaceutical compounds such as ibuprofen occurs through the co-metabolism of root exudates, including lipids, fatty acids, amino acids, and organic acids. Furthermore, they established a positive correlation between rhizosphere microbial activity and COD, indicating that COD serves as a C source that supports microbial nutrition and enhances pollutant degradation.

Microbes, including cyanobacteria, algae, and heterotrophic microorganisms, are collectively referred to as periphyton and are located on the submerged surfaces of aquatic plants. They can account for the removal of up to approximately 90% of contaminants from wastewater; in turn, aquatic vegetation provides nutrients to the microbial community.[12] In addition, the selection of suitable bed material supports vegetation growth and biofilm formation, playing a crucial role in wastewater treatment.[12]

Zhang *et al.*[26] reported that CWs provide C sequestration and wastewater treatment simultaneously. For example, a system planted with *Trema orientalis* achieved high pollutant removal efficiencies, reducing NH_4^+–N by 89.07%, COD by 79.32%, total phosphorus by 66.33%, and total N by 98.31%. At the same time, C fixation was enhanced, with a sequestration capacity of 1,806.94 g C/m^2/year. GHG fluxes included CH_4 at 2.37 mg/m^2/h (14.35%), CO_2 at 362.69 mg/m^2/h (81.36% of global warming potential), and N_2O at 0.07 mg/m^2/h (4.29%). These findings highlight that nutrient removal from wastewater directly fuels plant growth and microbial activity, thereby enhancing C storage while simultaneously influencing net GHG emissions. This demonstrates that wastewater purification and C cycling are tightly coupled, with hydrophytes driving both pollutant removal and C sequestration.

Furthermore, CWs have been widely explored to decontaminate nitrogenous substances through processes such as denitrification, anaerobic ammonia oxidation (anammox), and dissimilatory nitrate reduction to ammonium (DNRA). The efficient removal of N is mediated by rhizospheric microbes, including anaerobic, aerobic, and anoxic bacteria.[27] Nitrification occurs near the rhizosphere due to radial oxygen loss mediated by root activities, while denitrification is facilitated in the non-rhizosphere zone under anaerobic conditions. Recent evidence suggests that DNRA and anammox processes are hindered in the rhizosphere. This inhibition is linked to the presence of humic acid-like substances in root exudates and the accumulation of hydroxylamine during ammonia oxidation, which interferes with anammox activity and the expression of key functional genes.

In addition, the disruption of the symbiotic relationship between anammox and DNRA microorganisms further contributes to reduced N cycling efficiency in the rhizosphere.[27] Moreover, wastewater management through CWs facilitates nutrient recovery, promotes the reuse of treated effluent, and enables the extraction of valuable byproducts; it is also economically sustainable compared to conventional treatment infrastructure, thereby advancing the principles of the circular bioeconomy and supporting urban irrigation[24] (Figure 2). The key findings are summarized in Table 1, which presents selected studies demonstrating the role of CWs in wastewater treatment and C sequestration.

5. Challenges and future scope

Advanced CWs are widely recognized as reliable technologies for treating a broad range of wastewater types. However, limitations remain, particularly the relatively low efficiency of phosphorus removal, which must be considered when selecting treatment technologies. Earlier concerns regarding their safety and dependability have largely been dispelled. In addition, studies have demonstrated that CWs perform efficiently even under cold climatic conditions, and their relatively modest land requirements make them suitable for use in densely populated countries such as Denmark and the Netherlands.[38] CWs are also increasingly harnessed for their ability to mitigate non-point source pollution from agricultural runoff and livestock effluents,

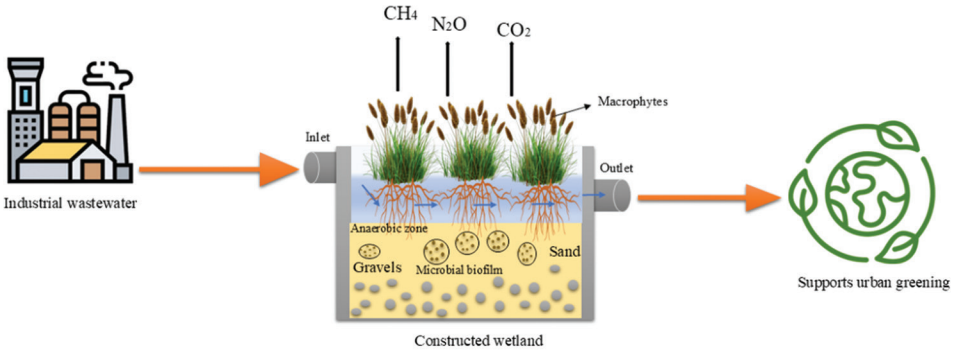

Figure 2. Representation of wastewater treatment through constructed wetlands. Image created by the authors by Microsoft power point (version 2019).

Table 1. Key findings on constructed wetlands for wastewater treatment and carbon sequestration

Key finding (s)	References
Restored inundated wetlands function as potential carbon sinks; however, their sequestration efficiency is influenced by restoration design, operational practices, and vegetation cover, with implications for climate change mitigation.	28
Coastal wetlands have a strong potential for carbon sequestration, but their efficiency is influenced by climate change, nitrogen inputs, vegetation management, and conservation practices.	29
The Zoige alpine wetland functions as a carbon sink; however, degradation alters environmental factors, reducing its sequestration efficiency.	30
Wetlands in West Bengal act as stronger carbon sinks than upland sites, storing 48.53–143.17 Mg C/ha in soils, with sequestration potential varying by wetland type and positively correlated with macrophyte coverage.	31
Montane fen wetlands in Korea act as significant carbon sinks (58.29–125.31 g C/m^2/y; 14.13–138.00 t C), with sequestration strongly influenced by dominant plant species (notably *Sphagnum palustre*) and reduced by disturbance, underscoring the importance of vegetation composition and conservation in wetland restoration.	32
In the Hangzhou Bay coastal wetlands, long-term reclamation (>1,000 years) increases surface soil carbon storage, with agricultural soils exhibiting the highest organic carbon content due to fertilization. However, SOC declines with depth, highlighting the importance of careful land management during early reclamation stages to minimize carbon loss.	33
CWs vegetated with *Pistia stratiotes* achieved significant pollutant removal (BOD=82%, total dissolved solids=83%, COD=81%, chloride=80%, sulfate=77%, TSS=82%, oil and grease=74%, and NH_3=84%), improved pH by 11.9%, and enhanced color and odor, with optimum treatment at 30 day hydraulic retention time. The effluent met national standards for irrigation use, and the system proved economical with minimal maintenance.	34
A pilot-scale CW-microbial fuel cell system using *Typha angustifolia* achieved high COD removal (97.56% in fedbatch; 82.8% in continuous mode) and enhanced bioelectricity generation (up to 58.55 mW/m^2, 229.6–283.3 mA/m^2) through auxiliary terracotta-based separator–electrode assemblies, demonstrating improved energetics and wastewater treatment efficiency.	35
Long-term monitoring of nature-based solutions in Italy showed that CWs and lagoon systems can improve reclaimed water quality for agricultural reuse, with CWs more effective at nitrogen removal (3.4 mg/L) and phosphorus removal (0.4 mg/L). However, further reductions in *Escherichia coli* (~100 CFU/100 mL), BOD (<25 mg/L), and TSS (up to 40 mg/L in the lagoon system) are needed to meet EU 2020/741 class A standards.	36
The novel biological-CW–microalgal wastewater process (sequencing batch reactor+CW+microalgal photobioreactor) achieved high PAH removal (90.58–97.50%), with adsorption dominating the removal of high-molecular-weight PAHs and microbial degradation increasing for lower-molecular-weight PAHs. Although toxic substituted PAHs formed during degradation, the microalgal unit removed 75.37–88.52% PAHs and 99.56–100% substituted PAHs via cytochrome P_{450} activity, reducing bacterial toxicity by 90.93% and genotoxicity by 93.08%. This highlights the critical role of microalgae in water security and the need to address the ecotoxicity of degradation byproducts.	37

Abbreviations: BOD: Biochemical oxygen demand; CFU: Colony-forming unit; COD: Chemical oxygen demand; CW: Constructed wetland; PAH: Polycyclic aromatic hydrocarbon; SOC: Soil organic carbon; TSS: Total soluble solid.

even under challenging conditions such as high altitudes. However, they still encounter significant challenges related to variable pollutant loads, climatic fluctuations, and long-term operational stability, highlighting the need for future designs that optimize treatment performance while ensuring environmental sustainability. In addition, tailored management strategies for different types and functions of CWs should be formulated to maximize their

societal, environmental, and economic benefits, while accounting for the ecological services and cost savings they can provide.

6. Conclusion

CWs are engineered systems that can achieve relatively low net C emissions while enhancing C sequestration, thereby reducing the C footprint and mitigating GHG emissions. In addition, they improve water quality by removing contaminants such as pharmaceuticals, antiseptics, and organic matter. Future designs must address current challenges, particularly phosphorus removal efficiency, resilience to climate change, and long-term operational stability. Optimizing hydrophyte selection and microbial communities will be critical to simultaneously enhance pollutant removal and C sequestration while minimizing CH_4 emissions. By integrating these approaches, CWs can provide resilient ecosystem services, improve water security, and safeguard communities when their deployment is supported by policies that tackle global climate change.

Acknowledgment

The authors acknowledge Kalinga Institute of Industrial Technology for support and encouragement in preparing this perspective article.

Funding

None.

Conflict of interest

The authors declare that they have no competing interests.

Author contributions

Conceptualization: All authors
Visualization: Basundhara Lenka
Writing–original draft: All authors
Writing–review & editing: Basundhara Lenka

Ethics approval and consent to participate

Not applicable.

Consent for publication

Not applicable.

Availability of data

Not applicable.

References

1. Vymazal J. Constructed wetlands for wastewater treatment: Five decades of experience. *Environ Sci Technol*. 2011;45(1):61-69.

   doi: 10.1021/es101403q

2. Chandra P, Enespa KM. Contribution of microbes in the renovation of wetlands. In: *Restoration of Wetland Ecosystem: A Trajectory Towards a Sustainable Environment*. Singapore: Springer Singapore; 2019. p. 101-124.

   doi: 10.1007/978-981-13-7665-8_8

3. Nag SK, Ghosh BD, Das BK, Sarkar UK. Wetlands function as carbon sink: Evaluation of few floodplains of middle Assam, Northeast India in the perspective of climate change. *J Environ Manage*. 2025;373:123841.

   doi: 10.1016/j.jenvman.2024.123841

4. Were D, Kansiime F, Fetahi T, Cooper A, Jjuuko C. Carbon sequestration by wetlands: A critical review of enhancement measures for climate change mitigation. *Earth Syst Environ*. 2019;3(2):327-340.

   doi: 10.1007/s41748-019-00094-0

5. Zhang Y, Zhang X, Fang W, *et al*. Carbon sequestration potential of wetlands and regulating strategies response to climate changes. *Environ Res*. 2025;269:120890.

   doi: 10.1016/j.envres.2025.120890

6. Wang Q, Xie H, Ngo HH, *et al*. Microbial abundance and community in subsurface flow constructed wetland microcosms: Role of plant presence. *Environ Sci Pollut Res Int*. 2016;23(5):4036-4045.

   doi: 10.1007/s11356-015-4286-0

7. Chen N, Zhang J, Hu Z, *et al*. Performance and mechanisms of reactive substrates in constructed wetlands: Emerging contaminant removal and greenhouse gas mitigation-a comprehensive review. *J Water Proc Eng*. 2025;69:106653.

   doi: 10.1016/j.jwpe.2024.106653

8. Muduli M, Choudharya M, Ray S. A review on constructed wetlands for environmental and emerging contaminants removal from wastewater: Traditional and recent developments. *Environ Dev Sustain*. 2024;26(12):30181-30220.

   doi: 10.1007/s10668-023-04190-0

9. Kaplan DI, Xu C, Huang S, *et al*. Unique organic matter and microbial properties in the rhizosphere of a wetland soil. *Environ Sci Technol*. 2016;50(8):4169-4177.

   doi: 10.1021/acs.est.5b05165

10. Du Y, Pan K, Yu C, *et al*. Plant diversity decreases net global warming potential integrating multiple functions in microcosms of constructed wetlands. *J Clean Prod*. 2018;184:718-726.

    doi: 10.1016/j.jclepro.2018.02.273

11. Rodgers JH, Dunn A. Developing design guidelines for constructed wetlands to remove pesticides from agricultural runoff. *Ecol Eng*. 1992;1(1-2):83-95.

doi: 10.1016/0925-8574(92)90026-X

12. Thakur TK, Barya MP, Dutta J, *et al*. Integrated phytobial remediation of dissolved pollutants from domestic wastewater through constructed wetlands: An interactive macrophyte-microbe-based green and low-cost decontamination technology with prospective resource recovery. *Water*. 2023;15(22):3877.

    doi: 10.3390/w15223877

13. Stefanakis AI. The role of constructed wetlands as green infrastructure for sustainable urban water management. *Sustainability*. 2019;11(24):6981.

    doi: 10.3390/su11246981

14. Vymazal J. Removal of nutrients in various types of constructed wetlands. *Sci Total Environ*. 2007;380(1-3):48-65.

    doi: 10.1016/j.scitotenv.2006.09.014

15. Moomaw WR, Chmura GL, Davies GT, *et al*. Wetlands in a changing climate: Science, policy and management. *Wetlands*. 2018;38(2):183-205.

    doi: 10.1007/s13157-018-1023-8

16. Yin X, Jiang C, Xu S, *et al*. Greenhouse gases emissions of constructed wetlands: Mechanisms and affecting factors. *Water*. 2023;15(16):2871.

    doi: 10.3390/w15162871

17. Bonetti G, Trevathan-Tackett SM, Hebert N, Carnell PE, Macreadie PI. Microbial community dynamics behind major release of methane in constructed wetlands. *Appl Soil Ecol*. 2021;167:104163.

    doi: 10.1016/j.apsoil.2021.104163

18. Wu H, Zhao Q, Gao Q, *et al*. Human activities inducing high CH4 diffusive fluxes in an agricultural river catchment in subtropical China. *Sustainability*. 2020;12(5):2114.

    doi: 10.3390/su12052114

19. Thauer RK. Functionalization of methane in anaerobic microorganisms. *Angew Chem Int Ed Engl*. 2010;49(38): 6712-6713.

    doi: 10.1002/anie.201002967

20. Wegener G, Krukenberg V, Riedel D, Tegetmeyer HE, Boetius A. Intercellular wiring enables electron transfer between methanotrophic archaea and bacteria. *Nature*. 2015;526(7574):587-590.

    doi: 10.1038/nature15733

21. Guerrero-Cruz S, Vaksmaa A, Horn MA, Niemann H, Pijuan M, Ho A. Methanotrophs: Discoveries, environmental relevance, and a perspective on current and future applications. *Front Microbiol*. 2021;12:678057.

    doi: 10.3389/fmicb.2021.678057

22. Ma S, Creed IF, Badiou P. New perspectives on temperate inland wetlands as natural climate solutions under different CO_2-equivalent metrics. *NPJ Clim Atmos Sci*. 2024;7(1):222.

    doi: 10.1038/s41612-024-00778-z

23. De Klein JJ, Van Der Werf AK. Balancing carbon sequestration and GHG emissions in a constructed wetland. *Ecol Eng*. 2014;66:36-42.

    doi: 10.1016/j.ecoleng.2013.04.060

24. Emeka UC, Chikwendu OC. Circular economy in wastewater management: Water reuse and resource recovery strategies. *Int J Latest Tech Eng Manage Appl Sci*. 2025;14(3):128-136.

    doi: 10.51583/IJLTEMAS.2025.140300016

25. Li Y, Lian J, Wu B, Zou H, Tan SK. Phytoremediation of pharmaceutical-contaminated wastewater: Insights into rhizobacterial dynamics related to pollutant degradation mechanisms during plant life cycle. *Chemosphere*. 2020;253:126681.

    doi: 10.1016/j.chemosphere.2020.126681

26. Zhang Y, Zhang X, Wang M, *et al*. Greenhouse gas emissions and carbon sequestration capacity of constructed wetlands with different hydrophytes. *J Water Proc Eng*. 2025;76:108292.

    doi: 10.1016/j.jwpe.2025.108292

27. Hu X, Xie J, Xie H, *et al*. Towards a better and more complete understanding of microbial nitrogen transformation processes in the rhizosphere of subsurface flow constructed wetlands: Effect of plant root activities. *Chem Eng J*. 2023;463:142455.

    doi: 10.1016/j.cej.2023.142455

28. Valach AC, Kasak K, Hemes KS, *et al*. Productive wetlands restored for carbon sequestration quickly become net CO_2 sinks with site-level factors driving uptake variability. *PLoS One*. 2021;16(3):e0248398.

    doi: 10.1371/journal.pone.0248398

29. Hao Q, Song Z, Zhang X, *et al*. Organic blue carbon sequestration in vegetated coastal wetlands: Processes and influencing factors. *Earth Sci Rev*. 2024;255:104853.

    doi: 10.1016/j.earscirev.2024.104853

30. Yang A, Kang X, Li Y, *et al*. Alpine wetland degradation reduces carbon sequestration in the Zoige Plateau, China. *Front Ecol Evol*. 2022;10:980441.

    doi: 10.3389/fevo.2022.980441

31. Nag SK, Das Ghosh B, Nandy S, Aftabuddin M, Sarkar UK, Das BK. Comparative assessment of carbon sequestration potential of different types of wetlands in lower Gangetic basin of West Bengal, India. *Environ Monit Assess*. 2023;195(1):154.

    doi: 10.1007/s10661-022-10729-x

32. Yu HY, Kim SH, Kim JG. Carbon sequestration potential in montane wetlands of Korea. *Glob Ecol Conserv*.

2022;37:e02166.

doi: 10.1016/j.gecco.2022.e02166

33. Wang F, Wang T, Gustave W, Wang J, Zhou Y, Chen J. Spatial-temporal patterns of organic carbon sequestration capacity after long-term coastal wetland reclamation. *Agric Ecosyst Environ*. 2023;341:108209.

doi: 10.1016/j.agee.2022.108209

34. Ali M, Aslam A, Qadeer A, *et al*. Domestic wastewater treatment by Pistia stratiotes in constructed wetland. *Sci Rep*. 2024;14(1):7553.

doi: 10.1038/s41598-024-57329-y

35. Kumar VK, Mohan KM, Manangath SP, Gajalakshmi S. Innovative pilot-scale constructed wetland-microbial fuel cell system for enhanced wastewater treatment and bioelectricity production. *Chem Eng J*. 2023;460:141686.

doi: 10.1016/j.cej.2023.141686

36. Mancuso G, Lavrnić S, Canet-Martí A, *et al*. Performance of lagoon and constructed wetland systems for tertiary wastewater treatment and potential of reclaimed water in agricultural irrigation. *J Environ Manage*. 2023; 348:119278.

doi: 10.1016/j.jenvman.2023.119278

37. Lu J, Zhang J, Xie H, *et al*. Transformation and toxicity dynamics of polycyclic aromatic hydrocarbons in a novel biological-constructed wetland-microalgal wastewater treatment process. *Water Res*. 2022;223:119023.

doi: 10.1016/j.watres.2022.119023

38. Rosli FA, Lee KE, Goh CT, *et al*. The use of constructed wetlands in sequestrating carbon: An overview. *Nat Environ Pollut Technol*. 2017;16(3):813-819.

ACCSCIENCE PUBLISHING

Explora: Environment and Resource

ORIGINAL RESEARCH ARTICLE

Synergistic GO/MgO nanocomposites with enhanced charge separation for photocatalytic dye degradation

Irfan Toqeer†*, Tahreem Fatima†, Muhammad Afzaal, and Abdul Ghuffar

Department of Physics, Faculty of Engineering and Applied Sciences, Riphah International University, Faisalabad, Punjab, Pakistan

Abstract

The development of efficient and chemically stable photocatalysts with improved charge separation is critical for the remediation of dye-contaminated wastewater. In this study, graphene oxide–magnesium oxide (GO/MgO) nanocomposites with ultralow GO loadings (0–0.05 wt.%) were synthesized through a co-precipitation route and evaluated for ultraviolet (UV)-driven methylene blue (MB) degradation. X-ray diffraction (XRD) results were consistent with the retention of the cubic MgO phase (JCPDS 45-0946) with crystallite refinement from 20.26 to 13.26 nm, while the slight peak-position variations were more consistent with interfacial strain than definitive lattice substitution. UV–visible diffuse reflectance spectra revealed a red shift and bandgap reduction from 5.11 to 4.71 eV. Fourier transform infrared (FTIR) and Raman spectra showed GO-related functional signatures and a decrease in the I_D/I_G ratio (0.886 → 0.830), suggesting strengthened interfacial interactions with increasing GO loading. The optimized 0.05 wt.% GO/MgO sample achieved 91.6% MB degradation within 180 min and exhibited a 5.24-fold enhancement in the apparent pseudo-first-order rate constant (k = 0.00290 min^{-1}) relative to pristine MgO (0.01518 min^{-1}). Photocatalytic efficiency was maximized at pH 7–9 with a catalyst dosage of 0.75 g L^{-1}, and post-reaction XRD/FTIR analysis indicated good structural stability. The enhancement is attributed to crystallite refinement and GO–MgO interfacial charge-transfer pathways inferred from consistent structural/optical–kinetic correlations.

Keywords: Graphene oxide; Magnesium oxide; Nanocomposites; Photocatalysis; Charge separation; Dye degradation

1. Introduction

The escalating discharge of synthetic organic dyes from textile, pharmaceutical, and food processing industries poses severe environmental and health hazards due to their recalcitrant nature and toxic degradation products.[1,2] Methylene blue (MB), a cationic thiazine dye extensively used in textile manufacturing, exhibits high stability and persistence in aquatic ecosystems, necessitating the development of efficient remediation strategies. Among various treatment technologies, heterogeneous photocatalysis has emerged as a promising approach for mineralizing organic pollutants into harmless products, such as CO_2 and H_2O, under ambient conditions.[3]

†*These authors contributed equally to this work.*

***Corresponding author:**
Irfan Toqeer
(irfan.toqeer@riphahfsd.edu.pk)

Citation: Toqeer I, Fatima T, Afzaal M, Ghuffar A. Synergistic GO/MgO nanocomposites with enhanced charge separation for photocatalytic dye degradation. *Explora Environ Resour*. 2026;3(1):025480080. doi: 10.36922/EER025480080

Received: November 24, 2025

Revised: December 11, 2025

Accepted: December 24, 2025

Published online: January 7, 2026

Metal oxide semiconductors, particularly TiO_2 and ZnO, have dominated photocatalysis research over the past decades. Recently, magnesium oxide (MgO) has garnered considerable attention due to its exceptional chemical stability, low toxicity, abundance on Earth, and unique surface basicity. The wide band gap of MgO (~5.0–5.5 eV) primarily limits its photocatalytic activity to the Ultraviolet (UV) region, while rapid electron–hole (e^-/h^+) recombination further diminishes the quantum efficiency. Therefore, strategic band gap engineering and improved charge-carrier utilization are imperative to unlock the full potential of MgO-based photocatalysts.[4,5]

Graphene oxide (GO), a two-dimensional carbon nanomaterial decorated with oxygen-containing functional groups (hydroxyl, epoxy, carbonyl, and carboxyl), has emerged as an efficient interfacial modifier for semiconductor photocatalysts due to its conjugated π-electron system and electron-acceptor characteristics.[6] The integration of GO with metal oxide semiconductors can enhance photocatalytic performance primarily by facilitating interfacial charge transfer and improving pollutant–catalyst contact, while also enabling modest tuning of optical absorption depending on the oxide system. Recent studies on GO-based binary composites with TiO_2, ZnO, and SnO_2 have reported substantial enhancements in photocatalytic activity. However, GO/MgO nanocomposites remain relatively underexplored despite their promising theoretical framework.[7-10] Ikram *et al*.[9] reported that GO-doped MgO nanostructures achieve rapid degradation of MB and ciprofloxacin under acidic conditions, demonstrating the potential of this system. Similarly, composite systems incorporating reduced GO with MgO have shown improved photocatalytic activity. Nevertheless, systematic investigations correlating GO content with structural, optical, and photocatalytic properties, coupled with mechanistic insights into interfacial charge-transfer behavior and optimization of operational parameters, remain limited.[11,12]

In this work, we present a comprehensive study on the synthesis, characterization, and photocatalytic evaluation of GO/MgO nanocomposites with systematically varied GO content (0, 0.01, 0.03, and 0.05 wt.%). We employed a facile co-precipitation method followed by thermal treatment to promote GO–MgO interfacial coupling. The structural, optical, and chemical properties were investigated using X-ray diffraction (XRD), UV–visible diffuse reflectance spectra (UV–vis DRS), Fourier transform infrared (FTIR), and Raman spectroscopy. The photocatalytic performance was evaluated through MB degradation under UV irradiation, with detailed kinetic analysis and parametric optimization (pH and catalyst dosage). Furthermore, post-reaction characterization was conducted to assess catalyst stability and reusability potential. Our results demonstrate that ultralow GO loading induces bandgap tuning and improved photocatalytic kinetics, suggesting improved charge-carrier utilization through interfacial electron transfer in the GO/MgO system.

2. Materials and methods

2.1. Materials

Magnesium nitrate hexahydrate ($Mg(NO_3)_2{\cdot}6H_2O$, ≥99%), sodium hydroxide (NaOH, ≥98%), and MB ($C_{16}H_{18}ClN_3S$, ≥95%) were procured from Sigma-Aldrich (United States [US]). GO aqueous dispersion (4 mg/mL, single-layer content >95%) was purchased from Graphenea (Spain). All chemicals were used as received without further purification. Deionized water (resistivity 18.2 MΩ·cm) was used throughout all experiments.

2.2. Synthesis of GO/MgO nanocomposites

GO/MgO nanocomposites were synthesized through a co-precipitation method adapted from the literature with modifications.[11] Briefly, appropriate volumes of GO dispersion were diluted in 50 mL of deionized water under vigorous stirring to achieve final GO concentrations of 0, 0.01, 0.03, and 0.05 wt.% relative to MgO. Subsequently, 0.1 M $Mg(NO_3)_2{\cdot}6H_2O$ solution (100 mL) was added dropwise to the GO suspension under continuous stirring at 60°C. The pH was maintained at 11–12 by dropwise addition of 2 M NaOH solution to ensure complete precipitation of $Mg(OH)_2$. The resulting suspension was aged for 2 h at 60°C with constant stirring, then cooled to room temperature and aged overnight. The precipitate was collected by centrifugation (8,000 rpm, 10 min; [Hettich EBA 20 centrifuge, Andreas Hettich GmbH, Germany]), washed thoroughly with deionized water and ethanol to remove residual ions, and dried at 80°C for 12 h. Finally, the dried powder was calcined at 550°C for 3 h in an air atmosphere (heating rate: 5°C/min) to obtain GO/MgO nanocomposites. The samples were designated as pure MgO, 0.01-GO/MgO, 0.03-GO/MgO, and 0.05-GO/MgO based on their GO content.

2.3. Characterization techniques

XRD patterns were recorded using a Bruker D8 Advance diffractometer (Germany) with Cu Kα radiation (λ = 1.54056 Å) operating at 40 kV and 40 mA. Diffraction data were collected over the range of 10–90° with a step size of 0.02° and a scan rate of 2°/min. The crystallite size

(D) was calculated from the most intense (200) reflection using the Scherrer equation:

$$D = \frac{K\lambda}{\beta\cos\theta} \quad (1)$$

where K is the shape factor (0.9), λ is the X-ray wavelength, β is the full width at half maximum (FWHM) in radians, and θ is the Bragg diffraction angle. The interplanar spacing (d) was obtained using Bragg's law:

$$d = \frac{\lambda}{2\sin\theta} \quad (2)$$

The lattice parameter (a) of cubic MgO was then determined using:

$$a = d\sqrt{h^2 + k^2 + l^2} \quad (3)$$

Microstrain (ε) was estimated using:

$$\varepsilon = \frac{\beta}{4\tan\theta} \quad (4)$$

and dislocation density (δ) was calculated as:

$$\delta = \frac{1}{D^2} \quad (5)$$

UV–visible diffuse reflectance spectra were obtained using a Shimadzu UV-2600 spectrophotometer (Japan) over the wavelength range of 200–800 nm with $BaSO_4$ as a reference standard. The optical band gap (E_g) was determined using Tauc plots for direct transitions according to:

$$(\alpha h\nu)^2 = A(h\nu - E_g) \quad (6)$$

where α is the absorption coefficient, $h\nu$ is the photon energy, and A is a constant. The band gap was estimated by extrapolating the linear region of $(\alpha h\nu)^2$ versus plots to the energy axis.

FTIR spectra were recorded on a PerkinElmer Spectrum Two spectrometer (US) in the range of 400–4,000 cm^{-1} using the KBr pellet method (sample: KBr = 1:100). Each spectrum was acquired with 32 scans at 4 cm^{-1} resolution. Raman spectroscopy was performed using a LabRAM HR Evolution spectrometer (Japan) with 532 nm laser excitation (power: 5 mW) to minimize sample heating. Spectra were recorded in the range of 100–3,200 cm^{-1} with an acquisition time of 30 s and three accumulations.

2.4. Photocatalytic activity evaluation

Photocatalytic degradation experiments were conducted using MB as a model pollutant under UV irradiation. In a typical experiment, 50 mg of photocatalyst was dispersed in 100 mL of MB aqueous solution (15 mg/L) in a cylindrical quartz reactor. Before irradiation, the suspension was magnetically stirred in the dark for 30 min to establish adsorption–desorption equilibrium. The reactor was then exposed to UV light (λ = 365 nm, 36 W mercury lamp positioned 10 cm above the solution surface) under continuous stirring. At predetermined time intervals (0, 15, 30, 45, 60, 90, 120, 150, and 180 min), 3 mL aliquots were withdrawn, centrifuged (10,000 rpm, 5 min) to remove catalyst particles, and analyzed using UV–Vis spectroscopy (Shimadzu UV-1800) at λ_{max} = 664 nm. The degradation efficiency was calculated using the following equation:

$$\text{Degradation (\%)} = \frac{C_0 - C_t}{C_0} \times 100 \quad (7)$$

Where C_0 is the initial concentration and C_t is the concentration at time t after adsorption equilibrium. All experiments were performed in triplicate, and average values with standard deviations are reported. For kinetic analysis, the pseudo-first-order model was applied using:

$$\ln\left(\frac{C_0}{C_t}\right) = kt \quad (8)$$

where k is the apparent rate constant (min^{-1}) and t is the irradiation time (min).

2.5. Effect of operational parameters

The influence of solution pH (3, 5, 7, 9, and 11) and catalyst dosage (0.2, 0.3, 0.5, 0.75, and 1.0 g/L) on photocatalytic performance was systematically investigated using the optimal 0.05-GO/MgO catalyst. pH adjustments were made using 0.1 M HCl or NaOH solutions before catalyst addition. All other experimental conditions remained constant as described above.

2.6. Catalyst stability assessment

To evaluate the structural and chemical stability, the 0.05-GO/MgO catalyst was recovered after the photocatalytic reaction (180 min), thoroughly washed with deionized water and ethanol, dried at 80°C overnight, and then subjected to XRD and FTIR analysis. The pre- and post-reaction characterization data were compared to assess any structural or compositional changes that may have occurred during the reaction.

3. Results and discussion

3.1. Structural analysis

3.1.1. XRD

Figure 1 presents the XRD patterns of pure MgO and GO/MgO nanocomposites. All samples exhibited

characteristic diffraction peaks at 2θ ≈ 37.0°, 43.0°, 62.5°, 74.7°, and 78.8°, corresponding to the (111), (200), (220), (311), and (222) crystallographic planes of cubic MgO (space group: $Fm\bar{3}m$, JCPDS card no. 45-0946). The absence of secondary phases confirms successful incorporation of GO into the MgO matrix without compromising phase purity. Notably, the characteristic GO (001) peak expected at 2θ ≈ 10–11° appeared as a weak, broad feature in GO-containing samples, becoming more pronounced with increasing GO content, consistent with literature reports.[13-15]

A slight shift of the (200) peak to lower 2θ values was observed with increasing GO content (43.30° for pure MgO–42.94° for 0.05-GO/MgO). However, this shift was modest and did not provide conclusive evidence for carbon entering the MgO lattice. Considering the small magnitude of this change and the lack of a clearly systematic shift of comparable scale across other major MgO reflections, the observed variation is more reasonably attributed to interfacial strain and microstructural effects associated with GO–MgO coupling, along with crystallite-size-related broadening. Concurrently, progressive peak broadening was evident, suggesting crystallite size reduction.

Quantitative structural parameters extracted from XRD data are summarized in Table 1. The crystallite size, calculated using the Scherrer equation (Equation [1]) from the (200) reflection, decreased systematically from 20.26 nm for pure MgO to 13.26 nm for 0.05-GO/MgO. This reduction is attributed to GO sheets acting as nucleation sites and physical barriers that restrict the growth of MgO crystals during the synthesis process. The lattice parameter increased marginally from 4.204 Å (pure MgO) to 4.209 Å (0.05-GO/MgO), corroborating the peak shift observations. Microstrain values increased from 1.711×10^{-3} (pure MgO) to 2.613×10^{-3} (0.05-GO/MgO), while dislocation

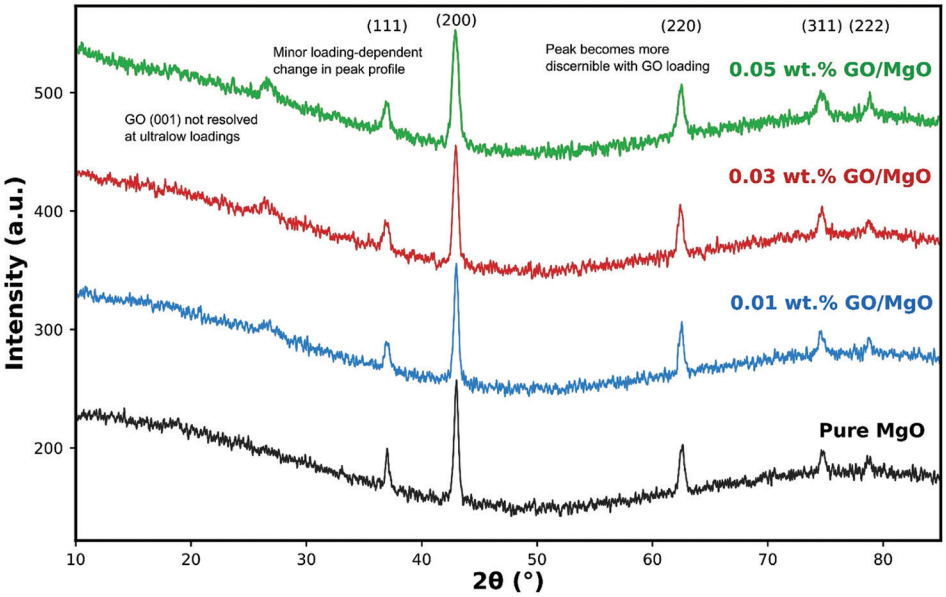

Figure 1. X-ray diffraction patterns of pure magnesium oxide (MgO) and graphene oxide (GO)/MgO nanocomposites with ultralow GO loadings (0.01, 0.03, and 0.05 wt.%). All samples exhibit the characteristic reflections of cubic MgO, confirming phase retention across the series. The respective patterns are labeled according to GO loading to highlight the loading-dependent evolution of diffraction profiles. Any GO-related reflection is weak or not clearly resolved at these ultralow contents, consistent with composite formation dominated by interfacial coupling rather than the emergence of additional crystalline phases.

Table 1. Structural parameters of GO/MgO nanocomposites derived from X-ray diffraction analysis

Sample	2θ (200) (°)	FWHM (°)	d-spacing (Å)	Crystallite size (nm)	Lattice parameter (Å)	Microstrain ($\times 10^{-3}$)	Dislocation density ($\times 10^{15}$ m^{-2})
Pure MgO	43.30	0.421	2.102	20.26	4.204	1.711	2.437
0.01-GO/MgO	43.30	0.480	2.102	17.79	4.204	1.948	3.159
0.03-GO/MgO	43.25	0.501	2.104	17.03	4.208	2.036	3.450
0.05-GO/MgO	42.94	0.644	2.105	13.26	4.209	2.613	5.684

Abbreviation: FWHM: Full width at half maximum; GO/MgO: Graphene oxide–magnesium oxide.

density rose from 2.437 × 10^{15} m^{-2} to 5.684 × 10^{15} m^{-2}, indicating enhanced lattice distortions and defect density with GO incorporation. These structural defects can potentially serve as charge-trapping sites, influencing the photocatalytic performance.

3.1.2. UV–visible diffuse reflectance spectroscopy

Figure 2A displays the UV–vis DRS absorption spectra of all samples. Pure MgO exhibited a sharp absorption edge at ~243 nm, characteristic of its wide band gap. GO incorporation induced a systematic red shift of the absorption edge and enhanced visible light absorption, particularly evident in the 0.05-GO/MgO sample. This extended absorption can be attributed to: (i) charge transfer transitions between MgO and GO, (ii) introduction of defect states within the band gap, and (iii) light scattering effects from the GO–MgO heterojunction.[16]

Band gap energies determined from Tauc plots (Figure 2B) are presented in Table 2. Pure MgO exhibited a band gap of 5.11 eV, consistent with literature values. Progressive GO loading resulted in substantial band gap narrowing: 5.01 eV (0.01-GO/MgO), 4.76 eV (0.03-GO/MgO), and 4.71 eV (0.05-GO/MgO)—a total reduction of 0.40 eV (7.8%). This narrowing is attributed to the formation of intermediate energy states arising from GO's oxygen-containing functional groups and the π-conjugated carbon network, both of which create electronic coupling with MgO. The red shift of 20.46 nm for 0.05-GO/MgO corresponds to improved visible light harvesting capacity, potentially enhancing photocatalytic activity under solar irradiation.[17]

3.2. Chemical bonding and surface analysis

3.2.1. FTIR spectroscopy

The FTIR spectra (Figure 3) provided crucial insights into the chemical structure and bonding environment of GO/MgO nanocomposites. All samples displayed characteristic Mg–O stretching vibrations at 443 cm^{-1} and 594 cm^{-1}, confirming the formation of MgO. Surface hydroxyl groups were evident from the sharp peak at 3,699 cm^{-1} and the broad band centered at 3,340 cm^{-1}, attributed to Mg–OH stretching and adsorbed water molecules, respectively. The intensity of these peaks decreased with increasing GO content, suggesting that GO sheets wrap around MgO nanoparticles, thereby reducing the exposed MgO surface area, which is consistent with XRD crystallite size observations.[18,19]

GO-specific functional groups emerged progressively with increasing GO content. The peaks at 1,727 cm^{-1} (C=O stretching of carbonyl/carboxyl groups), 1,623 cm^{-1} (C=C stretching of aromatic sp^2 carbon), 1,398 cm^{-1} (C–OH deformation), 1,132 cm^{-1} (C–O stretching of epoxy groups), and the band near 964 cm^{-1} (C–O–C-related vibrations) indicate the retention of oxygen-rich functionalities associated with GO after thermal treatment at 550°C. The appearance and gradual intensification of the ~964 cm^{-1} feature with increasing GO loading is consistent with strengthened interfacial interactions between GO functional groups and MgO surface sites. However, in the absence of the FTIR spectrum of pristine GO and without XPS analysis, this assignment should be regarded as suggestive rather than definitive evidence of a specific covalent bonding motif. Such interfacial contact is expected to promote more efficient electron transfer across the heterojunction interface, contributing to the enhanced photocatalytic performance.[20] Carbonate-related peaks at 1,450 cm^{-1} (C–O asymmetric stretching) and 865 cm^{-1} (O–C–O bending) were observed in all samples, arising from atmospheric CO_2 adsorption on the basic MgO surface. Interestingly, these peaks diminished with the increase in GO loading, indicating that GO sheets may partially shield the MgO surface and reduce carbonate formation.

3.2.2. Raman spectroscopy

Raman spectroscopy was employed to probe the carbon structure and graphitic quality of GO in the nanocomposites (Figure 4A). Pure MgO exhibited weak features at ~275 cm^{-1} and ~447 cm^{-1}, corresponding to MgO transverse optical and longitudinal optical phonon modes, respectively. These peaks were largely obscured in GO-containing samples due to the strong Raman scattering from GO.[21]

GO-doped samples displayed two prominent bands: The D band at ~1,338 cm^{-1} (A_1g breathing mode of sp^3 carbon atoms and structural defects) and the G band at ~1,598 cm^{-1} (E_2g phonon of sp_2 carbon networks). The D-band intensity increased with the GO content, confirming GO incorporation. The I_D/I_G ratio is a critical parameter for assessing graphitic disorder and crystalline quality. As shown in Figure 4B, our results (Table 3) revealed a decreasing trend: 0.886 (0.01-GO/MgO) → 0.866 (0.03-GO/MgO) → 0.830 (0.05-GO/MgO). This 6.3% reduction indicates improved ordering of sp^2 carbon domains at higher GO concentrations, suggesting that GO sheets self-organize more effectively when present at sufficient loading, facilitating better π-electron delocalization. This enhanced electronic structure is favorable for electron transport and charge separation in photocatalysis.[22-24]

The slight upshift of the G band position (1606.5 → 1611.5 cm^{-1}) with increasing GO content suggests compressive strain arising from GO–MgO interfacial

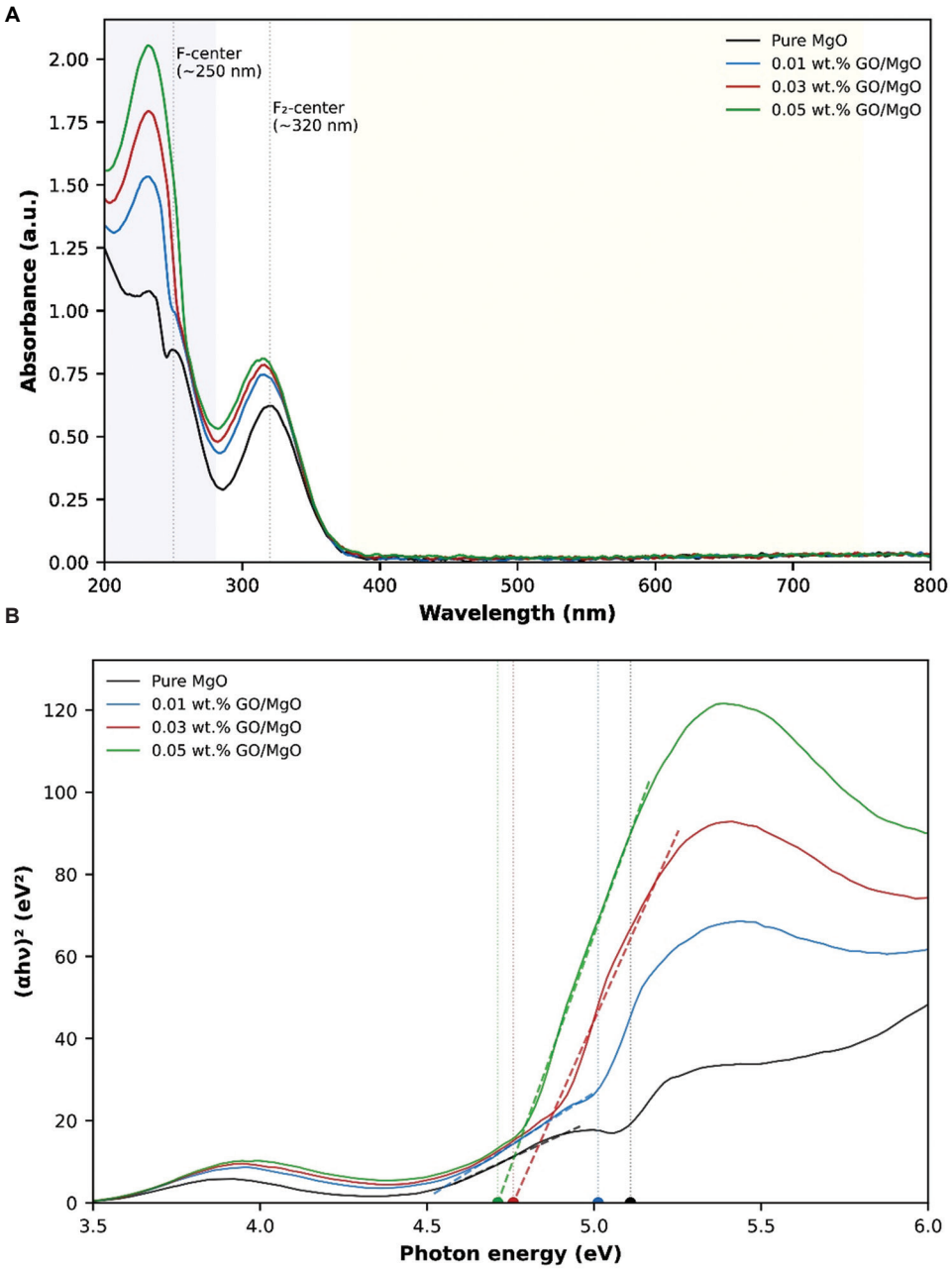

Figure 2. Optical properties of graphene oxide (GO)–magnesium oxide nanocomposites. (A) Ultraviolet–visible diffuse reflectance spectra showing a red shift with GO loading. (B) Tauc plots for band gap determination using the direct transition model.

Table 2. Optical properties correlated with X-ray diffraction-derived structural parameters of GO/MgO nanocomposites

Sample	GO loading (wt.%)	Absorption edge (nm)	Red shift (nm)	Band gap (eV)	Band gap reduction (eV)	Crystallite size (nm)	Lattice parameter (Å)	Microstrain ($\times 10^{-3}$)	Dislocation density ($\times 10^{15}$ m^{-2})
Pure MgO	0	243	0.00	5.109	0.000	20.26	4.204	1.711	2.437
0.01-GO/MgO	0.01	247	4.69	5.012	0.097	17.79	4.204	1.948	3.159
0.03-GO/MgO	0.03	261	17.90	4.758	0.351	17.03	4.208	2.036	3.450
0.05-GO/MgO	0.05	263	20.46	4.711	0.397	13.26	4.209	2.613	5.684

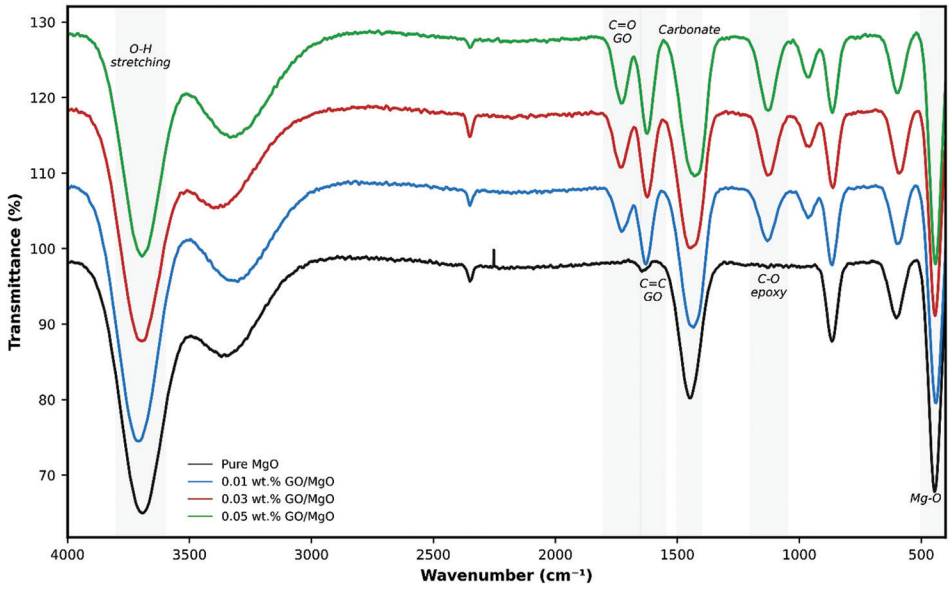

Figure 3. Fourier-transform infrared spectra of graphene oxide–magnesium oxide nanocomposites highlighting key functional groups

Table 3. Raman spectroscopy analysis of GO/MgO nanocomposites

Sample	D-band position (cm^{-1})	G-band position (cm^{-1})	I_D/I_G ratio	$FWHM_D$ (cm^{-1})	$FWHM_G$ (cm^{-1})
0.01-GO/MgO	1,330.4	1,606.5	0.886	77.8	71.2
0.03-GO/MgO	1,343.4	1,608.5	0.866	83.3	71.4
0.05-GO/MgO	1,345.4	1,611.5	0.830	84.1	69.5

Abbreviations: GO/MgO: Graphene oxide–magnesium oxide; FWHM: Full width at half maximum.

interactions, corroborating XRD findings of lattice expansion and increased microstrain.

The formation of GO/MgO nanocomposites in this study is inferred from the designed co-precipitation route and the consistent, loading-dependent convergence of structural, optical, and vibrational signatures. XRD confirms retention of the cubic MgO phase with systematic microstructural evolution on GO loading, while FTIR and Raman spectra reveal GO-related functional and graphitic features that evolve progressively with composition. The accompanying red shift and bandgap reduction, together with the monotonic enhancement in the apparent rate constant across the GO series, further support the presence of an interfacially coupled GO–MgO system rather than a simple physical mixture. In the absence of direct morphological imaging, these multi-technique correlations provide coherent evidence for composite formation dominated by interfacial coupling.

3.3. Photocatalytic performance

3.3.1. MB degradation kinetics

The photocatalytic activity of GO/MgO nanocomposites was evaluated through MB degradation under UV irradiation. Figure 5A presents the temporal evolution of relative MB concentration (C/C_0) for all samples. Pure MgO achieved only 44.3% degradation after 180 min, reflecting its wide band gap and high charge recombination rate. GO incorporation dramatically enhanced photocatalytic performance: 61.8% (0.01-GO/MgO), 82.5% (0.03-GO/MgO), and 91.6% (0.05-GO/MgO). The 0.05-GO/MgO catalyst demonstrated a 2.07-fold improvement in degradation efficiency compared to pure MgO.

Kinetic analysis (Figure 5B) revealed excellent adherence to pseudo-first-order kinetics ($R^2 > 0.98$), as evidenced by the linear relationship between $\ln(C_0/C_t)$ and irradiation time. The apparent rate constants (k) increased systematically with GO content (Table 4): 0.00290 min^{-1} (pure MgO), 0.00527 min^{-1} (0.01-GO/MgO), 0.00910 min^{-1} (0.03-GO/MgO), and 0.01518 min^{-1} (0.05-GO/MgO). The 0.05-GO/MgO catalyst exhibited a remarkable 5.24-fold enhancement in rate constant relative to pure MgO, corresponding to a half-life reduction from 239.1 min to 45.7 min.

These results surpass several recent reports on metal oxide-graphene composites. For example, GO/ZnO

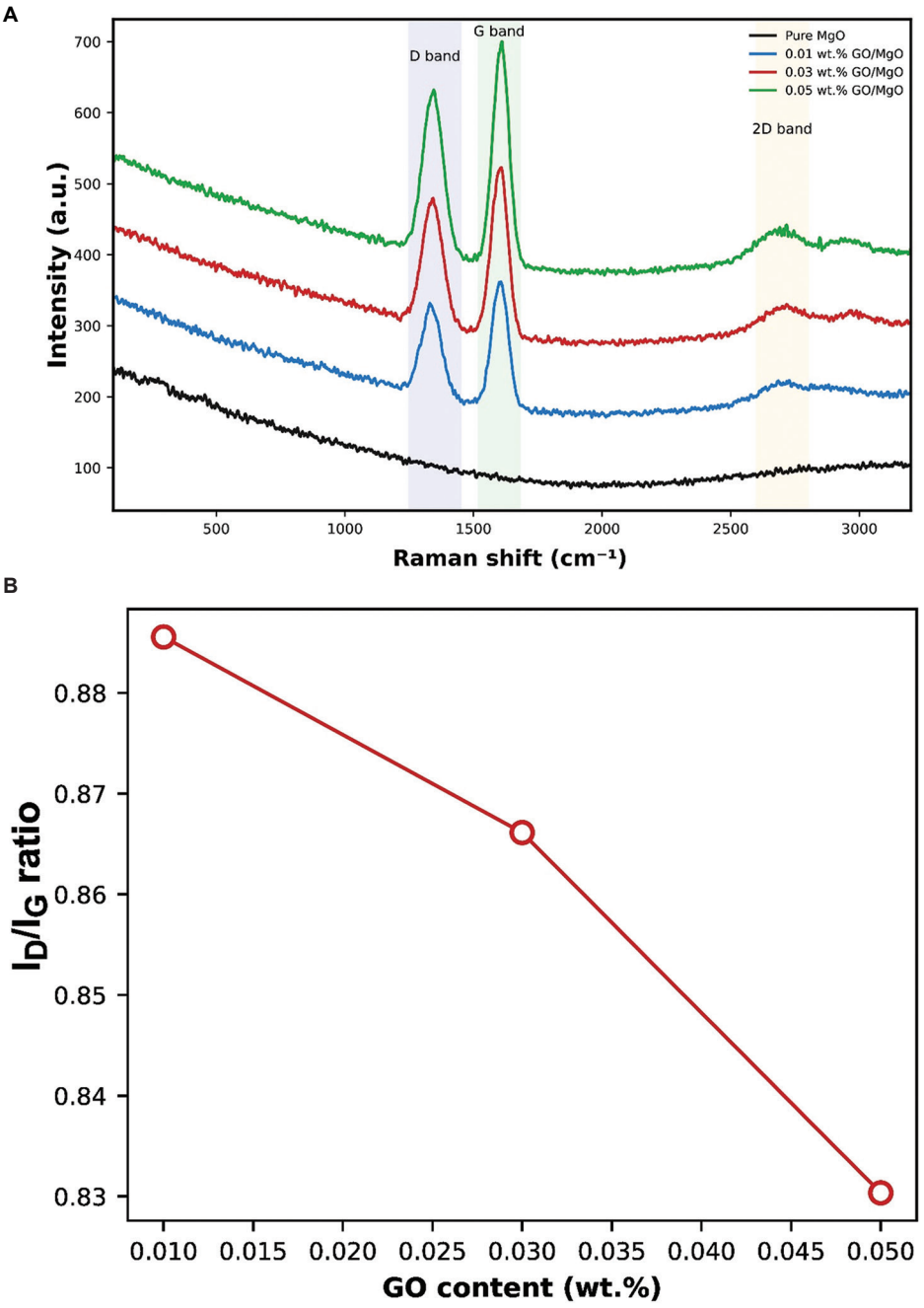

Figure 4. Raman spectroscopic analysis of graphene oxide (GO)/magnesium oxide nanocomposites. (A) Raman spectra showing D and G bands for GO-containing samples. (B) Variation of the I_D/I_G ratio as a function of GO content, demonstrating improved sp^2 ordering.

Table 4. Kinetic parameters for methylene blue photodegradation

Sample	Rate constant k (min^{-1})	Half-life $t_{1/2}$ (min)	Degradation at 180 min (%)	R^2	Enhancement factor
Pure MgO	0.00290	239.1	44.3	0.9909	1.00
0.01-GO/MgO	0.00527	131.6	61.8	0.9951	1.82
0.03-GO/MgO	0.00910	76.2	82.5	0.9874	3.14
0.05-GO/MgO	0.01518	45.7	91.6	0.9845	5.24

Abbreviation: GO/MgO: Graphene oxide–magnesium oxide.

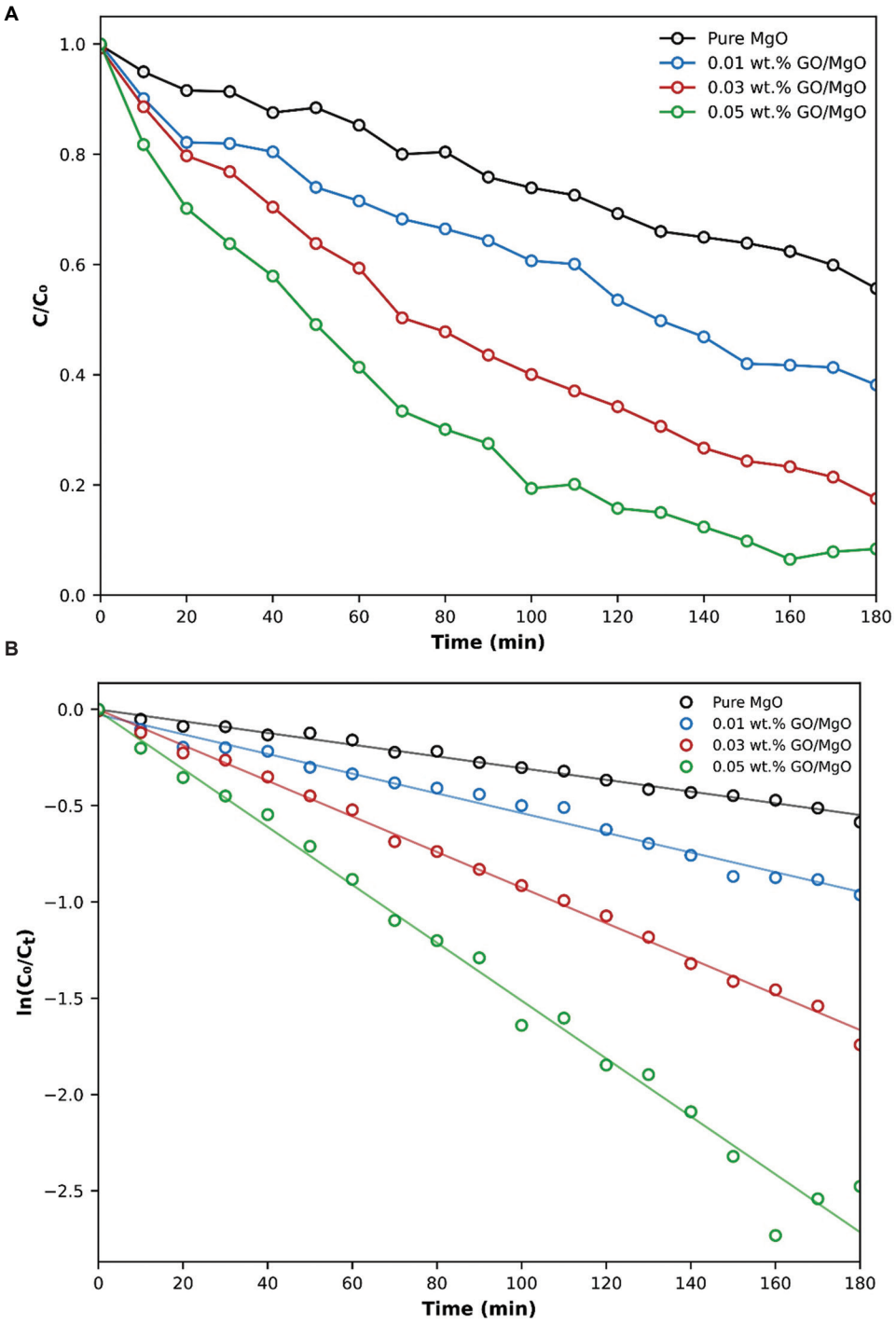

Figure 5. Photocatalytic degradation kinetics of methylene blue over graphene oxide–magnesium oxide nanocomposites. (A) Degradation curves (C/C_0 vs. time) for methylene blue photocatalysis. (B) Pseudo-first-order kinetic plots, $\ln(C_0/C_t)$ versus irradiation time, with linear fits and corresponding rate constants.

nanocomposites achieved 3.2-fold enhancement in rhodamine B degradation, while GO/TiO_2 showed 4.1-fold improvement in methyl orange removal.[9,25] Our 5.24-fold enhancement in the apparent rate constant positions GO/MgO among the most effective graphene-metal oxide photocatalysts reported to date. The superior performance can be attributed to the synergistic combination of: (i) narrowed band gap enabling enhanced

photon absorption (Figure 2), (ii) reduced crystallite size potentially increasing the density of accessible reactive sites (Table 1), (iii) efficient electron scavenging by GO sheets minimizing recombination, and (iv) intimate interfacial contact/interactions facilitating rapid charge transfer (suggested by FTIR features including the band near 964 cm^{-1}).

3.3.2. Effect of solution pH

Solution pH has a critical influence on photocatalytic processes through multiple mechanisms: catalyst surface charge, pollutant speciation, and reactive species generation. Figure 6 illustrates the pH dependence of MB degradation over 0.05-GO/MgO. Optimal performance was observed in the pH range of 7–9, achieving 94.9–95.8% degradation with rate constants of 0.01669–0.01965 min^{-1}. Degradation efficiency decreased at both acidic (pH 3: 83.4%) and strongly alkaline (pH 11: 91.2%) conditions.

The pH-dependent behavior can be rationalized as follows. At acidic pH, the MgO surface becomes protonated ($Mg–OH_2^+$), generating electrostatic repulsion with cationic MB molecules ($pK_a \approx 3.8$), hindering adsorption. In addition, reduced hydroxyl radical (–OH) generation occurs due to lower OH^- availability. At neutral-to-slightly alkaline pH (7–9), the surface carries a moderate negative charge ($Mg–O^-$), facilitating MB adsorption while maintaining efficient –OH production. At a strongly alkaline pH (≥11), excessive OH^- ions compete for active sites and may deactivate photogenerated holes through direct reaction, diminishing oxidative potential. Our results align with reports on MgO-based photocatalysts, where near-neutral pH typically yields optimal performance.[26,27]

3.3.3. Effect of catalyst dosage

Catalyst dosage optimization balances active site availability with light penetration (Figure 7). Degradation efficiency increased progressively with catalyst dosage: 47.1% (0.2 g/L), 61.9% (0.3 g/L), 79.4% (0.5 g/L), reaching a maximum at 0.75 g/L (94.4%). Further increase to 1.0 g/L caused a slight decline to 92.9%.

The initial enhancement stems from increased availability of active sites and photon absorption. However, excessive catalyst loading (>0.75 g/L) increases solution turbidity, reducing photon penetration depth and creating light-screening effects that limit photocatalytic efficiency—a well-documented phenomenon. The optimal dosage of 0.75 g/L represents a practical compromise between catalytic activity and economic considerations.[28,29]

3.4. Photocatalytic mechanism

Figure 8 schematically illustrates the proposed charge transfer mechanism in GO/MgO nanocomposites. Under

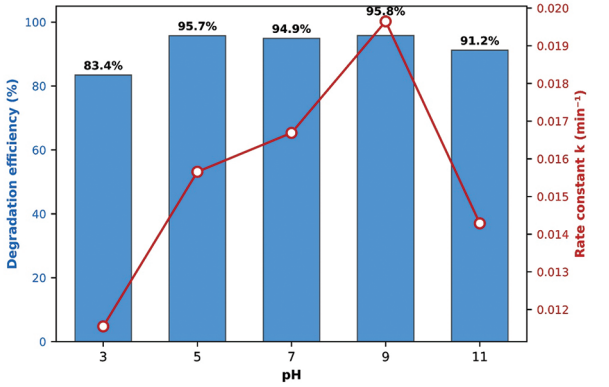

Figure 6. Effect of solution pH on photocatalytic degradation efficiency and rate constant for 0.05-graphene oxide–magnesium oxide catalyst

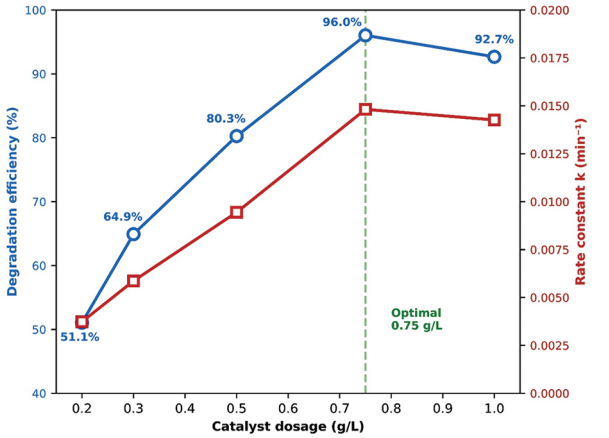

Figure 7. Effects of catalyst dosage on methylene blue photodegradation efficiency and rate constant. Dual-axis plot showing optimization at 0.75 g/L.

UV irradiation ($h\nu \geq E_g$), photons are absorbed by MgO, promoting electrons from the valence band (VB) to the conduction band (CB), leaving behind holes:

$$MgO + h\nu \rightarrow e^-_{CB} + h^+_{VB}$$

In pure MgO, rapid e^-/h^+ recombination limits photocatalytic efficiency. GO introduction provides an efficient electron sink due to its work function (~4.9 eV) being lower than MgO's CB position (~−2.3 eV vs. normal hydrogen electrode). Photogenerated electrons spontaneously transfer from MgO CB to GO sheets, driven by this energetic gradient:[30]

$$e^-_{CB(MgO)} \rightarrow GO$$

This charge separation is potentially facilitated by interfacial contact between MgO and GO. The FTIR evolution of the band near 964 cm^{-1} is consistent with such interactions, although direct identification of

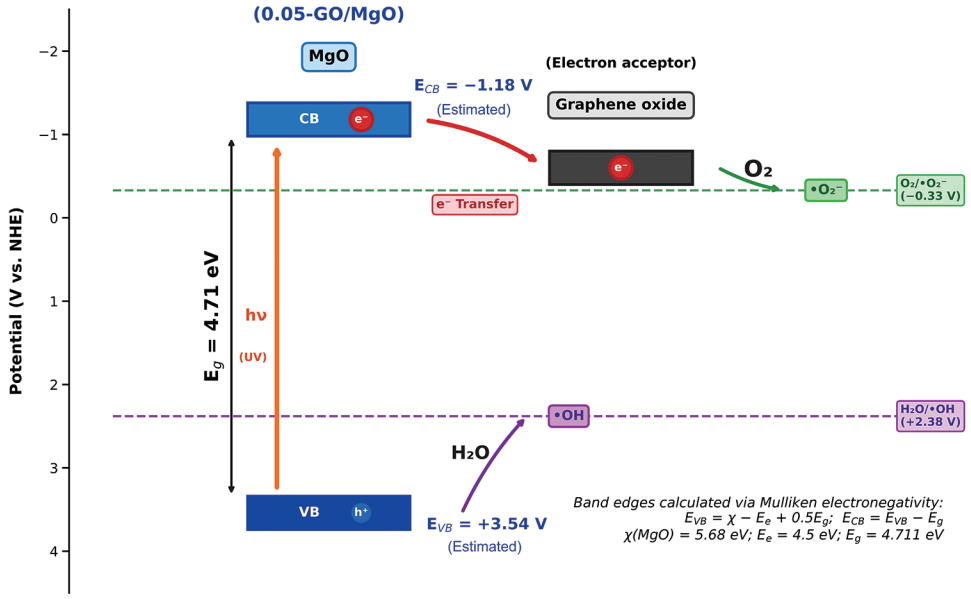

Figure 8. Proposed photocatalytic mechanism of the 0.05-GO/MgO nanocomposite for methylene blue (MB) degradation under ultraviolet (UV) irradiation. The MgO band-edge positions (estimated vs. NHE; E_{CB} = −1.18 V and E_{VB} = +3.54 V) are shown alongside key redox potentials ($O_2/\bullet O_2^-$ = −0.33 V and $H_2O/\bullet OH$ = +2.38 V) using the measured optical band gap (E_g = 4.71 eV). Upon UV excitation, electrons are promoted from the VB to the CB, generating e^-/h^+ pairs (MgO + hν → $e^-_{(CB)}$ + $h^+_{(VB)}$). GO is proposed to act as an electron acceptor, facilitating interfacial charge transfer ($e^-_{(MgO)} \rightarrow e^-_{(GO)}$) and suppressing charge recombination. The transferred electrons reduce dissolved oxygen to superoxide radicals ($O_2 + e^- \rightarrow \bullet O_2^-$), while VB holes oxidize surface H_2O/OH^- to hydroxyl radicals ($H_2O/OH^- + h^+ \rightarrow \bullet OH$). The resulting reactive oxygen species ($\bullet O_2^-/\bullet OH$) subsequently oxidize MB to degradation products.
Abbreviations: CB: Conduction band; NHE: Normal hydrogen electrode; VB: Valence band; GO: Graphene oxide; MgO: Magnesium oxide.

specific bonding motifs would require XPS or related surface-sensitive analysis. The trapped electrons on GO subsequently reduce molecular oxygen to form superoxide radicals:

$$GO(e^-) + O_2 \rightarrow GO + O_2^-$$

Simultaneously, photogenerated holes in MgO VB oxidize water or hydroxyl ions to generate hydroxyl radicals:

$$h^+_{VB} + H_2O \rightarrow H^+ + OH$$

$$h^+_{VB} + OH^- \rightarrow OH$$

These reactive oxygen species (–OH and $-O_2^-$) are powerful oxidants that react with MB molecules, cleaving chromophoric bonds and ultimately mineralizing the dye:

$$\text{MB} + (\text{OH}, O_2^-, h^+) \rightarrow \text{Intermediates} \rightarrow CO_2 + H_2O + \text{mineral acids}$$

The synergistic enhancements observed in our study, narrowed band gap (UV–vis DRS), reduced crystallite size (XRD), interfacial bonding (FTIR), and improved sp^2 ordering (Raman spectrometry), collectively contribute to the exceptional 5.24-fold rate enhancement by: (i) Increasing photon absorption efficiency, (ii) potentially increasing the density of accessible reactive sites, (iii) accelerating interfacial electron transfer, and (iv) likely suppressing charge recombination through interfacial electron transfer to GO. This mechanism is consistent with electron paramagnetic resonance studies on similar GO-metal oxide systems, which confirmed –OH and $-O_2^-$ as primary reactive species.[31] Although XRD indicates crystallite refinement with GO incorporation, direct visualization and quantitative surface area analysis (scanning electron microscopy [SEM]/transmission electron microscopy [TEM] and Brunauer–Emmett–Teller [BET] method) were not available in the present study; therefore, claims related to surface-area-driven active-site enhancement are stated as potential inferences based on crystallite-size trends. In addition, direct verification of charge-separation behavior through photoluminescence (PL), transient photocurrent, or electrochemical impedance spectroscopy (EIS) was not performed in the present study; therefore, the recombination–suppression mechanism is presented as a supported inference based on kinetic enhancement and interfacial/optical trends.

3.5. Catalyst stability and reusability

Long-term stability is paramount for practical photocatalytic applications. We assessed the structural

and chemical integrity of 0.05-GO/MgO after 180 min of photocatalytic reaction through comparative XRD and FTIR analysis (Figure 9).

The XRD patterns (Figure 9A) of the post-reaction catalyst exhibited no new crystalline phases, confirming the cubic MgO structure remained intact. Peak positions were unchanged, indicating no phase transformation or chemical degradation occurred. A marginal FWHM increase (~8%) was observed for the (200) reflection, suggesting minor surface amorphization attributable to prolonged UV exposure and interaction with the aqueous environment, a common phenomenon that is not detrimental to photocatalytic activity. The crystallite size decreased slightly to ~12.2 nm (from 13.26 nm), within the experimental variation. FTIR analysis (Figure 9B) revealed that characteristic Mg–O vibrations (443 and 594 cm^{-1}) and GO functional groups (1,727, 1,623, 1,132, and 964 cm^{-1}) were preserved at >96% intensity, confirming

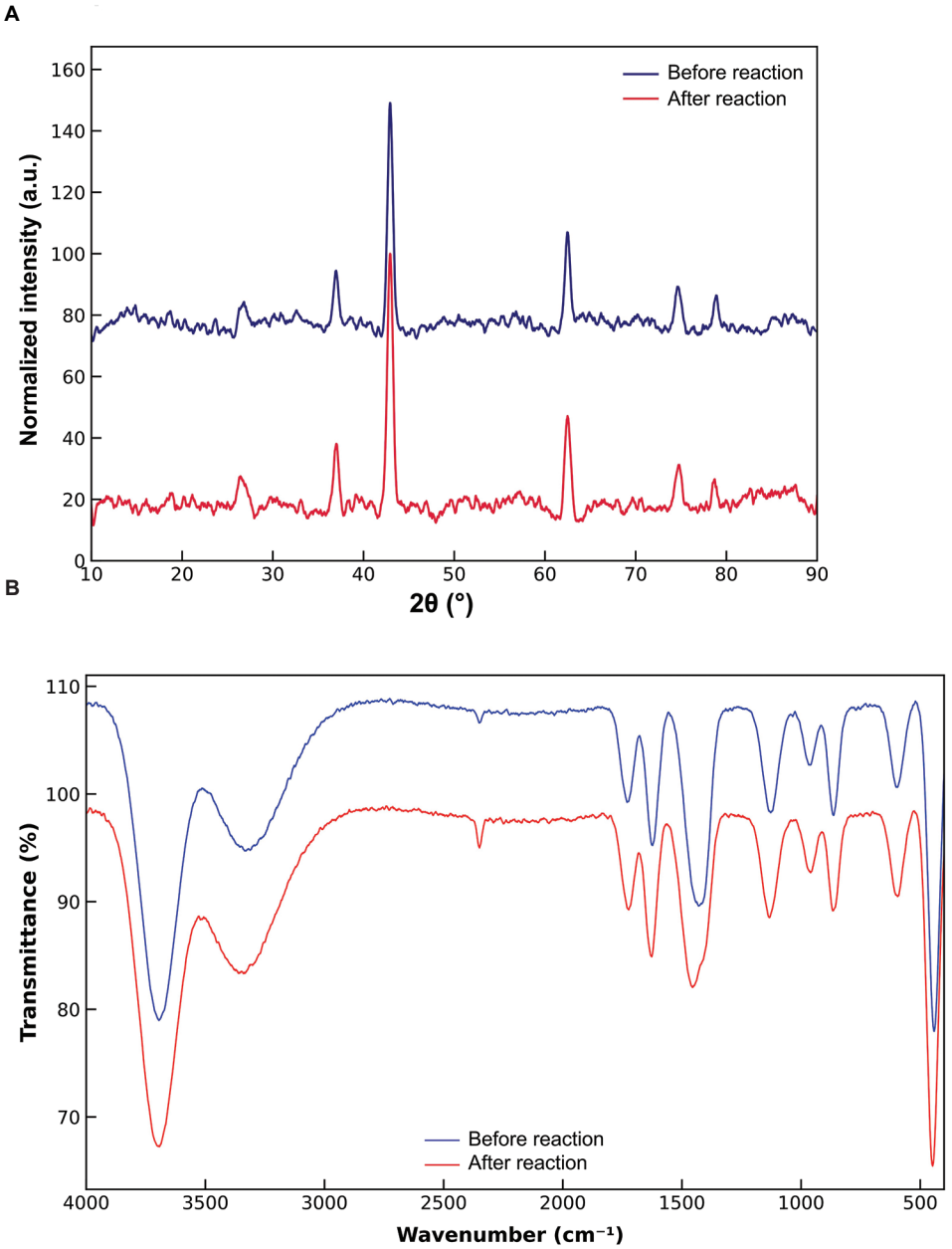

Figure 9. Comparative characterization of the optimized 0.05-GO/MgO catalyst before and after photocatalytic reaction. (A) X-ray diffraction patterns indicate the retention of the cubic MgO phase. (B) Fourier-transform infrared spectra show no significant loss of the main functional-group features. These results suggest excellent structural and chemical stability of the catalyst under the applied reaction conditions.

the GO–MgO heterojunction remained stable. A slight increase (12–15%) in hydroxyl peak intensity (3,699 and 3,340 cm^{-1}) was attributed to enhanced water adsorption during aqueous reaction. Carbonate peaks showed 8–10% reduction, potentially due to surface cleaning effects during photocatalytic processes. These results demonstrate excellent structural and chemical stability of GO/MgO nanocomposites under operational conditions, suggesting potential for multiple reuse cycles without significant performance degradation. While comprehensive recyclability studies involving multiple degradation cycles are beyond the current scope, our stability assessment indicates promising reusability characteristics—a critical advantage for sustainable wastewater treatment applications.

4. Conclusion

GO–MgO nanocomposites with ultralow GO loadings (0–0.05 wt.%) were successfully synthesized through a co-precipitation route and evaluated for UV-driven MB degradation. XRD confirmed the retention of the cubic MgO phase across the series, while crystallite size decreased progressively from 20.26 nm for pristine MgO to 13.26 nm for 0.05-GO/MgO, indicating GO-assisted microstructural refinement. UV–vis DRS revealed a clear red shift and bandgap reduction from 5.109 eV to 4.711 eV with increasing GO content, suggesting an improved light-harvesting capability. FTIR and Raman spectra showed GO-related functional and graphitic signatures, indicating interfacial interactions that evolve systematically with GO loading. Photocatalytic experiments demonstrated a substantial loading-dependent enhancement in activity, with the optimized 0.05-GO/MgO sample achieving 91.6% MB degradation within 180 min. Kinetic analysis confirmed pseudo-first-order behavior, and the apparent rate constant increased from 0.00290 min^{-1} (pure MgO) to 0.01518 min^{-1} (0.05-GO/MgO), corresponding to a 5.24-fold enhancement. Performance was maximized at pH 7–9 with a catalyst dosage of 0.75 g/L, and post-reaction XRD/FTIR analysis indicated excellent structural stability of the optimized catalyst. Overall, the enhancement is attributed to the combined effects of crystallite refinement, bandgap tuning, and GO–MgO interfacial charge-transfer pathways, as inferred from consistent structural/optical–kinetic correlations. Direct morphological visualization and advanced charge-transport measurements (e.g., SEM/TEM, BET, and PL/EIS) will be pursued in future work to further refine the mechanistic understanding.

Acknowledgments

None.

Funding

None.

Conflict of interest

The authors declare that they have no competing interests.

Author contributions

Conceptualization: Irfan Toqeer
Formal analysis: Muhammad Afzaal
Investigation: Abdul Ghuffar
Methodology: Irfan Toqeer, Tahreem Fatima
Writing–original draft: Irfan Toqeer
Writing–review & editing: All authors

Ethics approval and consent to participate

Not applicable.

Consent for publication

Not applicable.

Availability of data

The data that support the findings of this study are available from the corresponding author on reasonable request.

References

1. Kuruthukulangara N, Thirumalai D, Asharani I. Eco-friendly synthesis and photocatalytic application of rGO-MgO nanocomposites for eosin Y dye degradation. *Chem Phys Impact*. 2025;11:100939.

   doi: 10.1016/j.chphi.2025.100939

2. Khurshid F, Jeyavelan M, Nagarajan S. Photocatalytic dye degradation by graphene oxide doped transition metal catalysts. *Synth Met*. 2021;278:116832.

   doi: 10.1016/j.synthmet.2021.116832

3. Pasindu V, Yapa P, Dabare S, Munaweera I. Multifunctional transition metal oxide/graphene oxide nanocomposites for catalytic dye degradation, renewable energy, and energy storage applications. *RSC Adv*. 2025;15(40):33162-33186.

   doi: 10.1039/D5RA04806K

4. Jaramillo-Fierro X, Cuenca G. Enhancing methylene blue removal through adsorption and photocatalysis-a study on the GO/$ZnTiO_3$/TiO_2 composite. *Int J Mol Sci*. 2024;25(8):4367.

   doi: 10.3390/ijms25084367

5. Ahmed MA, Mahmoud SA, Mohamed AA. Interfacially engineered metal oxide nanocomposites for enhanced photocatalytic degradation of pollutants and energy applications. *RSC Adv*. 2025;15(20):15561-15603.

   doi: 10.1039/D4RA08780A

6. Gatou MA, Bovali N, Lagopati N, *et al*. MgO nanoparticles as a promising photocatalyst towards rhodamine B and rhodamine 6G degradation. *Molecules*. 2024;29(18):4299.

doi: 10.3390/molecules29184299

7. Al-Rawashdeh NA, Allabadi O, Aljarrah MT. Photocatalytic activity of graphene oxide/zinc oxide nanocomposites with embedded metal nanoparticles for the degradation of organic dyes. *ACS Omega*. 2020;5(43):28046-28055.

doi: 10.1021/acsomega.0c03652

8. Sahoo S, Bhuyan M, Sahu AK, Alagarsamy P, Sahoo D. Photodegradation of methylene blue by metal-nanoparticles-modulated graphene-based composites. *Solid State Sci*. 2023;142:107255.

doi: 10.1016/j.solidstatesciences.2023.107255

9. Ikram M, Inayat T, Haider A, *et al*. Graphene oxide-doped MgO nanostructures for highly efficient dye degradation and bactericidal action. *Nanoscale Res Lett*. 2021;16(1):56.

doi: 10.1186/s11671-021-03510-3

10. Sarojini P, Leeladevi K, Kavitha T, *et al*. Design of V_2O_5 blocks decorated with garlic peel biochar nanoparticles: A sustainable catalyst for the degradation of methyl orange and its antioxidant activity. *Materials (Basel)*. 2023;16(17):5800.

doi: 10.3390/ma16175800

11. Mosleh AT, Hassan AE, Sabry N, *et al*. Design of MgO/graphene nanocomposites for photocatalytic reduction of 4-nitrophenol. *Phys Scr*. 2024;99(12):125914.

doi: 10.1088/1402-4896/ad8381

12. Tung CH, Chang JH, Hsieh YH, *et al*. Comparison of hydroxyl radical yields between photo- and electro-catalyzed water treatments. *J Taiwan Inst Chem Eng*. 2014;45(4):1649-1654.

doi: 10.1016/j.jtice.2013.11.011

13. Liyanaarachchi H, Thambiliyagodage C, Jayanetti M, Ekanayake G, Wijayawardana S, Samarakoon U. The photocatalytic and antibacterial activity of graphene oxide coupled CoOx/MnOx nanocomposites. Environ Technol Innov. 2025;37:103984.

doi: 10.1016/j.eti.2024.103984

14. Jamjoum HAA, Umar K, Adnan R, Razali MR, Mohamad Ibrahim MN. Synthesis, characterization, and photocatalytic activities of graphene oxide/metal oxides nanocomposites: A review. *Front Chem*. 2021;9:752276.

doi: 10.3389/fchem.2021.752276

15. Heidarizad M, Şengör SS. Synthesis of graphene oxide/magnesium oxide nanocomposites for adsorption of methylene blue. *J Mol Liq*. 2016;224:607-617.

doi: 10.1016/j.molliq.2016.10.005

16. Zidane Y, Laouini SE, Bouafia A, *et al*. Green synthesis of multifunctional MgO@AgO/Ag_2O nanocomposite for photocatalytic degradation of methylene blue and toluidine blue. *Front Chem*. 2022;10:1083596.

doi: 10.3389/fchem.2022.1083596

17. Melese A, Wubet W, Abebe A, Hussen A. A comprehensive review on recent progress in synthesis methods of ZnO/CuO nanocomposites and their biological and photocatalytic applications. *Results Chem*. 2025;14:102141.

doi: 10.1016/j.rechem.2025.102141

18. Kwang Benno Park H, Kumar P, Kebaili I, *et al*. Optimization and modelling of magnesium oxide (MgO) photocatalytic degradation of binary dyes using response surface methodology. *Sci Rep.* 2024;14(1):9412.

doi: 10.1038/s41598-024-59412-6

19. Arshad A, Iqbal J, Siddiq M, *et al.* Graphene nanoplatelets induced tailoring in photocatalytic activity and antibacterial characteristics of MgO/graphene nanoplatelets nanocomposites. *J Appl Phys*. 2017;121(2):024901.

doi: 10.1063/1.4972970

20. Khan M, Tahir MN, Adil SF, *et al*. Graphene based metal and metal oxide nanocomposites: Synthesis, properties and their applications. *J Mater Chem A*. 2015;3(37):18753-18808.

doi: 10.1039/C5TA02240A

21. Kokulnathan T, Jothi AI, Chen SM, *et al*. GO-MgO nanocomposites for electrochemical detection. *J Environ Chem Eng*. 2021;9(6):106310.

doi: 10.1016/j.jece.2021.106310

22. Wang H, Li G, Fakhri A. Fabrication and structural of the Ag_2S-MgO/graphene oxide nanocomposites with high photocatalysis and antimicrobial activities. *J Photochem Photobiol B*. 2020;207:111882.

doi: 10.1016/j.jphotobiol.2020.111882

23. Kakade PM, Kachere A, Mandlik N, Rondiya SR, Jadkar S, Bhosale SV. Graphene oxide assisted synthesis of magnesium oxide nanorods. *ES Mater Manuf*. 2021;12(2):63-71.

doi: 10.30919/esmm5f1044

24. Muhaymin A, Mohamed H, Hkiri K, Safdar A, Azizi S, Maaza M. Green synthesis of magnesium oxide nanoparticles using hyphaene thebaica extract and their photocatalytic activities. *Sci Rep.* 2024;14(1):20135.

doi: 10.1038/s41598-024-70135-4

25. Rezvannasab SG, Safari N, Ghaedi AM. Synthesis and performance enhancement of GO/MgO/PEI composite for CO_2 capture: Effects of operating parameters. *J CO_2 Util*. 2025;102:103245.

doi: 10.1016/j.jcou.2025.103245

26. Bhargava R, Khan S. Superior dielectric properties and bandgap modulation in hydrothermally grown Gr/MgO

nanocomposite. *Phys Lett A*. 2019;383(14):1671-1676.

doi: 10.1016/j.physleta.2019.02.025

27. Al-Sharabi A, Sada'a KSS, Al-Osta A, Abd-Shukor R. Structure, optical properties and antimicrobial activities of MgO-Bi_2-x$CrxO_3$ nanocomposites. *Sci Rep*. 2022; 12(1):10647.

doi: 10.1038/s41598-022-14687-4

28. Barad C, Kimmel G, Opalińska A, Gierlotka S, Łojkowski W. Lattice variation as a function of concentration and grain size in MgO-NiO solid solution system. *Heliyon*. 2024;10(10):e311275.

doi: 10.1016/j.heliyon.2024.e31275

29. Khatua A, Kumari K, Khatak D, *et al*. Cerium-doped magnesium oxide nanoparticles. *J Funct Biomater*. 2023;14(2):112.

doi: 10.3390/jfb14020112

30. Yang L, Zhang L, Jiao X, Qiu Y, Xu W. The electrochemical performance of reduced graphene oxide prepared from different types of natural graphites. *RSC Adv*. 2021;11(7):4042-4052.

doi: 10.1039/D0RA09457A

31. Das A, Mandal AC, Roy S, Nambissam PM. Internal defect structure of calcium-doped magnesium oxide nanoparticles. *AIP Adv*. 2018;8(9):095206.

doi: 10.1063/1.5001105

ACCSCIENCE PUBLISHING

Explora: Environment and Resource

ORIGINAL RESEARCH ARTICLE

Spatiotemporal characteristics of population density, heat stress vulnerability, and effects of urban green spaces in Lagos, Nigeria

Vincent Nduka Ojeh*

Department of Geography, Faculty of Social Sciences, Taraba State University, Jalingo, Taraba, Nigeria

Abstract

Rapid urbanization in Lagos, Nigeria, has intensified population density and altered local microclimates, exposing residents to increased risks of heat stress. As one of Africa's largest megacities, Lagos faces challenges in balancing urban growth with environmental sustainability. This study investigates the spatiotemporal characteristics of heat stress vulnerability and the moderating effects of urban green spaces (UGSs) across 11 local government areas (LGAs) in Lagos, Nigeria. Land surface temperature (LST) for 2013, derived from Landsat 8 Operational Land Imager imagery, was analyzed alongside 2013 population statistics and household questionnaire data collected from residents nearest to 15 observation sites. Each LGA was represented as a polygon feature in ArcGIS. Exposure indicators included LST, population density, and LST hotspot clusters; sensitivity indicators included vulnerable age groups (0–4 and 65+ years), low educational attainment, and income classes; and adaptive-capacity indicators included ownership of air conditioners and fans, proximity to water bodies, and proximity to grass or green spaces. Results reveal five population density categories across the metropolis. Yaba exhibits extremely high density (93,320–339,100 persons/km^2), while areas such as Abule-Egba, Mushin, Ilupeju, and Shomolu fall within high to moderately high density ranges. LST hotspot analysis indicates that Amuwo-Odofin, Isolo, Yaba, Ilupeju, Shomolu, Alagbado, and Ikotun are statistically significant hotspot locations at the 95–99% confidence level. Conversely, Oko-Afo, Ajangbadi, City Hall, Marina market, and Abule-Egba were not classified as hotspots due to inherent adaptive capacities, while Oshodi and Ejigbo emerged as cold spots. Adaptation measures vary across the metropolis. Ownership of air conditioners and fans, along with proximity to vegetation and water bodies, were the dominant strategies for mitigating heat exposure. The study underscores the critical role of UGSs in reducing heat stress vulnerability and highlights the need for strategic urban planning interventions to enhance adaptive capacity in Lagos.

Keywords: Heat stress; Urban green space; Population density; Land surface temperature; Vulnerability; Lagos

***Corresponding author:**
Vincent Nduka Ojeh
(vinceojehnetwork@gmail.com)

Citation: Ojeh VN. Spatiotemporal characteristics of population density, heat stress vulnerability, and effects of urban green spaces in Lagos, Nigeria. *Explora Environ Resour*. 2026;3(1):025170034. doi: 10.36922/EER025170034

Received: April 25, 2025

Revised: December 10, 2025

Accepted: December 24, 2025

Published online: February 4, 2026

1. Introduction

Urban green spaces (UGSs) are declining globally due to rapid urbanization, increasing population density, and continuous spatial expansion. Lagos, like many large cities,

has experienced a major reduction in vegetated areas as built-up areas replace natural land cover. This trend contributes to higher city temperatures and intensifies the urban heat island (UHI) effect, a phenomenon widely documented across different climatic regions.[1] Rising temperatures in cities have been directly linked to the loss of UGSs, which play important roles in regulating local climates, improving air quality, supporting recreation, maintaining hydrological balance, reducing pollution, promoting social interaction, and enhancing the overall quality of urban life.[2]

Several foundational studies have established strong relationships between urban population characteristics and the development of UHI conditions. Oke's[3] early work demonstrated that UHI intensity decreases with higher regional wind speed and increases with city population size.[3] Later studies by Jauregui,[4] Hogan and Ferrick,[5] Montavez *et al.*,[6] and Smith and Levermore[7] also found that expanding cities with dense built surfaces and increased human-generated heat tend to exhibit greater UHI intensities. Debbage and Shepherd[8] showed that both compact high-density areas and sprawling urban layouts can intensify UHI conditions, while Steeneveld *et al.*[9] confirmed strong correlations between population density and extreme UHI events in European cities.

The combined influence of climate change, rapid urban growth, and demographic pressure has increased heat exposure risks in many tropical cities. In Lagos, where temperatures remain high year-round, residents who cannot afford cooling technologies, such as air conditioners, are highly vulnerable to heat stress.[10] High temperatures have direct effects on public health by increasing heat-related illness and physiological strain. Medical experts warn that extreme heat in Lagos may worsen the spread and severity of climate-sensitive diseases, including Lassa fever, meningitis, and cholera, as well as other infectious outbreaks.[11] The World Health Organization also notes that rapid demographic and environmental changes, together with climate change, are increasing the frequency and severity of infectious disease events around the world.[12]

Despite the pressures from urban growth, UGSs remain essential for improving thermal comfort within cities. Vegetation cools the environment through shading and evapotranspiration, reducing the amount of heat absorbed and re-emitted by built surfaces. Numerous studies have confirmed that UGSs and blue infrastructure, such as tree cover, parks, and water bodies, can reduce heat stress and lower heat-related mortality in cities.[13] Their importance is especially clear in fast-growing cities like Lagos, where built surfaces dominate, and green space scarcity increases heat accumulation.

Concerns about persistent extreme heat in Lagos highlight the need to understand how different populations experience heat risk and how UGSs can reduce that risk. The vulnerability framework used in this study, encompassing exposure, sensitivity, and adaptive capacity, provides a comprehensive approach to assessing how heat impacts diverse communities.[14] By combining satellite-based land surface temperature (LST), demographic information, and data on household adaptation practices, this study explores the spatial pattern of heat stress vulnerability in Lagos and emphasizes the value of green infrastructure in building environmental resilience.

Mitigating the impacts of the urban climate, especially the UHI effect, requires deliberate planning strategies that moderate thermal conditions within built environments. One of the most effective approaches is integrating urban greening initiatives, including planting trees and other vegetation, implementing green roofs and cool roofs, and using reflective paving materials on streets and sidewalks. These interventions help regulate surface temperature, reduce heat storage in buildings, and enhance overall comfort within cities.[15]

Public parks and private green areas surrounding residential and commercial buildings significantly contribute to the quality of urban environments. They help reduce surface and air temperatures, improve thermal comfort, and promote various ecological benefits. Studies have long recognized that even a single tree can contribute to localize cooling, although the effect is limited to a small area.[16] In contrast, large urban parks can influence thermal conditions beyond their boundaries and create cooler microclimates in the surrounding built-up areas. Vegetation does not always cool the air directly, but it moderates temperatures by shading surfaces and reducing the rate of heating.[2]

A growing body of research emphasizes that natural elements, such as parks, forests, tree belts, and water bodies, enhance the livability of cities. These features provide environmental benefits, including water purification, air filtration, noise reduction, and local climate stabilization. They also support social and psychological well-being by offering spaces for recreation and social interaction.[17] However, without strategic design, maintenance, and management, urban parks may become underutilized or poorly maintained. Recent studies indicate that the value of green spaces is contingent on their effective integration into broader urban sustainability goals, particularly in rapidly growing cities.[18]

In rural landscapes dominated by vegetation, cooling occurs primarily through shading and evapotranspiration, which transfers moisture from the surface to the

atmosphere.[19] Urban environments, however, are dominated by impervious materials, such as asphalt, concrete, and metal surfaces that absorb large amounts of heat during the day and release it at night. As cities expand and vegetation is cleared, reduced surface moisture limits the capacity for evaporative cooling. This contributes to higher daytime temperatures and persistent nighttime heat, intensifying both surface and atmospheric heat islands.[19]

Areas with extensive impervious cover, sometimes exceeding 75%, experience lower natural cooling than vegetated areas where impervious surfaces account for <10%.[20] To counter this, researchers have proposed several mitigation measures, including roof ponds, evaporative cooling systems, water features, and increased vegetation cover around residential and commercial structures.[21] Urban form also plays a crucial role; the orientation and geometry of buildings influence solar access and heat retention, making building design an important consideration in reducing urban heat.[22]

Vegetation reduces ambient temperatures by shading surfaces and through evapotranspiration, which converts incoming solar radiation into latent heat rather than sensible heat. The cooler surfaces then emit less long-wave radiation, reducing human exposure to heat.[23] The type, density, and spatial arrangement of vegetation near buildings can greatly influence indoor and outdoor temperatures, as well as energy demand for cooling. In dense subtropical cities, vegetation has been shown to reduce heat accumulation in buildings by more than 30%.[23]

Recent studies also highlight the role of urban morphology in determining when and how cooling can occur. For example, some cities experience morning cool islands where urban areas are temporarily cooler than surrounding rural areas. This effect depends largely on building configuration, vegetation cover, and human-generated heat.[24] In Lagos, where rapid urban growth has altered the landscape and reduced green cover, understanding these dynamics is essential for developing climate-resilient urban planning strategies.

2. Materials and methods

2.1. Study area

Lagos is the smallest state in Nigeria by land area, but it remains the most urbanized and industrialized part of the country. It ranks among the largest and fastest-growing metropolitan regions in the world, and it is currently the most populous urban center in sub-Saharan Africa. The state comprises 20 local government areas (LGAs), of which 16 form the densely populated metropolitan core.[25] Geographically, Lagos lies between longitudes 2°42' and 3°42' east and latitudes 6°22' and 6°42' north, occupying a coastal zone that contains a network of lagoons, creeks, barrier spits, and extensive wetlands (Figure 1).[26]

Population growth in Lagos is rapid. The population rose from 345,137 in 1952 to more than a million in 1963, over 5 million in 1988, and 9.1 million in 2006, according to census data.[27] Recent estimates suggest that the population to be 17,156,400 in 2025, with a 3.2% annual growth rate compared to 2.6% national population growth rate.[28,29] This sustained expansion has made Lagos one of the most rapidly growing cities in the world and a major destination for internal migration. Lagos serves as an economic and cultural hub, drawing residents from more than 250 ethnic groups in Nigeria.

According to recent urban area assessments, Lagos covers approximately 1,425 km^2, with a population density estimated at about 9,000 persons/km.[28,29] The city consumes more than half of Nigeria's electricity generation and accommodates over half of the country's vehicles, all concentrated within an already stressed road network. Nearly 80% of the population resides on just 37% of the land area. Economic activities, administrative functions, and commercial services are heavily concentrated within this metropolitan zone.

2.2. Climate and vegetation

Lagos experiences a wet equatorial climate influenced by its coastal location near the Gulf of Guinea and its proximity to the equator. The region features deep, poorly drained soils, and is characterized by a complex drainage network comprising lagoons, wetlands, and waterways that account for nearly one-quarter of the total land area.[29] Major water bodies include the Lagos and Lekki lagoons, the Ogun and Yewa rivers, and several creeks, such as the Ologe, Kuramo, and Five Cowries creeks. Combined, these water bodies and wetlands cover more than 40% of the state's area, and about 12% of the land is prone to seasonal flooding.[29]

Temperatures in Lagos remain high throughout the year. The mean annual temperature is about 28°C, with average maximum and minimum temperatures of 33°C and 26°C, respectively. Rainfall is substantial from May to November, though monthly variations in peak values are significant.[29] This combination of high temperature and high humidity increases the likelihood of urban heat discomfort and heat stress.

2.3. Methods

This study developed a heat-stress vulnerability index for Lagos by combining three components: exposure, sensitivity, and adaptive capacity. These components were used to assess how population characteristics, thermal

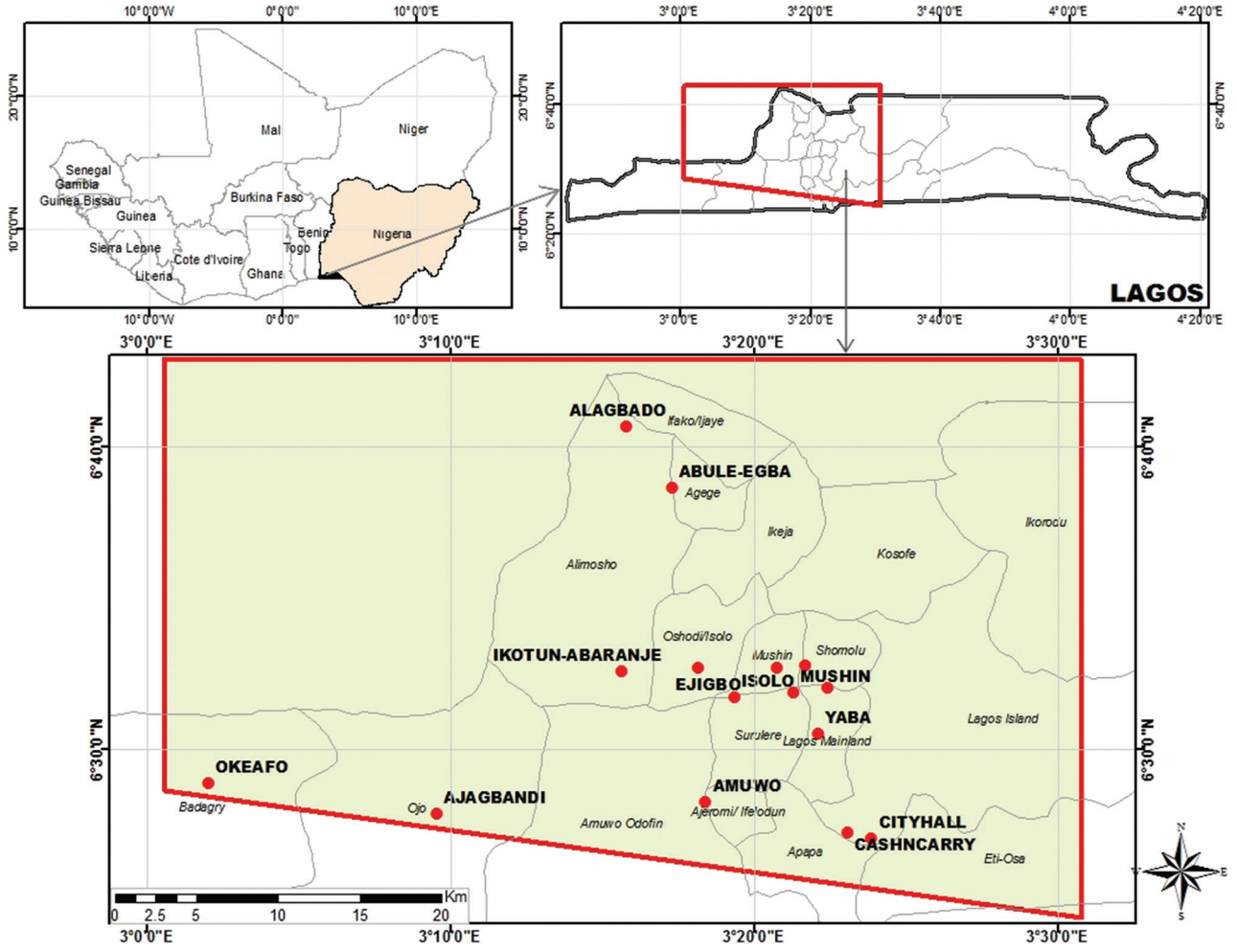

Figure 1. Map of the study area showing the locations of the study sites

conditions, and local environmental features influence vulnerability across different LGAs. The vulnerability framework employed in this study followed the exposure–sensitivity–adaptive capacity structure widely used in Intergovernmental Panel on Climate Change assessments and in several heat vulnerability index studies. Indicators were selected based on conceptual relevance and data availability within the Lagos context. Variables such as population density, age group, vegetation cover, and access to cooling devices have also been used in similar studies globally to represent components of heat exposure, sensitivity, and adaptative capacity. While several indicators, such as ownership of fans or air conditioners, function as proxies rather than complete measures of adaptive capacity, they reflect locally meaningful variations in a household's ability to regulate indoor temperatures. The conceptual framework is summarized in Figure 2.

LST data for 2013 were obtained from Landsat 8 Operational Land Imager imagery (metadata are provided in Appendix). Population data for the 11 LGAs included in the analysis (Alagbado, Abule-Egba, Ikotun, Isolo, Oshodi, Mushin, Shomolu, Yaba, Amuwo-Odofin, Ajangbadi and Oko-afo) were based on projections from 2013. Each LGA was represented as a polygon within ArcGIS (version 10.2, Environmental Systems Research Institute, United States of America), and spatial analysis incorporated population density, LST values, and cluster hotspot detection (Figure 3). In addition, questionnaires were administered to 200 households located near the 15 temperature observation sites across the 11 LGAs. These surveys provided information on exposure factors, sensitivity indicators, and adaptation practices. The remaining nine LGAs without temperature observation sites were classified as "no data" areas. A multi-stage purposive sampling procedure was employed to select respondents

for the household survey. The 200 households were drawn from communities located within the vicinity of the 15 temperature observation sites distributed across the 11 LGAs with available thermal and demographic data. This exploratory sampling frame allowed the study to capture adaptation behaviors and household-level characteristics that spatially correspond to measured LST patterns. The sample was therefore not intended to be statistically representative of the entire Lagos population, but rather to provide contextual insights into household-level sensitivity and adaptive capacity in areas experiencing varying heat conditions.

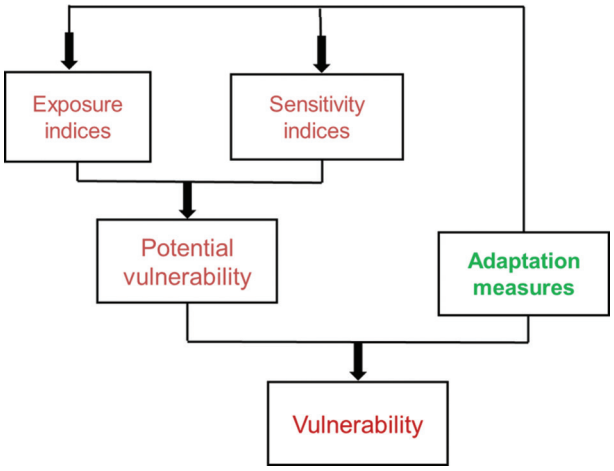

Figure 2. Conceptual model for heat stress vulnerability (adapted from Schroeter *et al.*[30] and Ebi *et al.*[31])

Adaptation strategies considered in the analysis included ownership of air conditioners and fans, proximity to vegetation or green spaces, and proximity to water bodies, such as open water or swimming pools. Adaptation capacity was grouped into three categories:

(i) High adaptation: Households that primarily rely on air conditioners and any other adaptation method
(ii) Medium adaptation: Households that rely mainly on fans and at least one additional strategy other than air conditioning
(iii) Low adaptation: Households that rely on any adaptation strategy but fall below the mean values for both air conditioner and fan ownership.

These adaptation measures, combined with exposure and sensitivity indicators, formed the basis for constructing the heat vulnerability index for Lagos. The analysis relied on 2013 Landsat LST data and 2013 population estimates because these were the only harmonized datasets that aligned with the period of the original household survey and were spatially complete for the 11 LGAs included in the study. At the time of analysis, recent LST and population datasets lacked full spatial coverage or consistent methodological processing across all LGAs, which would have introduced temporal or spatial inconsistencies into the vulnerability assessment. Therefore, the results should be interpreted as a 2013 baseline of urban heat exposure

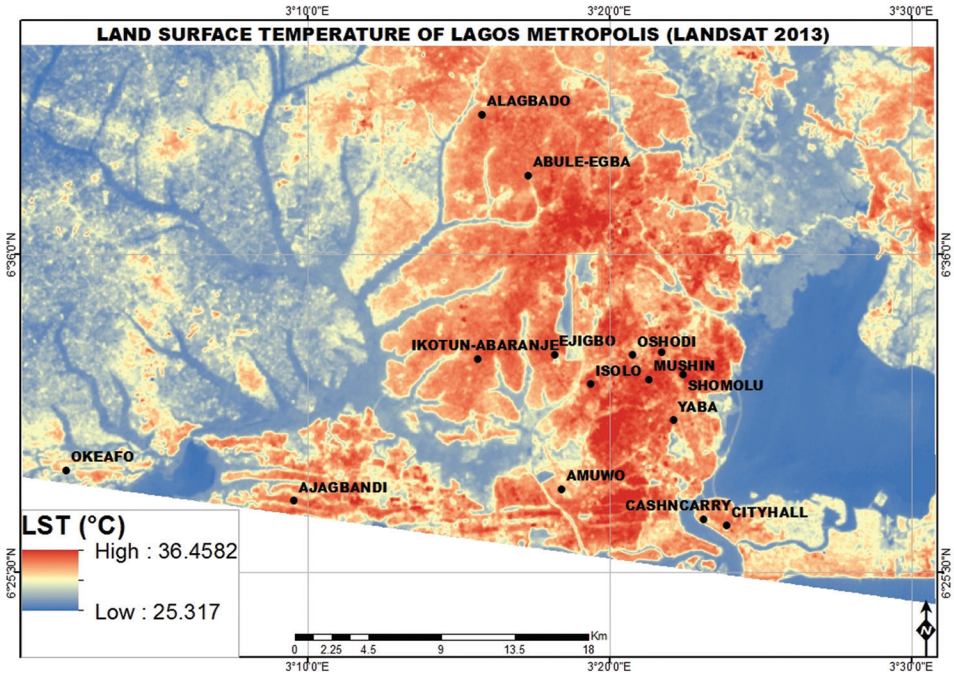

Figure 3. Land surface temperature of Lagos, 2013

and vulnerability rather than a representation of present-day conditions.

3. Results and discussion

The results of this study are primarily descriptive and reflect an exploratory spatial assessment of heat stress vulnerability using available thermal, demographic, and household-level data. The analysis provided insight into relative patterns of exposure and vulnerability across selected LGAs but does not constitute a predictive statistical model of heat risk. The descriptive approach is appropriate for the available data; however, advanced quantitative modeling would further strengthen the understanding of the drivers of vulnerability.

3.1. Exposure index

3.1.1. Heat exposure index of Lagos

Table 1 summarizes the heat vulnerability parameters obtained from the questionnaire survey. The exposure index included LST, population density, and LST hotspot classification. Sensitivity factors comprised the most vulnerable age groups (0–4 years and 65+ years), low educational attainment (no formal education, trade certificates, primary school certificates, and secondary school certificates), and income categories, including high income (₦ 100,000 and above), medium income (₦ 50,000–99,900), and low income (below ₦ 50,000). Adaptation factors included ownership of air conditioners and fans, living near water bodies, and proximity to green areas.

Figure 4 presents the population density distribution of Lagos based on projections from 2013. Five population density categories were identified. Yaba recorded the highest density, ranging from 93,320 to 339,100 persons/km^2. Abule-Egba, Mushin, Ilupeju, and Shomolu fell within the moderately high-density range of 45,360–93,310 persons/km^2. Isolo, Oshodi, and Ejigbo were classified as medium-density areas with populations ranging from 16,980 to 45,350 persons/km^2. Alagbado and Ikotun fell within the lower-density range of 6,417–16,970 persons/km^2. The observation sites with the lowest densities (88–6,416 persons/km^2) were City Hall, Marina market, Amuwo-Odofin, Ajangbadi, and Oko-Afo.

Table 1. Vulnerability index parameters covered in the questionnaire

Vulnerability index parameters	Variables
Exposure	• Land surface temperature • Population density • LST hotspot analysis areas
Sensitivity	• Most vulnerable age group (0–4 and 65+) • Low education levels (no formal education, • trade certificate, primary school certificate, and West African Examinations Certificate) • Income class (high [> ₦ 100,000], medium [₦ 50,000–99,900], and low [< ₦ 50,000])
Adaptation	• Ownership of air conditioners • Ownership of fans • Living close to a water body • Proximity to grass/green space

Abbreviation: LST: Land surface temperature.

These variations in density have direct implications for heat exposure. Densely populated areas, such as Yaba, experience greater heat stress because built-up areas replace natural cover and limit passive cooling opportunities, such as airflow, tree shade, and contact with water bodies. This pattern aligns with findings from other megacities. For example, in Mumbai, rapid urban expansion led to a nearly 20% loss of green spaces over three decades and a threefold increase in high-temperature zones.[27] Similar processes are occurring in Lagos.

3.1.2. LST cluster hotspot analysis

Figure 5 shows the LST cluster hotspots across Lagos. At the 95–99% statistical confidence level, Amuwo-Odofin, Isolo, Yaba, Ilupeju, Shomolu, Alagbado, Mushin, and Ikotun were classified as significant temperature hotspots. These areas are characterized by dense built environments and limited vegetative cover, conditions that promote the absorption and retention of heat.

In contrast, Oko-Afo, Ajangbadi, City Hall, Marina market, and Abule-Egba were not classified as hotspots. These areas possess natural or built features that enhance adaptive capacity, including open spaces, tree cover, and proximity to water bodies. At the same confidence level, Oshodi and Ejigbo were categorized as cold spots, likely due to the influence of surrounding vegetation, open land, or lower built density.

These observations correspond with recent findings. In eastern India, rapid urban expansion resulted in an 8.62% reduction in vegetated areas over a 10-year period, while the relationship between LST and the normalized difference vegetation index weakened significantly.[28] Similarly, research in Thiruvananthapuram, India, documented a 118% increase in built-up areas that resulted in a measurable rise in mean LST.[29] Additional studies show that expanding tree canopy cover can reduce peak thermal stress by more than 2°C in certain urban settings, demonstrating the moderating effect of vegetation on extreme heat.[30] These findings strongly mirror the thermal conditions observed in Lagos.

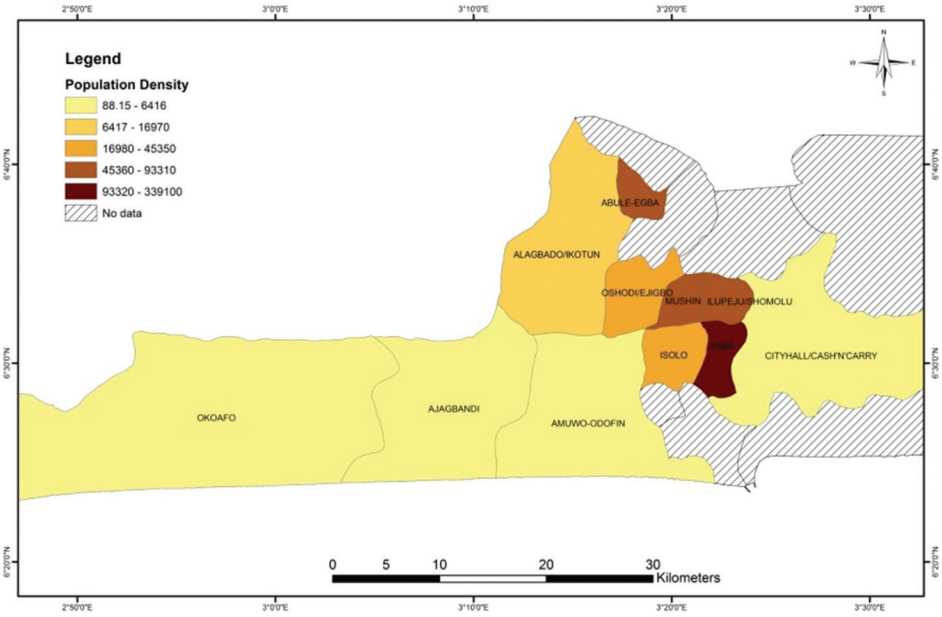

Figure 4. Population density map of Lagos

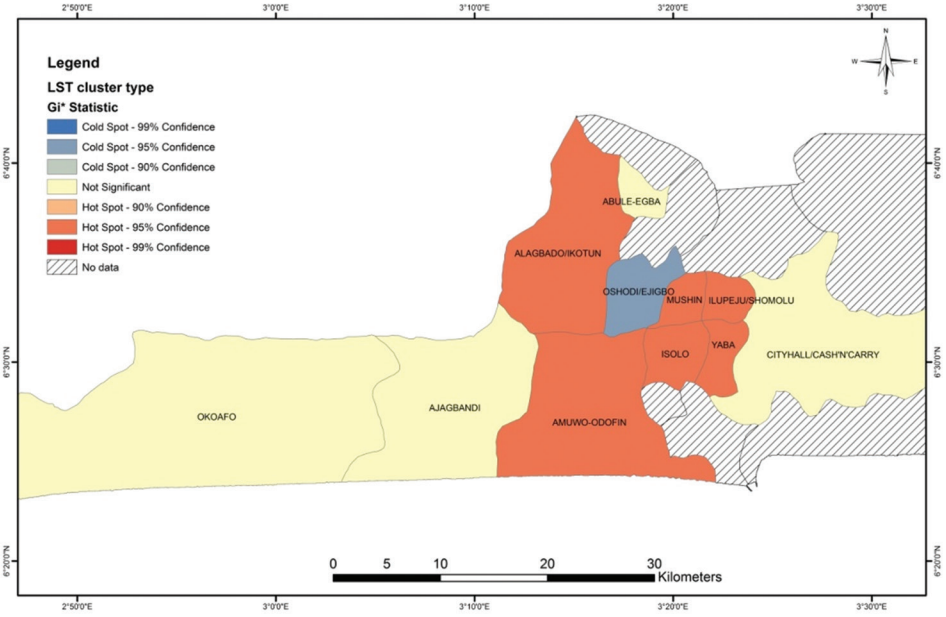

Figure 5. Land surface temperature cluster hotspot of Lagos metropolis
Abbreviation: GI: The Getis–Ord, Getis statistic at location i.

3.1.3. Heat exposure index of Lagos metropolis

Figure 6 shows the heat exposure index generated by combining population density and LST hotspot patterns. Yaba and Mushin were designated as high-exposure zones due to their high built density and limited natural cooling resources. Amuwo-Odofin, Isolo, Ilupeju, and Shomolu constituted moderate-exposure zones, reflecting a mix of built-up areas and available green spaces. Alagbado and Ikotun exhibited low exposure levels, while Oko-Afo, Ajangbadi, City Hall, Marina market, Oshodi, Ejigbo, and Abule-Egba showed minimal exposure, attributed to vegetation cover, open areas, or proximity to water bodies.

These patterns follow trends observed in other cities. For

example, a fine-scale assessment in Augsburg, Germany, reported that vegetation cover and surface imperviousness have a strong influence on daytime temperatures, while building form affects nighttime conditions.[31] Lagos exhibits similar dynamics, with densely occupied neighborhoods displaying higher heat exposure and areas with vegetation and open land demonstrating greater thermal resilience.

3.2. Sensitivity index for Lagos

3.2.1. Distribution of the sensitive age group in Lagos metropolis

Figure 7 shows the spatial distribution of the most vulnerable age groups, specifically children aged 0–4 years and adults aged 65 years and above. These groups are widely recognized in heat-vulnerability studies as the most physiologically sensitive to extreme temperatures due to limited thermoregulatory capacity and higher susceptibility to heat-related illness.[32]

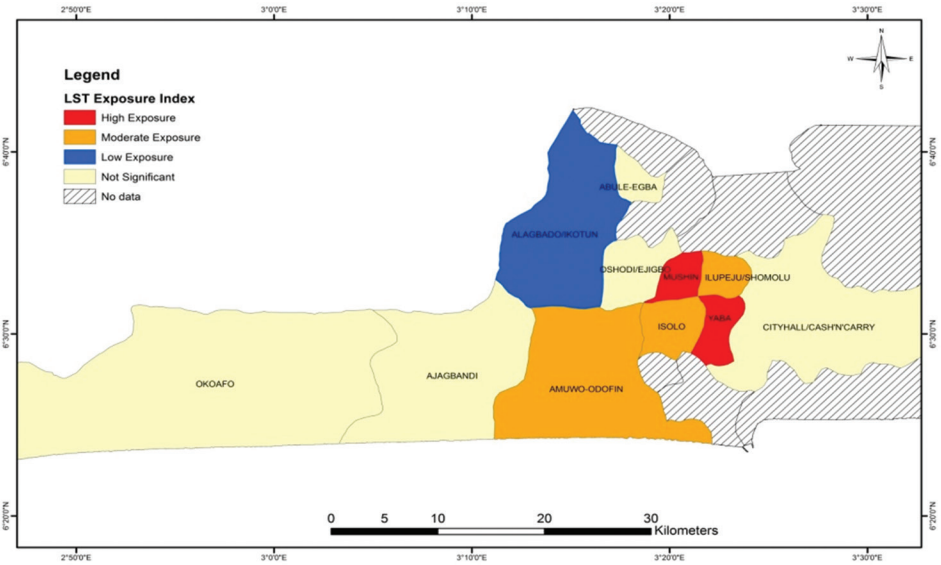

Figure 6. The land surface temperature (heat) exposure index of Lagos metropolis

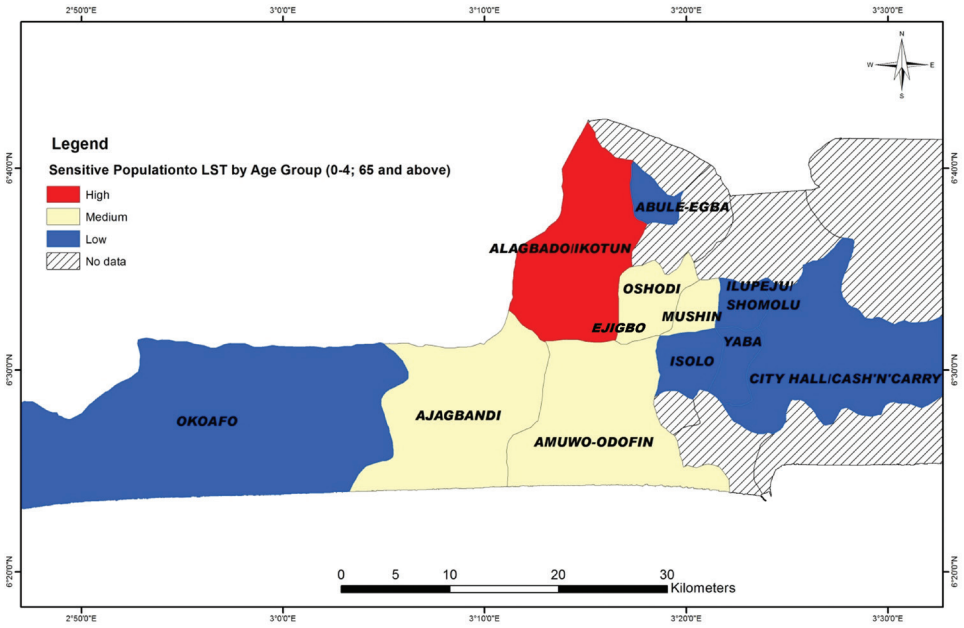

Figure 7. Distribution of the sensitive age group in Lagos metropolis

In Lagos, high populations of these age groups were found in Alagbado and Ikotun. A medium-sized population resided in Ajangbadi, Amuwo-Odofin, Oshodi, Ejigbo, and Mushin. Areas such as Oko-Afo, Isolo, Yaba, City Hall, Marina market, Shomolu, Ilupeju, and Abule-Egba had relatively low populations of the vulnerable age groups.

These patterns suggest that the western and northwestern parts of the metropolis have a higher proportion of residents susceptible to heat stress, whereas the central business district and coastal zones have lower populations of these demographic categories.

3.2.2. Educational attainment of the population in Lagos

Figure 8 illustrates the distribution of individuals with low levels of education, defined as residents without formal schooling, trade certificates, primary school certificates, or secondary school certificates. Educational attainment is a key determinant of heat vulnerability because it influences access to information, awareness of heat risks, and the ability to adopt effective adaptive behaviors.

The map indicates that the highest distribution of populations with low educational attainment was observed in Isolo, Mushin, Oshodi, and Ejigbo. High populations of low-educated individuals were also observed in Oko-Afo, Alagbado, and Ikotun. A moderate number of low-educated individuals resided in Abule-Egba. Low populations of individuals with low education levels were found in Yaba, City Hall, Marina market, and Ajangbadi, whereas Amuwo-Odofin, Ilupeju, and Shomolu have the lowest populations of individuals with low education levels.

These spatial patterns reflect the socioeconomic landscape of Lagos, where low-income, high-density neighborhoods often overlap with areas of limited educational opportunities. Such areas are likely to exhibit greater heat sensitivity due to reduced access to resources and lower adaptive capacity.

3.2.3. Population distribution of Lagos by income level

Figure 9 presents the income-based population distribution for Lagos. Income level is a major determinant of vulnerability because it affects the capacity to acquire cooling technologies, modify living environments, or relocate during extreme heat events.

High-income areas included Amuwo-Odofin, City Hall, and Marina market. These neighborhoods have access to better infrastructure, improved housing conditions, and greater purchasing power for cooling devices. Middle-income areas included Yaba, Mushin, Oshodi, and Ejigbo, whereas low-income areas included Oko-Afo, Ajangbadi, Alagbado, Ikotun, Abule-Egba, Isolo, Ilupeju, and Shomolu.

Low-income households often face the greatest challenges during extreme heat due to overcrowding, poor building materials, and limited access to cooling strategies. These socioeconomic factors strengthen the heat sensitivity component of the vulnerability assessment.

3.2.4. Combined heat sensitivity index

Figure 10 presents the combined heat sensitivity index, integrating vulnerable age groups, low educational attainment, and income levels. The results reveal that Abule-Egba, Alagbado, Ikotun, Isolo, and Oko-Afo exhibited high heat sensitivity. A medium sensitivity was observed in Ajangbadi, Oshodi, Ejigbo, Mushin, and Yaba, whereas Amuwo-Odofin, City Hall, Marina market, Ilupeju, and Shomolu exhibited low sensitivity.

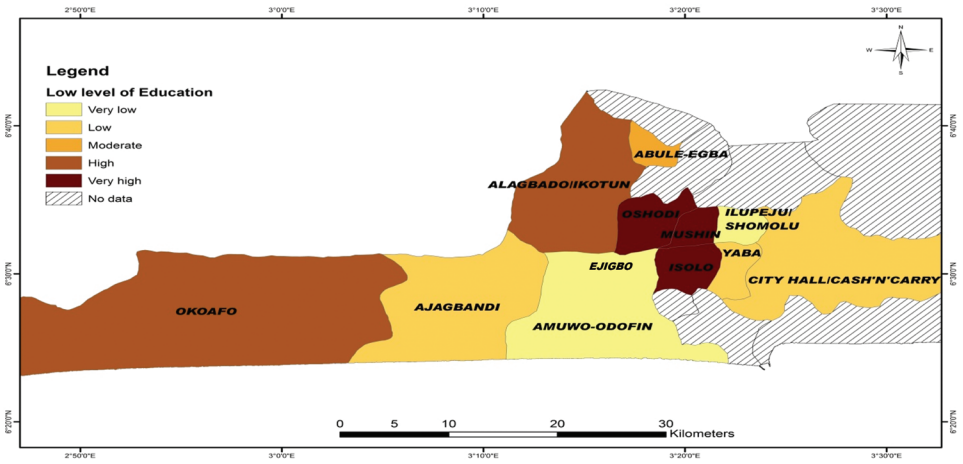

Figure 8. Distribution of population with low educational levels in Lagos metropolis

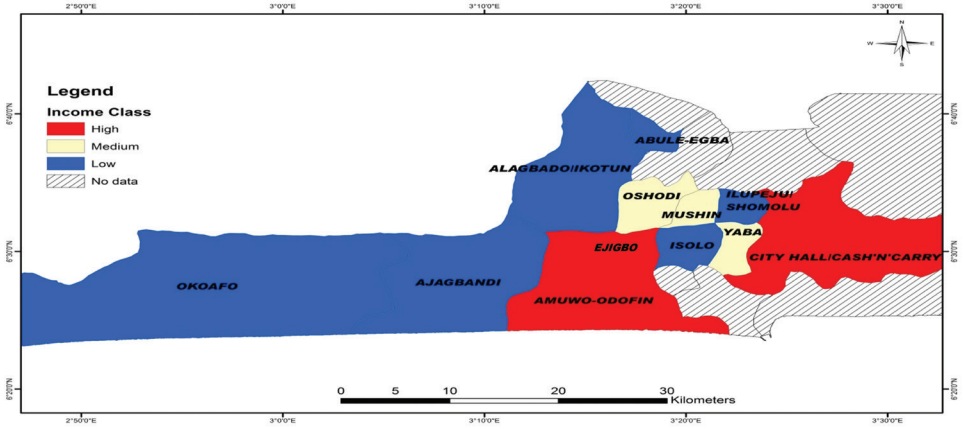

Figure 9. Population distribution in Lagos metropolis by income level

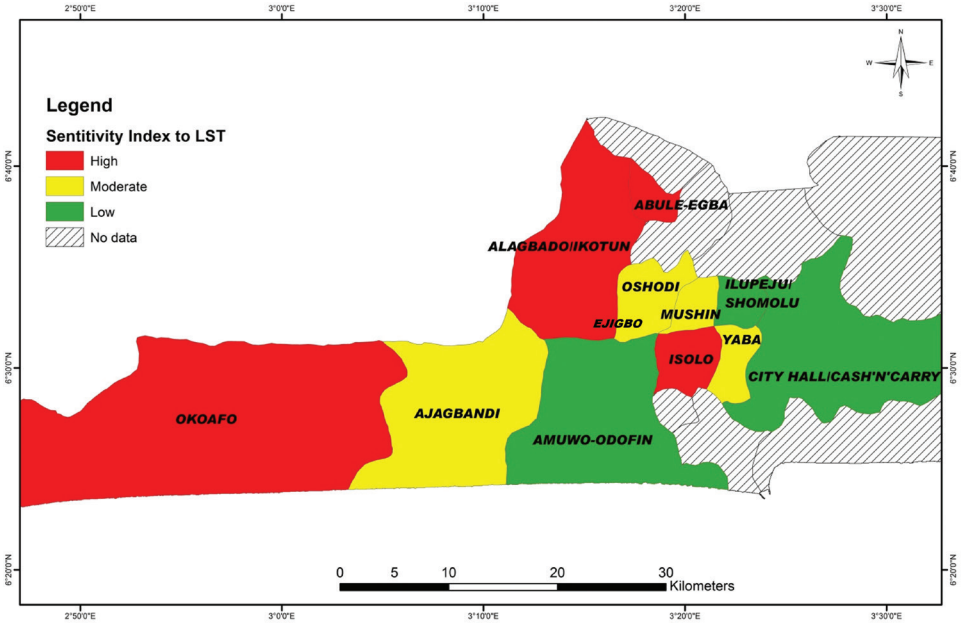

Figure 10. Overall heat sensitivity index of Lagos Metropolis

These findings align with broader research on urban heat vulnerability. For instance, a recent assessment in the Pearl River Delta region of China found that heat vulnerability is driven primarily by frequent heatwave events, demographic sensitivity, and disparities in economic and healthcare infrastructure.[21] Similar drivers are evident in Lagos, where densely populated neighborhoods with limited incomes and educational opportunities face heightened heat sensitivity.

3.3. Adaptation strategies to heat stress in Lagos

Adaptation capacity reflects the resources available to households to cope with high temperatures. In this study, adaptation strategies included ownership of air conditioners or fans, proximity to trees or green spaces, and proximity to water bodies. These strategies help reduce exposure to heat and are important indicators of communities' ability to manage thermal discomfort.

High adaptation capacity was defined as locations where the mean air conditioner ownership exceeds the overall average of 3.36 recorded across the 11 LGAs. Medium adaptation capacity refers to locations where fan ownership exceeds the overall mean of 6.63 and where residents employ at least one additional cooling strategy beyond air conditioning. Low adaptation capacity refers to LGAs that fall below the mean for both air conditioner and fan ownership

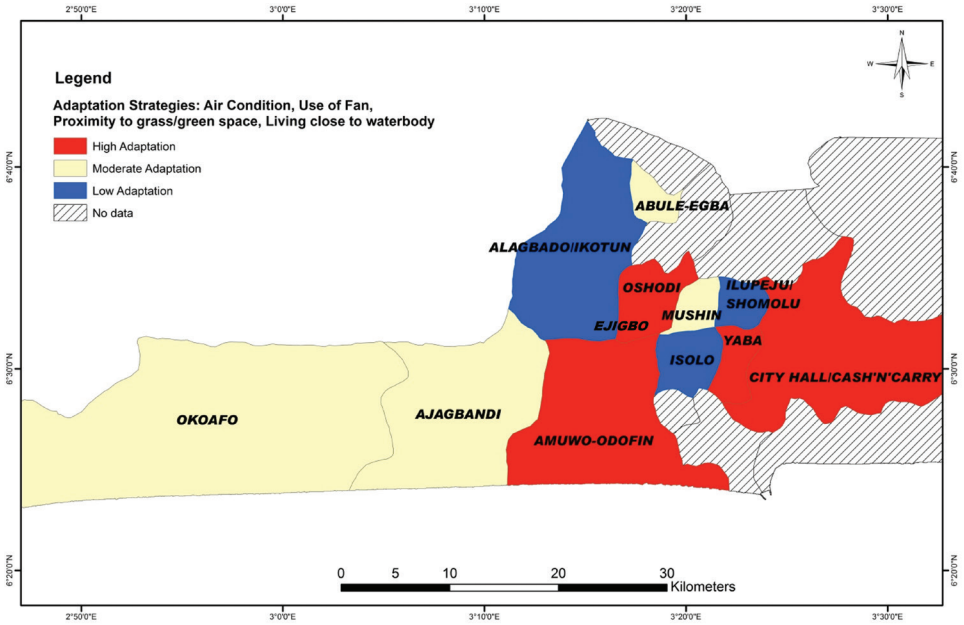

Figure 11. Distribution of adaptive strategies to heat stress in Lagos metropolis

and that rely primarily on other cooling strategies.

Figure 11 presents the spatial distribution of adaptation strategies across Lagos. The results show that Amuwo-Odofin, Oshodi, Ejigbo, Marina market, City Hall, and Yaba demonstrated high adaptation capacity. These locations benefited from relatively better housing quality, higher income levels, or improved access to infrastructure that supports mechanical cooling.

A moderate adaptation capacity was observed in Oko-Afo, Ajangbadi, Abule-Egba, and Mushin. These areas rely primarily on fans and complementary strategies, such as shading from trees or the presence of nearby water bodies. Although mechanical cooling is used, it is not as widespread as in high-adaptation zones.

A low adaptation capacity was reported in Alagbado, Ikotun, Isolo, Ilupeju, and Shomolu. These areas have limited access to mechanical cooling technologies and rely heavily on informal or natural methods to reduce heat stress. Lower adaptation levels in these neighborhoods may be linked to socioeconomic constraints, housing characteristics, or limited access to green spaces.

Overall, the spatial pattern of adaptation capacity suggests that thermal resilience in Lagos is unevenly distributed. Areas with greater economic resources and improved infrastructure exhibit greater adaptation potential, whereas low-income areas face greater challenges in coping with extreme heat conditions. These disparities highlight the need for targeted interventions that expand access to cooling resources and enhance environmental infrastructure in the most heat-sensitive communities.

3.4. Potential vulnerability to heat stress in Lagos

The combined effects of exposure, sensitivity, and adaptation determine the potential vulnerability of communities to heat stress. Figure 12 presents the integrated vulnerability classification for the 11 LGAs examined in this study. The results show distinct spatial variations, reflecting the interaction between demographic characteristics, built environment features, and access to cooling resources.

High potential vulnerability was observed in Mushin and Yaba. These neighborhoods experience combinations of high sensitivity, moderate-to-high exposure, and low adaptation capacity. In most of these areas, built density is high, informal settlements are widespread, and household access to air conditioners is limited. These conditions limit the ability of residents to cope with extreme heat. Medium vulnerability was observed in Ajangbadi, Ejigbo, Isolo, and Oshodi. A low adaptation capacity was reported in Alagbado, Ikotun, Isolo, Ilupeju, and Shomolu. These areas have limited access to mechanical cooling technologies and rely heavily on informal or natural methods to reduce heat stress. Lower adaptation levels in these neighborhoods may be linked to socioeconomic constraints, housing characteristics, or limited access to green spaces. Although not as vulnerable as the high-risk zones, these areas still require targeted interventions to improve heat resilience. From the figure, these locations fall into low-income categories.

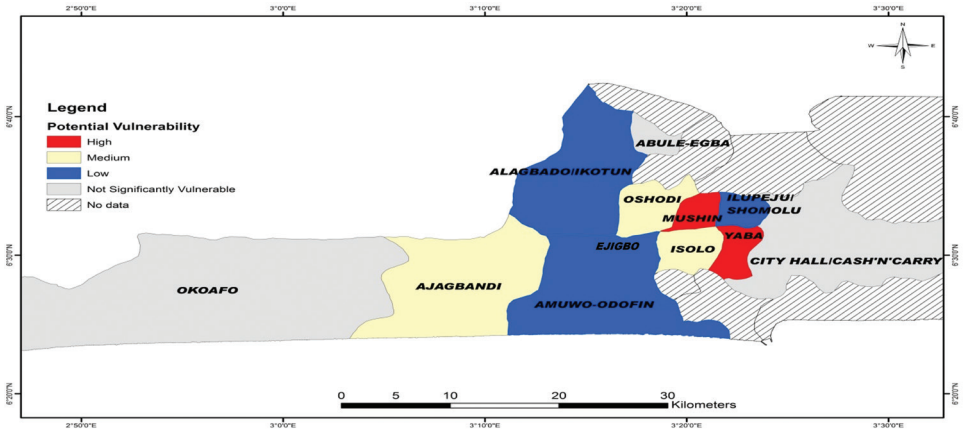

Figure 12. Potential heat vulnerability map of Lagos metropolis

The spatial distribution of potential vulnerability in Lagos reflects broader global patterns in tropical megacities, where vulnerability is often the highest in low-income areas with poor infrastructure, limited green spaces, and high population densities. Studies in cities such as Manila, Rio de Janeiro, and Dhaka similarly report that vulnerability hotspots are concentrated in rapidly urbanizing districts with limited adaptive capacity and high environmental stress.[33] The results for Lagos align with this trend, underscoring the importance of equity-focused adaptation strategies that prioritize the most vulnerable communities.

3.5. Heat vulnerability index and spatial distribution

Figure 12 shows the heat vulnerability index of Lagos and the spatial distribution of vulnerability across the metropolitan area. The results demonstrate that most of the study area falls within the medium- to high-vulnerability zones, reflecting the combined influence of dense built environments, demographic pressure, and limited adaptation capacity.

High vulnerability was observed in Abule-Egba, Ajangbadi, Alagbado, Ikotun, Ilupeju, Isolo, Oko-Afo, and Shomolu. These areas exhibit persistent high temperatures, significant proportions of sensitive populations, and limited access to cooling resources such as air conditioners or shade from vegetation. Many of these neighborhoods contain informal settlements, inadequate housing, and limited access to green spaces. These factors heighten susceptibility to heat stress and reduce households' ability to manage extreme temperatures.

Medium vulnerability was recorded in Mushin, Oshodi, and Ejigbo. These areas experience moderate exposure and sensitivity but have relatively higher adaptation capacity than the high-vulnerability zones. Residents of these areas frequently rely on mechanical cooling devices, such as fans and, in some cases, air conditioners, to reduce exposure to daytime heat. However, their vulnerability remains significant due to high population density and limited access to natural cooling features.

Low vulnerability occurred in Amuwo-Odofin, City Hall, Marina market, and Yaba. These locations benefit from lower exposure levels, reduced sensitivity, and strong adaptation capacity. Higher income levels, better building materials, and proximity to vegetated or water-based environments contribute to improved resilience. These neighborhoods demonstrate the importance of socioeconomic advantages in moderating the impacts of extreme heat.

The overall vulnerability pattern in Lagos mirrors findings from other tropical megacities. Studies in cities such as Bangkok, Jakarta, and Ho Chi Minh City show that vulnerability is shaped by a combination of demographic characteristics, LST, and access to cooling infrastructure.[34] As in Lagos, the urban poor tend to reside in the most heat-exposed and least adapted neighborhoods, reinforcing the need for policies that enhance resilience in underserved communities.

This study has several limitations. First, the use of 2013 LST and population data reflects the period for which complete and harmonized datasets were available and should be interpreted as a baseline rather than current conditions. Second, the analysis was restricted to 11 LGAs due to the absence of comparable temperature observation points and survey data in the remaining LGAs, which may limit the generalizability of the results to the wider Lagos metropolis. Third, the household survey sample of 200 respondents is small relative to the population of Lagos and was selected purposively near observation sites; therefore, the findings describe local adaptation behaviors but are not statistically representative of the entire population.

Fourth, some indicators used to operationalize exposure, sensitivity, and adaptive capacity are proxies, and the composite vulnerability index has not been validated with independent datasets. Fifth, the mapping outputs represent relative classes of vulnerability and are not probabilistic risk estimates. Future research should incorporate recent thermal datasets, larger probability-based surveys, and formal statistical or machine learning models to strengthen the predictive capacity of heat vulnerability assessments.

4. Recommendations

This study highlights the need for a more systematic approach to understanding and managing heat stress across Lagos. Future assessments should use recent, high-resolution thermal datasets, updated demographic information, and complete spatial coverage across all LGAs. Large and representative household surveys, combined with advanced analytical methods such as multivariate regression, geographically weighted regression, and machine learning, can improve scientific understanding of the relationships among LST, vegetation, population density, and social vulnerability.

From a policy perspective, Lagos requires a coordinated and proactive framework to mitigate heat-related risks. Priority actions include expanding and protecting urban green areas, incorporating heat-risk indicators into land-use planning and building regulations, promoting cool roofs and reflective building materials, and improving ventilation and shading in high-density neighborhoods. Strategies such as strengthening early warning systems, improving access to cooling options, and directing support to vulnerable groups, such as low-income households, the elderly, and those living in densely populated settlements, can help mitigate the impacts of heat.

Effective action will require collaboration among urban planners, environmental agencies, public health institutions, researchers, and community organizations. Integrating heat risk considerations into urban development, housing, public health, and climate adaptation strategies will help build a more heat-resilient and sustainable Lagos.

Continuous monitoring of LST, urban vegetation, and population health outcomes will help policymakers evaluate the effectiveness of adaptation measures and improve resilience strategies.

5. Conclusion

This study assessed the spatial pattern of heat stress vulnerability in Lagos by integrating LST, population density, demographic sensitivity, and adaptation capacity across 11 LGAs. The results show that vulnerability to heat stress varied considerably across the metropolitan area, with the highest levels concentrated in densely populated and economically disadvantaged neighborhoods. These areas experience higher temperatures, contain larger proportions of sensitive populations, and have limited access to cooling resources or green spaces.

Medium vulnerability areas benefit from improved adaptation practices, although high built density and persistent warm temperatures still present significant risks. Low vulnerability zones display strong adaptation capacity, lower sensitivity, and, in some cases, reduced exposure, largely due to better infrastructure, improved housing, and access to vegetation or water bodies.

The findings demonstrate that heat vulnerability in Lagos is shaped by the combined effects of rapid urban growth, limited green space, socioeconomic inequality, and uneven access to cooling infrastructure. As Lagos continues to expand, addressing these factors will be critical for reducing the health and environmental impacts of extreme heat. The framework from this study provides a valuable spatial insight into developing targeted adaptation strategies that support resilience in the most vulnerable communities. While the present analysis provides a useful exploratory baseline of heat vulnerability patterns across the selected LGAs, the findings highlight the need for future studies to integrate more recent thermal datasets, expand the spatial extent to include all LGAs, and apply quantitative modeling techniques, such as regression or geographically weighted regression, to further examine the relationships between vegetation cover, population density, and LST.

Acknowledgments

The author acknowledges all who contributed to this work. A special recognition to my supervisors, Prof. A.A. Balogun and Prof. A.A. Okhimamhe, for improving the quality of the work.

Funding

This study is part of the PhD work of Vincent Nduka Ojeh, supported by the West African Science Service Center on Climate Change and Adapted Land Use (grant no.: WASC-20130902).

Conflict of interest

The author declares no conflict of interest.

Author contributions

This is a single-authored article.

Ethics approval and consent to participate

Not applicable.

Consent for publication

Not applicable.

Availability of data

Data for the study are available from the author on reasonable request.

Further disclosure

Part of the findings (temperature difference) was published in 2016 by MDPI in *Climate* with the title "Urban-Rural Temperature Differences in Lagos." (https://doi.org/10.3390/cli4020029)

References

1. Akbari H, Bell R, Brazel T, *et al*. *Reducing Urban Heat Islands: Compendium of Strategies-Urban Heat Island Basics*. Perrin Quarles Associates Inc.; 2014. p. 1-19. Available from: https://www.epa.gov/sites/default/files/2014-06/documents/basicscompendium.pdf [Last accessed on 2025 Dec 10].
2. Chiesura A. The role of Urban parks for the sustainable city. *Landsc Urban Plan*. 2004;68(1):129-138.

   doi: 10.1016/j.landurbplan.2003.08.003
3. Oke TR. City size and the Urban heat island. *Atmos Environ*. 1973;7(8):769-779.

   doi: 10.1016/0004-6981(73)90140-6
4. Jauregui E. Influence of a large Urban park on temperature and convective precipitation in a tropical city. *Energy Build*. 1990;15:457-463.

   doi: 10.1016/0378-7788(90)90021-A
5. Hogan A, Ferrick M. Winter morning air temperature. *J Appl Meteorol Climatol.* 1997;36:52-69

   doi: 10.1175/1520-0450(1997)036<0052:WMAT>2.0.CO;2
6. Montavez JP, Gonzalez-Rouco JF, Valero F. A simple model for estimating the maximum intensity of nocturnal Urban heat island. *Int J Climatol*. 2008;28:235-242.

   doi: 10.1002/joc.1526
7. Smith C, Levermore G. Designing urban spaces and buildings to improve sustainability and quality of life in a warmer world. *Energy Policy.* 2008;36:4558-4562.

   doi: 10.1016/j.enpol.2008.09.011
8. Debbage N, Shepherd JM. The Urban heat island effect and city contiguity. *Comput Environ Urban Syst*. 2015;54:181-194.

   doi: 10.1016/j.compenvurbsys.2015.08.002
9. Steeneveld GJ, Koopmans S, Heusinkveld BG, Van Hove LW, Holtslag AA. Quantifying UHI effects and comfort for cities of varying size. *J Geophys Res*. 2011;116:D20129.

   doi: 10.1029/2011JD015988
10. Kunda JJ, Gosling SN, Foody GM. The effects of extreme heat on human health in tropical Africa. *Int J Biometeorol*. 2024;68(6):1015-1033.

    doi: 10.1007/s00484-024-02650-4
11. Muanya C. *Anxiety as Extremely Hot, Humid Weather Persist in Lagos, Others*. Guardian Newspaper; 2022. Available from: https://guardian.ng/tag/global-temperatures [Last accessed on 2025 Dec 10].
12. Rostika F, Haerawati I, Desheila A, editors, *et al.* The Impact of Climate Change on Infectious Disease Transmission. In: *2nd Sriwijaya International Conference of Public Health (SICPH). Proceedings of Conference Held 6-7 November 2019*. Indonesia: Sriwijaya University; 2019.
13. Hondula DM, Davis RE, Georgescu M. Clarifying the connections between green space, Urban climate, and heat-related mortality. *Am J Public Health*. 2018;108(S2):S62-S63.

    doi: 10.2105/AJPH.2017.304295
14. Alexandri E, Jones P. Temperature decreases in an Urban canyon due to green walls and green roofs in diverse climates. *Build Environ*. 2008;43(4):480-493.

    doi: 10.1016/j.buildenv.2006.10.055
15. Rinner C, Patychuk D, Nasr K, Bassil K, Gower S, Campbell M. The role of maps in neighborhood-level heat vulnerability assessment for the City of Toronto. *Cartogr Geogr Inf Sci*. 2010;37(1):31-44.

    doi: 10.1559/152304010790588089
16. Nolan J, Lang W. *Mitigating Heat Island Effect in the Urban Environment*. Austin: UTSoA Seminar in Sustainable Architecture, University of Texas; 2002.
17. Blocken B, Carmeliet J. High-resolution wind-driven rain measurements on a low-rise building-experimental data for model development and model validation. *J Wind Eng Ind Aerodyn*. 2005;93(12):905-928.

    doi: 10.1016/j.jweia.2005.09.004
18. Blocken B, Carmeliet J. Validation of CFD simulations of wind-driven rain on a low-rise building facade. *Build Environ*. 2007;42(7):2530-2548.

    doi: 10.1016/j.buildenv.2006.07.032
19. Dobbs C, Escobedo FJ, Zipperer WC. A framework for developing urban forest ecosystem services and goods indicators. *Landsc Urban Plan*. 2011;99:196-206.

    doi: 10.1016/j.landurbplan.2010.11.004
20. Krüger EL, Pearlmutter D. The effect of urban evaporation on building energy demand in an arid environment. *Energy Build*. 2008;40(11):2090-2098.

    doi: 10.1016/j.enbuild.2008.06.002
21. Wang J, Li Y, Liu W, Gou A. Spatial and temporal evolution

characteristics and factors of heat vulnerability in the pearl river delta Urban agglomeration from 2001 to 2022. *Heliyon*. 2024;10(13):e34116.

doi: 10.1016/j.heliyon.2024.e34116

22. Rahaman S, Jahangir S, Haque S, Chen R, Kumar P. Spatio-temporal changes of green spaces and their impact on Urban environment of Mumbai, India. *Environ Dev Sustain*. 2020;23:6481-6501.

doi: 10.1007/s10668-020-00882-z

23. Anupriya RS, Rubeena TA. Spatio-temporal urban land surface temperature variations and heat stress vulnerability index in Thiruvananthapuram city of Kerala, India. *Geol Ecol Landsc*. 2025;9(1):262-278.

doi: 10.1080/24749508.2023.2182088

24. Halder B, Bandyopadhyay J, Al-Hilali AA, *et al*. Assessment of Urban green space dynamics influencing the surface Urban heat stress using advanced geospatial techniques. *Agronomy*. 2022;12(9):2129.

doi: 10.3390/agronomy12092129

25. Ojeh VN, Balogun AA, Okhimamhe AA. Urban-rural temperature differences in Lagos. *Climate*. 2016;4(2):29.

doi: 10.3390/cli4020029

26. Sangwan A, Saraswat A, Kumar N, Pipralia S, Kumar A. *Urban Green Spaces Prospects and Retrospects*. London: *IntechOpen*; 2022.

doi: 10.5772/intechopen.102857

27. Nkeki FN, Ojeh VN. Flood risks analysis in a littoral African city. In: Nielson D, editor. *Geographic Information Systems: Techniques, Applications and Technologies*. Nova Science Publishers; 2014. p. 279-316.

28. Available from: https://worldpopulationreview.com/cities/nigeria/lagos [Last accessed on 2025 Dec 10].

29. Arup. *Reducing Urban Heat Risk: Mapping and Visualization Study*. London: Greater London Authority; 2014.

30. Schroeter D, Acosta-Michlik L, Arnell AW, *et al*. *The ATEAM Final Report 2004 - Detailed Report Related to Overall Project Duration. Advanced Terrestrial Ecosystem Analysis and Modelling*. Potsdam, Germany: Potsdam Institute for Climate Impact Research; 2004. p. 139. Available from: https://www.pik-potsdam.de/ateam/ateam_final_report_sections_5_to_6.pdf [Last accessed on 2025 Dec 10].

31. Ebi KL, Smith JB, Hitz S. Adaptation to climate variability and change from a public health perspective. In: Ebi KL, Smith JB, Burton I, editors. *Integration of Public Health with Adaptation to Climate Change*. London, U.K: Taylor and Francis; 2005. p. 1-17.

32. Séguin J, Clarke KL. In: Seguin J, editor. *Human Health in a Changing Climate*. Canada: Health Canada; 2008.

33. Walker A. *Vulnerability: Who is Most at Risk*? *Climate Change: Preparing for Health Impacts*. Canada: Health Canada; 2006.

34. Yildiz S, Oğuz Z. Designing sustainable Urban parks: A proposal backed by research. *Explora Environ Resour*. 2025;2(1):5839.

doi: 10.36922/eer.5839

Appendix

LANDSAT 2013 METADATA

ORIGIN = "Image courtesy of the U.S. Geological Survey"
LANDSAT_SCENE_ID = "LC81910552013352LGN00"
TARGET_WRS_PATH = 191
TARGET_WRS_ROW = 55
DATE_ACQUIRED = 2013-12-18 December 18, 2013 (DAY-TIME)
SCENE_CENTER_TIME = 10:04:25.3497966Z (10:04 am GMT)

ACCSCIENCE PUBLISHING

Explora: Environment and Resource

ORIGINAL RESEARCH ARTICLE

Water treatment using silver-iron-modified biochar for enhanced disinfection and sustainability

Chee Chung Wong[1†], Yong Yee Chua[1†], Peter Nai Yuh Yek[1*], Chee Swee Wong[1], Tung Chuan Tiong[1], Yie Hua Tan[2,3], Rock Keey Liew[4], Shin Ying Foong[5], Su Shiung Lam[5,6*], and Ding Lu[7]

[1]Centre for Research of Innovation and Sustainable Development, School of Engineering and Technology, University of Technology Sarawak, Sibu, Sarawak, Malaysia

[2]Department of Chemical and Energy Engineering, Faculty of Engineering, Universiti Teknologi Brunei, Gadong, Brunei Darussalam

[3]Department of Chemical and Petroleum Engineering, Faculty of Engineering, Technology and Built Environment, UCSI University, Kuala Lumpur, Malaysia

[4]Department of Psychiatry, Saveetha Medical College and Hospital, Saveetha Institute of Medical and Technical Sciences, Chennai, Tamil Nadu, India

[5]Higher Institution Centre of Excellence (HICoE), Institute of Tropical Aquaculture and Fisheries (AKUATROP), Universiti Malaysia Terengganu, Kuala Nerus, Terengganu, Malaysia

[6]University Centre for Research and Development, Department of Chemistry, Chandigarh University, Gharuan, Mohali, Punjab, India

[7]School of Resources and Environmental Engineering, Institute of Clean Coal Technology, East China University of Science and Technology, Shanghai, China

[†]*These authors contributed equally to this work.*

***Corresponding authors:**
Peter Nai Yuh Yek
(peter.yek@uts.edu.my)
Su Shiung Lam
(lam@umt.edu.my)

Citation: Wong CC, Chua YY, Yek PNY, *et al*. Water treatment using silver-iron-modified biochar for enhanced disinfection and sustainability. *Explora Environ Resour*. 2026;3(1):025480081. doi: 10.36922/EER025480081

Received: November 26, 2025

Revised: January 19, 2026

Accepted: January 26, 2026

Published online: February 12, 2026

Abstract

The contamination of water resources by pathogenic microorganisms remains a critical global challenge, predominantly in low- and middle-income countries. Conventional water treatment technologies, such as chlorination and filtration, often face drawbacks, including the formation of harmful byproducts and high operational costs. The increasing demand for efficient, sustainable, and scalable solutions necessitates the exploration of advanced materials for water disinfection. This study investigates the potential of silver-iron (Ag-Fe)-modified biochar as a photocatalyst under visible light to achieve high microbial inactivation. The material demonstrates dual functionality through the antibacterial effects of Ag and the photocatalytic activity of Fe, integrated within a renewable biochar. Elemental composition analysis shows that a composition of 4.3 wt% Ag and 30.0 wt% Fe enhances antimicrobial performance. Experimental results indicate bacterial inactivation under visible light conditions. Ag-Fe-modified biochar presents a potential alternative to conventional disinfection methods.

Keywords: Photocatalysis; Biochar; Water disinfection; Silver; Iron catalysis

1. Introduction

The contamination of water resources by pathogenic bacteria, including *Escherichia coli*, *Salmonella*, and *Vibrio cholerae*, represents a significant challenge to public health

worldwide. These microorganisms are introduced into water supplies through agricultural runoff, untreated sewage, and stormwater, contributing to an estimated 1.2 million deaths annually from waterborne diseases, particularly in low- and middle-income regions.[1,2] Traditional water treatment technologies, such as chlorination, sand filtration, and boiling, have been widely employed to manage microbial contamination.[3] However, these methods present limitations that reduce their suitability for large-scale or resource-constrained applications. Chlorination, for example, produces potentially carcinogenic byproducts, such as trihalomethanes, while sand filtration is often ineffective at removing certain microbial contaminants, and boiling is energy-intensive and impractical for widespread use in energy-limited settings.[3,4] These shortcomings necessitate the development of advanced technologies capable of providing safe and sustainable water treatment solutions.

Advanced oxidation processes (AOPs), ultraviolet (UV) irradiation, and membrane filtration systems have been proposed as alternatives to conventional methods.[5-7] AOPs generate reactive radicals that degrade pollutants and inactivate microorganisms, while UV irradiation provides non-chemical disinfection without producing harmful byproducts, and membrane filtration effectively separates contaminants through physical barriers. However, the widespread adoption of these advanced methods is constrained by high operational costs, significant infrastructure requirements, and challenges associated with scalability. Membrane fouling increases operational costs by 30%, while the initial capital investment for UV and AOP systems limits their feasibility in resource-limited settings.[8] Furthermore, the emergence of antimicrobial resistance introduces additional challenges to ensuring reliable disinfection performance.

In this context, biochar, a porous carbonaceous material produced through the pyrolysis of biomass, has attracted considerable interest as a platform for environmental remediation due to its high surface area, tunable surface chemistry, and renewable origin. Recent research has focused on enhancing biochar properties through the incorporation of metals, such as silver (Ag) and iron (Fe), creating multifunctional photocatalysts with superior antibacterial and photocatalytic activities.[9,10] Ag exhibits antimicrobial properties through mechanisms that disrupt bacterial cell membranes and interfere with intracellular processes, while Fe enhances photocatalytic performance by facilitating the production of reactive oxygen species (ROS) under visible light conditions. The integration of Ag and Fe within a biochar matrix produces a composite material with dual functionality, where the antibacterial effects of Ag are complemented by the photocatalytic properties of Fe.[11,12] This approach not only improves the efficiency of water disinfection but also reduces energy demands by utilizing solar energy, making it a potentially sustainable and cost-effective solution for microbial water contamination.

Recent studies increasingly treat metal-modified biochar as a multifunctional disinfection material rather than a purely adsorptive carbon. Ag-modified biochar is synthesized by immobilizing Ag on porous biochar and incorporating it into beads or hydrogels intended for drinking-water purification, where the antibacterial performance is typically attributed to contact-mediated effects and controlled Ag species release. A chitosan-coated biochar–nanoAg composite reported sustained antibacterial activity and reusability in a drinking-water context, highlighting the practicality of immobilizing Ag onto a recoverable scaffold.[13] Similarly, porous Ag-loaded biochar was embedded into polymer gel beads to suppress bacteria, a strategy that improves handling and reduces direct nanoparticle dispersion while still achieving strong antibacterial outcomes in laboratory tests.[14] For Fe-modified biochar, the emphasis was on the redox/photochemical routes, frequently involving oxidant activation or visible light assistance, which can yield strong disinfection but also introduce condition-dependence. Maghemite-impregnated biochar with visible light-assisted disinfection of *E. coli* has been investigated, where the Fe-bearing phases can participate in photo-assisted inactivation rather than purely contact killing.[15] Fe_3O_4-loaded magnetic hydrochar with bacterial inactivation reported that iron–carbon composites can support radical-driven disinfection under visible light. The $FeCl_3$-activated biochar/peroxymonosulfate system was evaluated for *E. coli* inactivation in real secondary-treated urban wastewater, and the interference effects of microplastics on disinfection performance were explicitly examined.[16] Meanwhile, Ag–Fe hybrid concepts have also been explored in photocatalytic/radical frameworks, where Ag_3PO_4/Fe_3O_4-activated biochar was used under visible light, emphasizing that dual-metal systems can be designed for recoverability and enhanced photo-redox performance.[17] Ag-biochar has been tested in sand filtration columns and reported >90% *E. coli* removal from wastewater samples, demonstrating that deployment-like configurations can yield measurable microbial reductions.[18]

This research investigates the antibacterial and photocatalytic properties of Ag–Fe-modified biochar and assesses its application in realistic conditions of pond water. The preparation of Ag and Fe within the biochar matrix represents an alternative approach to

achieving dual functionality, combining antimicrobial and photocatalytic properties. The dual-action nature of this material not only enhances disinfection efficiency but also reduces reliance on synthetic materials and minimizes environmental impact, offering a practical and sustainable solution for water treatment.[19] The current development of Ag–Fe-modified biochar as a photocatalyst for water disinfection has been carried out as proof-of-concept through lab-scale validation. This study also aims to address limitations in existing water treatment technologies by preparing a material that operates effectively under visible light and achieves high microbial inactivation. In adition, biochar, derived from biomass waste, aligns with the principles of resource recovery and waste valorization, supporting the sustainability objectives of modern water treatment systems. The practical implications of Ag–Fe-modified biochar are significant, particularly for regions with limited access to advanced water treatment infrastructure. The use of visible light as an energy source ensures that the Ag–Fe-modified biochar can be applied in low-resource settings, providing a low-cost and scalable solution for microbial water contamination. These findings align with the objectives of the United Nations Sustainable Development Goal 6, which focuses on ensuring clean water and sanitation for all.

2. Materials and methods

2.1. Water sample collection

Water samples from a pond located at Sibu, Sarawak (2.361275, 111.956743) were collected from three different points in July 2018 to assess the disinfection efficacy of Ag-Fe-modified biochar on natural microbial communities. Representative samples were collected to reflect the native microbial community and key physicochemical characteristics of the source water, thereby enabling evaluation of the disinfection process under conditions that are relevant to practical application. Samples were placed in a cooler containing ice packs to maintain a controlled temperature range of 1–4°C to reduce microbial metabolic activity, thereby preventing structural or compositional changes within the microbial community.

2.2. Preparation and characterization of photocatalyst

The preparation of Ag–Fe-modified biochar was conducted at room temperature using a liquid-phase reduction method. Palm kernel shell biochar was carbonized at 500°C for 2 h, ground, and sieved to achieve a fineness of 200 mesh. This ensures a uniform particle size, which is critical for consistent surface modification. The process commenced with the preparation of a coating solution by dissolving 0.05 g of polyethylene glycol and 2–3 g of ferrous sulfate heptahydrate ($FeSO_4 \cdot 7H_2O$) in 50 mL of distilled water.[20] The polyethylene glycol acts as a stabilizing agent, while the FeSO4 provides the Fe source required for subsequent reactions. Following the preparation of the coating solution, 2 g of palm kernel shell biochar powder was introduced into the solution. The mixture was subjected to magnetic stirring for 30–60 min, which facilitated the deposition of nano-zero valent Fe (nZVI) onto the biochar surface, resulting in the formation of the nZVI–biochar composite.[21] Magnetic stirring ensured homogeneous dispersion and interaction between the Fe precursor and the biochar, enhancing the uniformity of the coating.

The resulting composite was then immersed in 50 mL of a sodium borohydride solution (22.7 g/L) and subjected to vigorous stirring. This step induces the reduction of Fe ions to their zero-valent state, a critical transformation for the desired photocatalytic activity.[22] After the reduction process, the nZVI–biochar composite was thoroughly washed with distilled water and ethanol to eliminate any residual reactants or byproducts that might interfere with subsequent reactions or applications. In the final stage, 30 mL of a silver nitrate ($AgNO_3$) solution containing 0.013–0.018 g of $AgNO_3$ was introduced into the nZVI-biochar mixture. The solution was stirred for an additional 30–60 min to facilitate the reduction of Ag ions and their deposition onto the nZVI surface.[23] The reduction and deposition of Ag ions onto the composite surface are critical for enhancing the antibacterial and photocatalytic properties of the material. The resulting product, Ag–Fe-modified biochar, represents a multifunctional composite material designed for potentially efficient water disinfection through the synergistic effects of its antimicrobial and photocatalytic properties. This methodical preparation process ensures the reproducibility and uniformity of the Ag–Fe-modified biochar composite, which is essential for achieving consistent performance in subsequent experimental applications.

Scanning electron microscopy with energy-dispersive X-ray spectroscopy (SEM-EDX) analysis was performed using a scanning electron microscope (M JSM-6010 Plus/LV, JEOL, Japan) equipped with an EDX (Oxford Instruments, United Kingdom) system operated in high-vacuum mode. Before imaging, dried samples were mounted on aluminum stubs using double-sided conductive carbon tape. Secondary electron images were acquired at a field of view consistent with a 50 μm scale bar (×500 magnification), using an accelerating voltage of 15 kV. The working distance was maintained at approximately 10 mm, and the beam current size was set to a moderate level to balance spatial resolution and count

rate. Elemental acquisition was conducted at multiple locations (six-point spectra) across the sample surface to capture compositional heterogeneity.

2.3. Pond water treatment with photocatalyst

A 500 mL batch reactor system was employed for laboratory-scale experiments to evaluate the disinfection performance of the Ag–Fe-modified biochar photocatalyst. In these experiments, 100 mL of pond water and 0.5 g of photocatalyst (solution pH was adjusted to 4) were introduced into a closed reaction system, and all experiments were conducted in triplicate to ensure reproducibility and enable reporting of averaged results with associated variability. The setup was designed to allow precise control of experimental conditions, including light exposure, reaction time, and temperature. Natural sunlight was utilized where feasible due to its cost-effectiveness and practical relevance. Key operational parameters, such as reaction time and light intensity, were systematically monitored and adjusted to optimize the interaction between the photocatalyst and the contaminants. These parameters are critical to maximizing the photocatalytic efficiency and ensuring accurate assessment of the disinfection process. Control experiments were conducted in parallel, in which pond water samples were exposed to identical conditions without the addition of the photocatalyst. These controls were essential for distinguishing the photocatalytic effects of the Ag–Fe-modified biochar from other processes, such as natural microbial die-off or photolysis caused by direct light exposure.

Water samples were collected at predefined intervals during the experimental period to track changes in microbial populations and contaminant levels. Microbial plate counting techniques were employed to quantify the reduction in bacterial counts and assess the efficacy of the treatment.[24] These techniques provided a quantitative evaluation of the disinfection process, offering critical insights into the performance of the photocatalyst under varying experimental conditions. The rigorous application of these methodologies ensured that the findings were robust, reproducible, and reflective of the practical potential of the photocatalyst for water disinfection applications.

2.4. *E. coli* detection

To prepare a 5 mM solution of $AgNO_3$, 0.085 g of $AgNO_3$ was accurately weighed using an analytical balance. The $AgNO_3$ was then transferred into a 100 mL volumetric flask, and distilled water was added to the calibration mark to achieve the desired concentration. The flask was gently swirled to ensure the complete dissolution of the $AgNO_3$, resulting in a homogeneous solution ready for experimental use. Two sample sets were prepared for the experiment. For the treated sample, 50 mL of the water sample was mixed with 50 mL of the 5 mM $AgNO_3$ solution in a 250 mL volumetric flask, creating a total volume of 100 mL. This mixture was stirred continuously for 1 h using a magnetic stirrer to ensure thorough mixing and to promote the interaction between the Ag ions and the microbial contaminants present in the water. For the control sample, 50 mL of the same water sample was combined with 50 mL of distilled water. This mixture served as a baseline to compare the effectiveness of the Ag treatment.

The Quanti-Tray Sealer (Hach, United States) was preheated according to the manufacturer's instructions.[25] Both the treated and control samples were vigorously shaken to ensure homogeneity. Each sample was then transferred into a test bottle, to which one packet of Colilert reagent (Hach, United States) was added. The bottles were capped and shaken until the reagent was mostly dissolved. Subsequently, the contents of each bottle were poured into a Quanti-Tray/51 (Hach, United States), which contains 51 wells for microbial enumeration. Special care was taken to fill each well uniformly and eliminate air bubbles by gently tapping the trays on a hard surface. The filled Quanti-Trays were sealed using the Quanti-Tray Sealer following the manufacturer's guidelines. The sealed trays were then incubated at a temperature of 35 ± 0.5°C for 24 h to optimize the growth and detection of coliform bacteria and *E. coli*.

After incubation, the trays were examined under normal lighting to count the wells that turned yellow, indicating the presence of total coliform bacteria. To identify wells containing *E. coli*, the trays were illuminated with a UV lamp at 365 nm, and wells exhibiting fluorescence were recorded. These results were used to assess the effectiveness of the Ag treatment by comparing the microbial presence in treated versus control samples. The counts of yellow and fluorescent wells from each tray were meticulously recorded and referenced against the most probable number table included with the Colilert system. This table allows the estimation of bacterial concentrations based on the number of positive wells, facilitating the quantification of disinfection efficacy.

3. Results and discussion

3.1. Characteristics of the photocatalyst

Figure 1 and Table 1 show the surface morphology and elemental composition of biochar samples before and after modification with Ag and Fe, providing quantitative evidence of the modification process efficacy and its influence on the material properties for disinfection applications. Table 1 presents the elemental composition

Table 1. Elemental analysis using scanning electron microscopy with energy-dispersive X-ray spectroscopy analysis

No.	Sample	Carbon (wt%)	Oxygen (wt%)	Silicon (wt%)	Silver (wt%)	Iron (wt%)
1	Biochar	97.3±8.7	2.1±3.3	0.6±0.2	N/A	N/A
2	Silver-iron-modified biochar	24.6±4.6	41.1±6.1	N/A	4.3±2.2	30.0±5.8

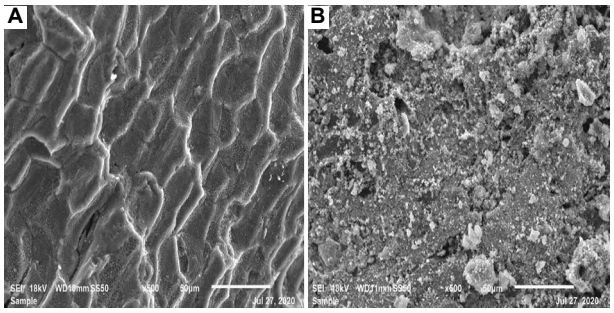

Figure 1. Scanning electron microscopy images. (A) Biochar. (B) Silver-iron-modified biochar. Scale bar: 50 μm; magnification: ×500.

in weight percentages (wt%) of carbon, oxygen, silicon, Ag, and Fe for both the raw biochar and the Ag–Fe-modified biochar. In biochar, carbon constitutes 97.3 wt%, which reflects the high carbon content of biochar derived from biomass pyrolysis. Oxygen accounts for 2.1 wt%, which shows limited oxygen-containing functional groups on the biochar surface. Silicon is detected at 0.6 wt%, which likely originated from inorganic components inherent to the biomass.

In the Ag–Fe-modified biochar, notable compositional changes were observed. The carbon content decreased to 24.6 wt%, oxygen increased to 41.1 wt%, and silicon was not detected after modification. These reductions correspond to the incorporation of Ag and Fe, evidenced by the addition of 4.3 wt% Ag and 30.0 wt% Fe. The significant presence of Ag and Fe indicates successful deposition onto the biochar matrix, which is critical for achieving the intended functionalities of the material. The elevated Fe content supports enhanced photocatalytic activity by facilitating the generation of ROS under visible light. These ROS are able to degrade organic pollutants and inactivate microbes. Similarly, the high Ag content provides strong antibacterial properties as Ag^{+} ions disrupt bacterial membranes and interfere with essential cellular processes.

The modified biochar plays a dual-purpose role as an adsorbent and a photocatalyst. The increased oxygen content after Ag–Fe loading further confirms that the biochar surface has been substantially modified. During impregnation, Fe and Ag precursors are converted mainly to their oxide or hydroxide forms. These new oxygen-containing phases and functionalities replaced part of the original carbon matrix, explaining the sharp drop in carbon and the large rise in oxygen detected by EDX. The dense metal oxide domains can also screen the underlying carbon from the detector, which, after normalization of the data to 100 wt%, further amplified the apparent oxygen proportion. This higher oxygen content is not only a compositional change but also directly benefits the material performance. Polar oxygenated groups improve the hydrophilicity of the surface and provide active sites for binding pollutants, thereby enhancing adsorption capacity.[26,27] Simultaneously, surface hydroxyls on Fe and Ag oxides act as reaction centers for the generation of ROS under light irradiation. These species, such as hydroxyl and superoxide radicals, are important for photocatalytic degradation of contaminants. Hence, the enrichment of oxygen indicates the formation of an oxygen-rich metal oxide-biochar interface that underpins the dual role of the modified biochar as an efficient adsorbent and a robust photocatalyst.

3.2. Treatment of pond water using the photocatalyst

Figure 2 presents the results of a Quanti-Tray test conducted to evaluate the presence of coliform bacteria (e.g., *E. coli*) in water samples treated with Ag-Fe-modified biochar under ambient and UV light conditions. This experimental setup demonstrates the material's dual functionality in water disinfection, combining the antimicrobial effects of Ag and the photocatalytic activity of Fe embedded within a biochar matrix. Under ambient light conditions, the untreated water sample (Figure 2A) showed a high prevalence of yellow wells, indicative of total coliform bacteria, while the treated water samples (Figure 2B) showed a significant reduction. This reduction suggests that Ag–Fe-modified biochar is potentially effective in mitigating microbial contamination. Similarly, under UV light, fluorescence observed in the untreated sample indicates the presence of *E. coli* (Figure 2C), a critical indicator of fecal contamination and a key public health concern. The absence of fluorescence in the treated sample demonstrates the material efficacy in targeting pathogenic bacteria (Figure 2D).

The Ag–Fe-modified biochar reduced microbial contamination effectively by inactivating bacteria under visible light conditions. However, several considerations require critical evaluation to contextualize the results

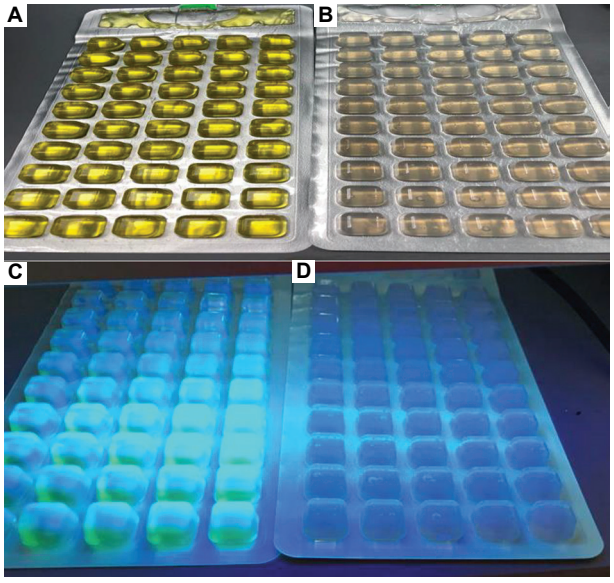

Figure 2. The differences between untreated pond water and treated pond water. Untreated pond water under (A) ambient light and (C) ultraviolet light. Treated pond water under (B) ambient light and (D) ultraviolet light.

and assess their broader implications. Mechanistically, the dual actions of Ag and Fe contribute to the material's antibacterial effectiveness. Ag ions disrupt bacterial membranes and interfere with essential cellular processes, while Fe enhances the production of ROS, which oxidatively degrade organic contaminants and inactivate microorganisms. However, the specific contributions of Ag and Fe to the disinfection process remain unclear. Quantitative studies to separate and assess the individual roles of these components are needed to optimize the material design and performance.

The influence of environmental factors, such as turbidity, organic matter content, and competing ions, on the material performance in real-world water systems must be addressed. High organic loads in natural water systems may interfere with the availability of Ag ions or hinder ROS generation by scavenging reactive species. The performance of Ag–Fe-modified biochar should also be benchmarked against established disinfection technologies, such as chlorination, UV treatment, and AOPs. Comprehensive studies on the environmental impact of Ag and Fe leaching are critical for ensuring sustainability. While Ag–Fe-modified biochar shows significant promise as a sustainable and cost-effective water treatment solution, further research is necessary to ensure its practicality, scalability, and environmental compatibility in real-world applications. These efforts are essential to advancing this material from laboratory studies to practical implementation in global water quality improvement efforts.

3.3. Mechanisms underlying bacterial inactivation by the silver-iron-modified biochar

The antibacterial performance of Ag-Fe-modified biochar is discussed in the current proof-of-concept study. The experiments demonstrated successful incorporation of Ag and Fe on the biochar surface based on SEM-EDX elemental detection and a clear reduction in total coliform/*E. coli*. At the material level, SEM-EDX confirmed surface-associated enrichment of Ag and Fe in raw biochar, indicating that the modification procedure successfully introduced metal-bearing domains onto the porous carbon. The biochar provides a high surface area and surface heterogeneity that can promote microbe–surface interactions. In disinfection systems, porous carbonaceous substrates can concentrate microorganisms at solid–liquid interfaces through adsorption and physical entrapment, thereby increasing the frequency and intimacy of contact between bacteria and active surface sites.[28]

The presence of Ag on the biochar provides a basis for antibacterial activity, as Ag-bearing surfaces are widely associated with contact-mediated bacterial stress and, potentially, release of Ag species that interfere with cellular envelope integrity and essential metabolic functions.[29] In this study, the observed reduction in coliform/*E. coli* indicators after exposure to the Ag–Fe-modified biochar suggests that Ag-associated antimicrobial functionality is accessible in the pond water matrix under the tested conditions. The Fe on the biochar surface further contributed to photo/redox processes at the metal–oxide/carbon interface. Many Fe-bearing composites facilitate the formation of oxidative intermediates that damage cells.[30]

The reduced number of positive wells in the Quanti-Tray test indicates that the microbial suppression may reflect a combination of inactivation and physical removal/partitioning, including adsorption of bacteria onto the solid phase, followed by sedimentation. Ag-associated antibacterial action may occur through contact killing or limited Ag species release, while Fe-associated photo/redox activity may contribute under the applied irradiation conditions. Therefore, while the current results demonstrate that Ag–Fe-modified biochar can suppress coliform/*E. coli* indicators in pond water under specified laboratory conditions, mechanistic attribution, and claims of synergistic coupling between Ag and Fe remain beyond the scope of the present evidence.

3.4. Current developments in biochar-based water disinfection technologies

Silver was selected in this study due to its well-established and broad-spectrum antimicrobial potency, which can be achieved at relatively low mass fractions, offering the

possibility of high disinfection efficacy without excessive material dosing.[31] When Ag is immobilized onto a solid support, it can deliver rapid bacterial suppression through contact-mediated effects and limited ion release, providing a strong benchmark for proof-of-concept development and mechanistic framing. Ag was incorporated onto a recoverable biochar, which was intended to reduce uncontrolled dispersion and enable physical separation after treatment. This immobilization strategy is also aligned with a scalability pathway, as biochar is abundant and low-cost, and can be processed into retrievable forms (e.g., packed media, beads, or supported beds) that minimize direct release. The scope of this study is positioned as a laboratory-scale validation of an Ag-containing composite design concept, with direct performance evidence under defined conditions. In subsequent work, Ag leaching, reusability across cycles, and performance retention in varying water matrices will be evaluated to determine whether the observed disinfection efficacy can be maintained with acceptable environmental risk.

Biochar-based technologies for water disinfection illustrate a clear transition from conventional adsorption-focused applications toward multifunctional materials capable of catalytic and photocatalytic inactivation of diverse microbial contaminants.[32] Biochar has the potential as a cost-effective adsorbent with tunable physicochemical properties for pollutant removal, but it has a limited intrinsic antibacterial capacity. Hence, metal functionalization, surface modification, and carbon–metal electron-transfer pathways have been explored to transform biochar into an active disinfection platform capable of generating ROS, releasing controlled antimicrobial ions, and stabilizing catalytic sites for persistent microbial inactivation. These advancements have laid the groundwork for integrated systems that combine adsorption, photocatalysis, and metal-induced oxidative stress within a single material framework.

Iron-modified biochar can activate persulfate to generate powerful sulfate radicals, enabling rapid destruction of antibiotic-resistant bacteria and suppressing the spread of antibiotic resistance genes.[33] Fe–biochar facilitates electron transfer, accelerates radical generation, and maintains activity under environmentally relevant conditions. The mechanistic elucidation shows that well-characterized pathways, including Fe(II)/Fe(III) redox cycling, surface-bound radical formation, and oxidative membrane rupture, are central to designing next-generation biochar disinfectants. These insights guide the engineering of multifunctional composite materials where catalytic activation, radical-driven oxidation, and microbial membrane disruption occur simultaneously. The recent research shows the role of visible light-driven photocatalysis as a sustainable and low-energy approach for water disinfection.[34] Fe-assisted photocatalysis is particularly attractive as Fe sites in biochar can narrow the bandgap, promote photoexcited electron–hole separation, and generate ROS under natural sunlight without UV-based systems that require higher energy input. The incorporation of metallic nanoparticles (i.e., Ag, copper, or Fe oxides) onto biochar matrices creates synergistic effects that outperform individual components. Ag modification provides potent antimicrobial action through ion release and protein inactivation, while Fe enhances ROS formation and stabilizes charge carriers.[35] Together, these mechanisms create a multifaceted antibacterial system capable of addressing not only general coliforms but also more resilient microbial groups. The trend toward hybrid designs reflects the replacement of chemical-intensive disinfection with environmentally benign, sunlight-responsive materials that can operate effectively in rural, decentralized, or emergency contexts.

Recent studies emphasize that the presence of natural organic matter, turbidity, suspended solids, and competing ions can limit ROS availability, alter metal speciation, or interfere with bacterial interactions.[36,37] In addition, greater attention is now given to the environmental safety of metal-doped biochar, including metal leaching dynamics, long-term structural stability, and potential ecological impacts. Engineering strategies of strong metal–biochar bonding, surface oxidation for nanoparticle immobilization, and moderate metal loading have been recognized as necessary approaches to balance disinfection efficiency with environmental stewardship. This also aligns with global themes in circular economy principles, sustainable materials design, and decentralized water treatment for underserved regions. The integration of catalytic activation, visible light responsiveness, and sustainability considerations represents the newest direction in biochar-based disinfection that emphasizes accessibility, environmental safety, and advanced performance under real-world conditions.

3.5. Limitations, future directions, and real-world implications

The study on Ag–Fe-modified biochar as a photocatalyst for water disinfection identified several limitations that require further analysis to improve its performance and applicability. The stability and reusability of the photocatalyst present challenges, as the potential leaching of Ag and Fe nanoparticles could reduce its long-term effectiveness and pose environmental hazards. The experimental conditions, which were controlled and simplified, may not fully reflect the complexities of real-

world water systems. Environmental factors such as turbidity, organic content, and competing ions are likely to affect the material functionality in practical applications. In addition, the research focused primarily on bacterial inactivation, leaving its effectiveness against other waterborne pathogens, including viruses and antibiotic-resistant microorganisms, unexplored. The study also does not include an evaluation of the economic viability or scalability of producing the Ag–Fe-modified biochar for deployment in low-resource contexts.

Future investigations should prioritize assessing the environmental impact of nanoparticle leaching and developing strategies to improve material stability, such as advanced coating techniques or stabilizing element incorporation. Field tests in diverse water matrices, including municipal and industrial wastewater, are necessary to understand the material's performance in varying environmental conditions. Studies should also expand to include their disinfection capacity against a broader range of microorganisms, including viruses and biofilm-forming species, to provide a comprehensive evaluation. Furthermore, conducting techno-economic analyses is essential to assess the cost-effectiveness and scalability of this material, particularly in comparison to established water treatment methods. Exploring the integration of Ag–Fe-modified biochar with other advanced treatment technologies could enhance its overall efficacy and broaden its application scope.

The implications of this Ag–Fe-modified biochar for practical water treatment are significant. By utilizing visible light as an energy source, Ag–Fe-modified biochar offers a sustainable and cost-efficient approach to microbial water disinfection, particularly in regions lacking advanced water treatment infrastructure. The use of biomass-derived biochar aligns with principles of resource recovery and waste utilization, providing an environmentally sustainable approach to developing functional materials for water treatment. Its demonstrated ability to inactivate bacteria suggests it could play an important role in reducing waterborne diseases, especially in underserved regions. Furthermore, avoiding chemical-intensive disinfection methods, such as chlorination, reduces the generation of harmful byproducts and lowers the environmental impact of water treatment processes.

4. Conclusion

This study presents an evaluation of Ag–Fe-modified biochar as a photocatalyst for water disinfection, demonstrating its potential as an advanced solution for addressing microbial contamination. The dual functionality of the material was achieved through the integration of Ag and Fe nanoparticles within a biochar matrix. Ag exhibits antibacterial properties by disrupting bacterial membranes and interfering with intracellular processes, while Fe enhances photocatalytic activity through the generation of ROS. The biochar substrate contributes additional benefits for adsorption and stabilization, which collectively enhance the disinfection performance. The research presents the material's ability to achieve significant microbial reduction under visible light, offering an energy-efficient and sustainable approach to water treatment, and the strategic integration of renewable biochar with functional properties to develop a cost-effective adsorbent as an alternative to conventional water disinfection technologies. Moreover, the reliance on biomass-derived biochar aligns with environmental sustainability objectives, promoting the valorization of waste materials and reducing dependence on chemical-intensive methods.

Acknowledgments

None.

Funding

The authors Tiong Tung Chuan and Peter Nai Yuh Yek would like to thank the University of Technology Sarawak for providing financial support under the UTS Internal Research Grant (UCTS/RESEARCH/<3/2023/02) to perform this project.

Conflict of interest

Su Shiung Lam is an Associate Editor of this journal, but was not in any way involved in the editorial and peer-review process conducted for this paper, directly or indirectly. The authors declare they have no competing interests.

Author contributions

Conceptualization: Peter Nai Yuh Yek, Chee Chung Wong
Formal analysis: Yie Hua Tan, Chee Swee Wong, Shin Ying Foong
Investigation: Chee Swee Wong, Tung Chuan Tiong, Ding Lu
Methodology: Rock Keey Liew, Tung Chuan Tiong, Shin Ying Foong
Writing–original draft: Chee Chung Wong, Yong Yee Chua
Writing–review & editing: Peter Nai Yuh Yek, Su Shiung Lam

Ethics approval and consent to participate

Not applicable.

Consent for publication

Not applicable.

Availability of data

Data will be made available on request to the corresponding author.

References

1. Mei Z, Fu Y, Wang F, *et al*. Magnetic biochar/quaternary phosphonium salt reduced antibiotic resistome and pathobiome on pakchoi leaves. *J Hazard Mater*. 2023;460:132388.

   doi: 10.1016/j.jhazmat.2023.132388

2. Zhang JB, Dai C, Wang Z, *et al*. Resource utilization of rice straw to prepare biochar as peroxymonosulfate activator for naphthalene removal: Performances, mechanisms, environmental impact and applicability in groundwater. *Water Res*. 2023;244:120555.

   doi: 10.1016/j.watres.2023.120555

3. Gwenzi W, Chaukura N, Noubactep C, Mukome FND. Biochar-based water treatment systems as a potential low-cost and sustainable technology for clean water provision. *J Environ Manag*. 2017;197:732-749.

   doi: 10.1016/j.jenvman.2017.03.087

4. Wu XN, Yuan CJ, Huo ZY, *et al*. Reduction of byproduct formation and cytotoxicity to mammalian cells during post-chlorination by the combined pretreatment of ferrate(VI) and biochar. *J Hazard Mater*. 2023;458:131935.

   doi: 10.1016/j.jhazmat.2023.131935

5. Zheng J, Zhang P, Li X, Ge L, Niu J. Insight into typical photo-assisted AOPs for the degradation of antibiotic micropollutants: Mechanisms and research gaps. *Chemosphere*. 2023;343:140211.

   doi: 10.1016/j.chemosphere.2023.140211

6. Sun W, Dong H, Wang Y, *et al*. Ultraviolet (UV)-based advanced oxidation processes for micropollutant abatement in water treatment: Gains and problems. *J Environ Chem Eng*. 2023;11(5):110425.

   doi: 10.1016/j.jece.2023.110425

7. Zhang R, Ding A, Cai X, *et al*. Break through the trade-off between membrane fouling and pathogen removal in ultrafiltration process by poly(amino acid)s modified biochar. *Sep Purif Technol*. 2025;356:129847.

   doi: 10.1016/j.seppur.2024.129847

8. Coccia M, Bontempi E. New trajectories of technologies for the removal of pollutants and emerging contaminants in the environment. *Environ Res*. 2023;229:115938.

   doi: 10.1016/j.envres.2023.115938

9. Yu C, Tang J, Liu F, Chen Y. Green synthesized nanosilver-biochar photocatalyst for persulfate activation under visible-light illumination. *Chemosphere*. 2021;284:131237.

   doi: 10.1016/j.chemosphere.2021.131237

10. Zhou X, Diao Y, Zhu Y, Quan G, Yan J, Zhang W. Release of biochar-derived dissolved organic matter and the formation of chlorination disinfection by-products: Effects of pH and chlorine dosage. *Environ Pollut*. 2024;342:123025.

    doi: 10.1016/j.envpol.2023.123025

11. Kumar A, Rana A, Sharma G, *et al*. High-performance photocatalytic hydrogen production and degradation of levofloxacin by wide spectrum-responsive Ag/Fe_3O_4 bridged $SrTiO_3/g\text{-}C_3N_4$ plasmonic nanojunctions: Joint effect of Ag and Fe_3O_4. *ACS Appl Mater Interfaces*. 2018;10(47):40474-40490.

    doi: 10.1021/acsami.8b12753

12. Nicoara AI, Ene VL, Voicu BB, *et al*. Biocompatible ag/fe-enhanced Tio_2 nanoparticles as an effective compound in sunscreens. *Nanomaterials (Basel)*. 2020;10(3):570.

    doi: 10.3390/nano10030570

13. Hu Z, Zhang L, Zhong L, Zhou Y, Xue J, Li Y. Preparation of an antibacterial chitosan-coated biochar-nanosilver composite for drinking water purification. *Carbohydr Polym*. 2019;219:290-297.

    doi: 10.1016/j.carbpol.2019.05.017

14. Zhao H, Li X, Zhang L, Hu Z, Zhong L, Xue J. Preparation and bacteriostatic research of porous polyvinyl alcohol/biochar/nanosilver polymer gel for drinking water treatment. *Sci Rep*. 2021;11(1):12205.

    doi: 10.1038/s41598-021-91833-9

15. Basu A, Behera M, Maharana R, *et al*. To unsnarl the mechanism of disinfection of *Escherichia coli* via visible light assisted heterogeneous photo-Fenton reaction in presence of biochar supported maghemite nanoparticles. *J Environ Chem Eng*. 2021;9(1):104620.

    doi: 10.1016/j.jece.2020.104620

16. Adeel M, Cirillo C, Sarno M, Rizzo L. Urban wastewater disinfection by FeCl3-activated biochar/peroxymonosulfate system: *Escherichia coli* inactivation and microplastics interference. *Environ Pollut*. 2024;359:124607.

    doi: 10.1016/j.envpol.2024.124607

17. Talukdar K, Jun BM, Yoon Y, Kim Y, Fayyaz A, Park CM. Novel Z-scheme Ag_3PO_4/Fe_3O_4-activated biochar photocatalyst with enhanced visible-light catalytic performance toward degradation of bisphenol A. *J Hazard Mater*. 2020;398:123025.

    doi: 10.1016/j.jhazmat.2020.123025

18. Zhu L, Chattopadhyay S, Elijah Akanbi O, *et al*. Biochar and zero-valent iron sand filtration simultaneously removes contaminants of emerging concern and *Escherichia coli* from wastewater effluent. *Biochar*. 2023;5(1):41.

    doi: 10.1007/s42773-023-00240-y

19. Xie Y, Liu A, Bandala ER, Goonetilleke A. TiO_2-biochar composites as alternative photocatalyst for stormwater disinfection. *J Water Process Eng*. 2022;48:102913.

doi: 10.1016/j.jwpe.2022.102913

20. Dong H, Deng J, Xie Y, *et al*. Stabilization of nanoscale zero-valent iron (nZVI) with modified biochar for Cr(VI) removal from aqueous solution. *J Hazard Mater*. 2017;332:79-86.

doi: 10.1016/j.jhazmat.2017.03.002

21. Ahmad S, Liu X, Tang J, Zhang S. Biochar-supported nanosized zero-valent iron (nZVI/BC) composites for removal of nitro and chlorinated contaminants. *Chem Eng J*. 2022;431:133187.

doi: 10.1016/j.cej.2021.133187

22. Zhang K, Suh JM, Choi JW, Jang HW, Shokouhimehr M, Varma RS. Recent advances in the nanocatalysts-assisted $NaBH_4$ reduction of nitroaromatics in water. *ACS Omega*. 2019;4:483-95.

doi: 10.1021/acsomega.8b03051

23. Jayeoye TJ, Eze FN, Olatunde OO, Benjakul S, Rujiralai T. Synthesis of silver and silver@zero valent iron nanoparticles using *Chromolaena odorata* phenolic extract for antibacterial activity and hydrogen peroxide detection. *J Environ Chem Eng*. 2021;9(3):105224.

doi: 10.1016/j.jece.2021.105224

24. Wang X, Liang R, Pu X, *et al*. Application of the electrical microbial growth analyzer method for efficiently quantifying viable bacteria in ready-to-eat sea cucumber products. *Microorganisms*. 2024;12:2301.

25. McNair JN, Rediske RR, Hart JJ, Jamison MN, Briggs S. Performance of colilert-18 and qPCR for monitoring *E. coli* contamination at freshwater beaches in Michigan. *Environments*. 2025;12:21.

26. Mirzaeian M, Abbas Q, Hunt MRC, Hall P. Pseudocapacitive effect of carbons doped with different functional groups as electrode materials for electrochemical capacitors. *Energies*. 2020;13:5577.

27. Allahkarami E, Monfared AD. Activated carbon adsorbents for the removal of emerging pollutants and its adsorption mechanisms. In: Hadi Dehghani M, Karri RR, Tyagi I, editors. *Sustainable Remediation Technologies for Emerging Pollutants in Aqueous Environment*. Ch. 5. Netherlands: Elsevier; 2024. p. 79-109.

28. Afrooz ARMN, Boehm AB. *Escherichia coli* removal in biochar-modified biofilters: Effects of biofilm. *PL_OS One*. 2016;11(12):e0167489.

doi: 10.1371/journal.pone.0167489

29. Yin IX, Zhang J, Zhao IS, Mei ML, Li Q, Chu CH. The antibacterial mechanism of silver nanoparticles and its application in dentistry. *Int J Nanomedicine*. 2020;15: 2555-2562.

doi: 10.2147/ijn.S246764

30. Arabzadeh Nosratabad N, Yan Q, Cai Z, Wan C. Exploring nanomaterial-modified biochar for environmental remediation applications. *Heliyon*. 2024;10(18):e37123.

doi: 10.1016/j.heliyon.2024.e37123

31. Peng H, Guo H, Gao P, Zhou Y, Pan B, Xing B. Reduction of silver ions to silver nanoparticles by biomass and biochar: Mechanisms and critical factors. *Sci Total Environ*. 2021;779:146326.

doi: 10.1016/j.scitotenv.2021.146326

32. Wang X, Guo Z, Hu Z, Zhang J. Recent advances in biochar application for water and wastewater treatment: A review. *PeerJ*. 2020;8:e9164.

doi: 10.7717/peerj.9164

33. Duan R, Ma S, Ma Y, *et al*. Efficient inactivation of antibiotic resistant bacteria by iron-modified biochar and persulfate system: Potential for controlling antimicrobial resistance spread and mechanism insights. *J Hazard Mater*. 2025;492:138182.

doi: 10.1016/j.jhazmat.2025.138182

34. Qiu P, Zhu J, Zhang C, *et al*. Visible light-supported efficient photocatalytic disinfection using a robust silver-doped boron photocatalyst. *J Environ Chem Eng*. 2023;11(5):111058.

doi: 10.1016/j.jece.2023.111058

35. Mondal SK, Chakraborty S, Manna S, Mandal SM. Antimicrobial nanoparticles: Current landscape and future challenges. *RSC Pharm*. 2024;1(3):388-402.

doi: 10.1039/d4pm00032c

36. Oladimeji TE, Oyedemi M, Emetere ME, Agboola O, Adeoye JB, Odunlami OA. Review on the impact of heavy metals from industrial wastewater effluent and removal technologies. *Heliyon*. 2024;10(23):e40370.

doi: 10.1016/j.heliyon.2024.e40370

37. Pontoni L, La Vecchia C, Boguta P, *et al*. Natural organic matter controls metal speciation and toxicity for marine organisms: A review. *Environ Chem Lett*. 2021;20:797-812.

doi: 10.1007/s10311-021-01310-y

ACCSCIENCE PUBLISHING

Our Journals

Microbes & Immunity is a multidisciplinary peer-reviewed journal dedicated to advancing the understanding of the interactions between microbes and the immune system. The journal provides an open access publishing platform for researchers, clinicians, and scientists to disseminate their original research, reviews, and perspectives related to various aspects of microbes and immunity. The journal aims to foster collaboration and knowledge exchange in the fields of microbiology, immunology, infectious diseases, and related disciplines. *MI* covers subject areas, including but not limited to the following:

- Host-Microbe Interactions
- Microbial Pathogenesis
- Immunomodulation by Microbes
- Microbiome and Immunity
- Vaccines and Immunotherapeutics
- Host Defense Mechanisms
- Microbial Genomics and Proteomics
- Diagnostic Methods and Technologies

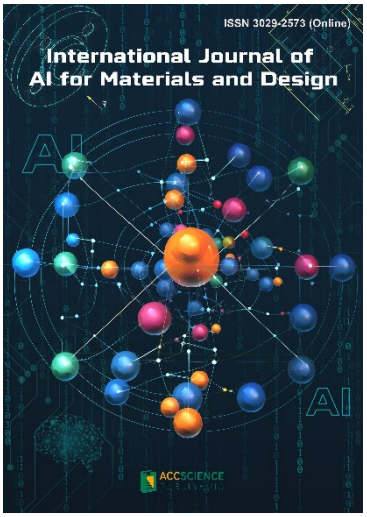

International Journal of AI for Materials and Design is an international, peer-reviewed open-access journal that aims to bridge the cutting-edge research between AI and materials, AI and design. In recent years, the tremendous progress in AI is leading a radical shift of AI research from a mainly academic endeavor to a much broader field with increasing industrial and governmental investments. The maturation of AI technology brings about a step change in the scientific research of various domains, especially in the world of materials and design. Machine learning (ML) algorithms enable researchers to analyze extensive datasets on material properties and accurately predict their behavior in different conditions. This subsequently impact the industry to leverage on big data and advanced analytics to build scientific strategies, scale operational performance of processes and drive innovation. In addition, AI and ML are uniquely positioned to enable advanced manufacturing technologies across the value chain of different industries. Integration of multiple and complementary AI techniques, such as ML, search, reasoning, planning, and knowledge representation, will further accelerate advances in scientific discoveries, engineering excellence and the future of cyber-physical systems manufacturing.

International Journal of AI for Materials and Design covers the following topics: AI or machine learning for material discovery, AI for process optimization, AI and data-driven approaches for product or systems design, application of AI in advanced manufacturing processes such as additive manufacturing, IoT, sensors, robotics, cloud-based manufacturing, intelligent manufacturing for various applications, autonomous experiments, material intelligence, energy intelligence, and AI-linked decarbonization technologies.

Start a new journal

Write to us via email if you are interested to start a new journal with AccScience Publishing. Please attach your CV, professional profile page and a brief pitch proposal in your email. We shall inform you of our decision whether we are interested to collaborate in starting a new journal.

Contact: info@accscience.com

https://accscience.com/journal/EER

Access Science Without Barriers

Contact

www.accscience.com
2 Venture Drive, #07-06 Vision Exchange,Singapore 608526
E-mail: editorial@accscience.com
Phone: +65 8182 1586